An Examination of the Neural Correlates of Interoceptive Processes in the Macaque Monkey

Dissertation

zur Erlangung des Grades eines Doktors

der Naturwissenschaften

der Mathematisch-Naturwissenschaftlichen Fakultät

und

der Medizinischen Fakultät

der Eberhard-Karls-Universität Tübingen

vorgelegt von

Renee Elizabeth Hartig

aus Smithtown, New York, United States of America

September 2019

Tag der mündlichen Prüfung:	10. Dezember 2019
Dekan der Math.-Nat. Fakultät:	Prof. Dr. W. Rosenstiel
Dekan der Medizinischen Fakultät:	Prof. Dr. I. B. Autenrieth
1. Berichterstatter:	Dr. Henry C. Evrard
2. Berichterstatter:	Prof. Andreas Bartels
3. Berichterstatter:	
Prüfungskommission:	Dr. Henry C. Evrard
	Prof. Andreas Bartels
	Prof. Cornelius Schwarz
	Prof. Nikos K. Logothetis

I hereby declare that I have produced the work entitled “An Examination of the Neural Correlates of Interoceptive Processes in the Macaque Monkey” submitted for the award of a doctorate, on my own (without external help), have used only the sources and aids indicated and have marked passages included from other works, whether verbatim or in content, as such. I s wear upon oath that these statements are true and that I have not concealed anything. I am aware that making a false declaration under oath is punishable by a term of imprisonment of up to three years or by a fine.

Tübingen, 30 September 2019

Renee Elizabeth Hartig

To the wise that came before my time

ABSTRACT

Several well-established methods exist for recording and measuring the underlying signals of the brain. Methods such as electrophysiology and fMRI, when taken together, have the capacity to disclose local and global neuronal activity. Here, both techniques were employed to refine the working functional model of the insular cortex, a recipient of sensory afferents relaying information about the body's physiological state. This dissertation serves to extend the current knowledge relating to the sensory afferent pathways relaying gustatory and interoceptive information to the brain, with special considerations of the role of the insular cortex. A series of fMRI experiments were conducted in the anesthetized macaque; whereby, responses to different types of interoceptive stimulation were measured (e.g. lower gastrointestinal distention, cutaneous thermal stimulation, auricular vagus nerve stimulation, and taste). The gross anatomical localization of these functions were mapped, providing a foundation for subsequent electrophysiological sampling across the insula. Using these methods, our results revealed a topographic organization of multi-modal interoceptive responses and the evidence garnered was analyzed within the context of insular cortex connectivity and its association with limbic and higher-order cortical areas. Our results support previous evidence of a topographic representation of interoceptive afferents in the human insula and contribute to the working model of insular cortex function in non-human primates. The manner in which interoceptive information is organized may disclose how upstream regions integrate sensory information to form a conscious percept of the body's physiological state, shaping cognition, and contribute to emotional embodiment. The present work serves as a basis for mapping functional responses with more involved paradigms designed to assess the emotional and cognitive responses to interoceptive sensations in the awake behaving state.

CONTENTS

Appended Manuscripts

ABBREVIATIONS

ABVN	auricular branch of the vagus nerve
ACC	anterior cingulate cortex
AIC	anterior insular cortex
ANOVA	analysis of variance
ANS	autonomic nervous system
AP	anteroposterior axis
BOLD	blood-oxygen-level-dependent
CN	cranial nerve
CNS	central nervous system
DV	dorsolateral axis
ECG	electrocardiogram
EGG	electrogastrogram
fMRI	functional magnetic resonance imaging
FOV	field-of-view
FWHM	full-width at half-maximum
HPC	heat-pinch-cold cell
Idfa/dAIC	dorsal fundus of the anterior insular cortex
Idfm	dorsal fundus of the mid-insular cortex
Idfp	dorsal fundus of the posterior insular cortex
GLM	General Linear Model
LFP	local field potential
MCC	midcingulate cortex
MDvc	mediodorsal thalamic nucleus ventrocaudal portion

MDEFT	modified driven equilibrium Fourier transform
ML	mediolateral axis
MUA	multi-unit activity
NHP	non-human primate
NTS	nucleus tractus solitarius
PAG	periaqueductal gray
PBN	parabrachial nucleus
PGA	Primary Gustatory Area
PIC	Primary Interoceptive Cortex
PFC	prefrontal cortex
PSFS	peripheral suction fluid stimulator
RD	rectal distention
Ri	retro-insula
ROI	Region-of-Interest
SDF	spike density function
ssGLS	suction-sealed gustolingual stimulator
vAIC	ventral Anterior Insular Cortex
VEN	von Economo Neuron
VMb	ventromedial thalamic nucleus basal portion
VMpo	ventromedial thalamic nucleus posterior portion

SYNOPSIS

"Sense-objects are always present, and thus when a sense organ—the subtle matter that allows you to see, hear, and so forth— develops, an eye consciousness, ear consciousness, nose consciousness, tongue consciousness, or body consciousness will be produced."

(Dalai Lama, 2000)

CHANNELING THE SENSES

The brain is an avid processor of the world around us and the world within us. The processing of these environments, and the signals arising from them, is crucial for survival and the maintenance of a healthy, balanced life. This dissertation examines the representation of different sensory modalities in the brain, with particular attention to signals arising from the body.

The underlying neural activity representing these sensory processes was analyzed to refine the concept of a somatotopographically organized insular cortex in the macaque monkey, a region with multiple functional domains encoding different aspects of bodily processing. The evidence presented here was compared to the topographic organization of the human insula, as determined by fMRI, and to prior tract-tracing studies previously targeting thalamic nuclei known to project to the insula. From this comparative research, we learn that the topographic innervation of afferents is conserved from the spinal cord to the cortex and that distinct anatomical subregions support the integration of multi-modal information.

While a plethora of functional modules exist within the neuroanatomical construct of the brain, this intricate system is often parsimoniously described for general education purposes. What has been commonly taught to students about the central nervous system (CNS) largely concerns the input of information to the brain and outputs in terms of emotions, behavior and physiological changes. There are five *classical senses* everyone learns by adulthood: taste, touch, smell, vision and hearing. It is generally understood that the brain receives visual input from the eyes, auditory

input from the ears, taste input from the mouth, olfactory input from the nose and tactile input from the skin. By this framework, each sense has its own specialized organ for transducing the relevant information. But, to consider the processing of sensory information only within this framework would surely lead to the exclusion of other senses including, in particular, interoception.

Interoception plays an essential role in maintaining a balanced internal world, or homeostatic state. The term, coined by Charles Sherrington in the early 1900s, originally referred to the sense of visceral organ function. Over time, however, Sherrington's interoception was redefined as the sense of the physiological condition of all the organs and tissues of the body (Craig, 2002). Thereby, interoception includes skin and body temperature, respiration, cardiovascular activity and noxious stimuli, among others. This modern definition of interoception has already been adopted by contemporary researchers in the field (Tsakiris & De Preester, 2018; Garfinkel & Critchley, 2013).

A prevailing dichotomy distinguishes interoception from exteroception, whereby the latter relates to stimuli originating externally without a direct effect on the body's physiology. This terminology has been employed by multiple research groups to investigate exteroceptive vs. interoceptive attention (Farb, Segal, & Anderson, 2013), sensory discrimination (Fukushima, Tanaka, & Myowa, 2018), and multi-sensory integration (Suzuki, Garfinkel, Critchley, & Seth, 2013). An illustration of the anatomical relay of interoceptive and exteroceptive sensory modalities from the periphery to the CNS helps to classify these different sensory modalities (Fig. 1).

By examining the underlying anatomical pathway of all incoming stimuli, one may classify them based on their relay to the brain. The taste pathway, for example, is remarkably distinct from that of olfaction and vision, whereby taste afferents relay to the ventromedial thalamus like other interoceptive modalities. A categorization based upon this anatomical distinction would group taste together with interoception. Whereas, olfaction and vision would not fall within this category - as vision has its own specialized processing nuclei in the thalamus and olfaction bypasses the thalamus entirely on its way to the cortex, making vision and olfaction independent senses in their own right.

We can discretely categorize sensory processes, but must acknowledge their interdependence and relatedness. For instance, the senses of taste and smell transduce chemical stimuli arising from the environment, which in turn interact with the oral and retro-nasal cavities, respectively. It is the retro-nasal activation by odorants that also activates the gustatory pathway by means of swallowing (Marciani et al., 2006). A similar, albeit slightly less direct concept can be

applied to visual stimuli, which once transduced by cells in the retina, can influence the body's physiological state. Take for example, gruesome images that evoke a certain churning sensation in the stomach. Here, the inherent connectedness between the external and internal worlds is evident.

Each sensory organ has its own specialized set of receptors. For instance, the tongue contains numerous metabo- and iono-tropic receptor cells embedded within its epithelium (Carleton, Accolla, & Simon, 2010). Visceral organs are largely innervated by the 'free'-nerve endings of C-fibers and vagal afferents (Bonaz, Bazin, & Pellissier, 2018; Haupt, Jänig, & Kohler, 1983; Ozaki & Gebhart, 2001; Sugiura, Terui, & Hosoya, 1989), and a collection of different cell types, nestled within the skin, supports the transmission of both exteroceptive and interoceptive information. There are specific receptors for haptic sensation (e.g. Pacinian corpuscle for mechano- and vibro-reception) innervated by thickly myelinated Aβ-fibers, and additional sensory afferents (i.e. unmyelinated C-fibers and thinly myelinated Aδ-fibers), which relay information related to skin temperature (Craig, 2004), among other interoceptive modalities, such as affiliative touch, baroreception, and ergoreception. Thus, the sensory afferent fibers connecting the skin to the CNS are characterized not only by their anatomical relay to the cortex but also by fiber type. This categorization classifies the skin as both an exteroceptive and interoceptive organ, depending on the stimulus modality relayed.

The processing of interoceptive stimuli is crucial for the maintenance of homeostasis. Such information reaches the CNS by vagal (Mayer, 2011) or craniofacial (Galizia & Lledo, 2013) afferents, or via the lateral spinothalamic tract (Han, Zhang, & Craig, 1998). Peripheral afferents relay to the superficial (lamina I) spinal dorsal horn and crossover immediately to the contra-lateral lemniscus, thereby ascending to the first homeostatic relay center in the brainstem – the nucleus tractus solitarius (NTS). Afferents innervating more rostral parts of the body, for example, baroreceptors, enter via lamina I of the trigeminal dorsal horn (Bereiter, Hirata, & Hu, 2000).

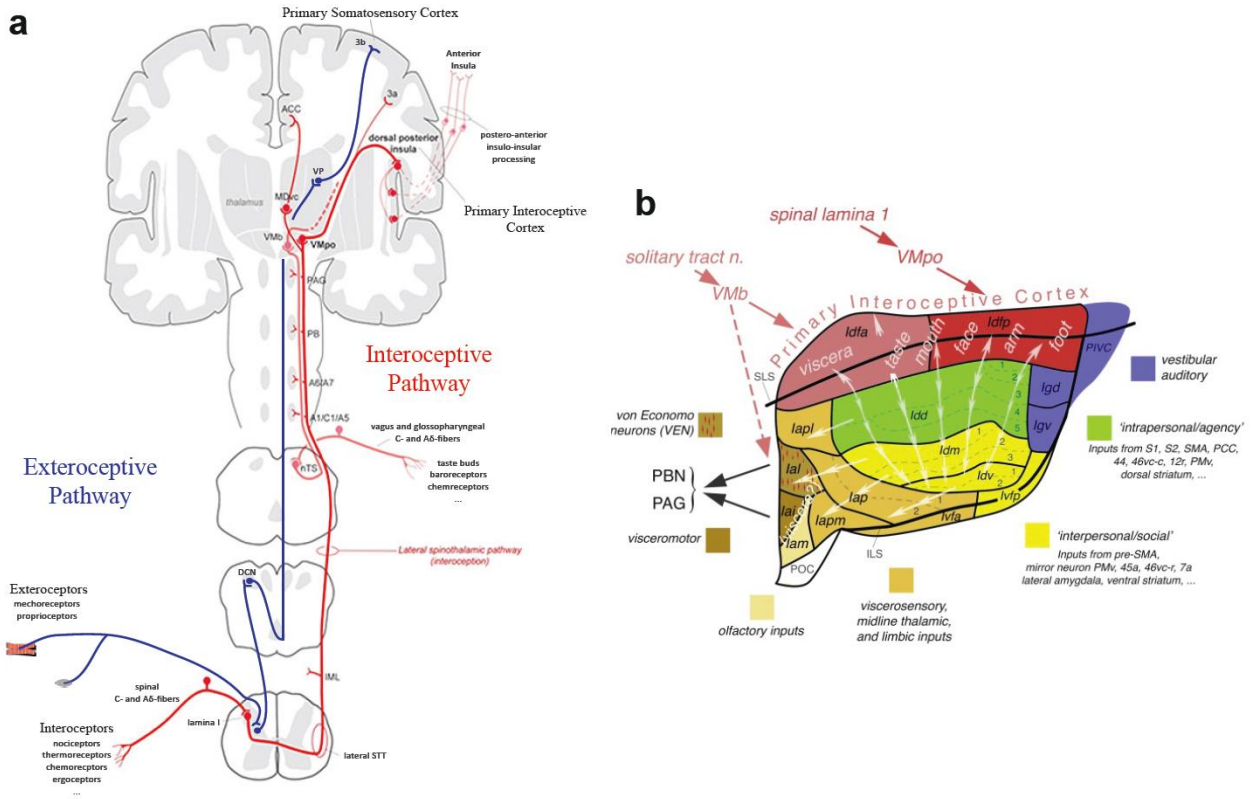

Fig. 1: The ascending pathways and working model of the insular cortex. (**a**) The ascending interoceptive and exteroceptive pathways relaying modality-specific information in a conserved topographic manner up the central nervous system hierarchy, whereby interoceptive information ultimately relays to the insular cortex, exteroceptive information relays to the somatosensory cortex (area 3b). Figure adapted from Craig (2015). (**b**) The working functional neuroanatomical model for the insular cortex, as reproduced with permission from Evrard (2018).

It is at the level of the medulla that the NTS receives input from the spinothalamic tract as well as from facial (CN VII), glossopharyngeal (CN IX), trigeminal (CN V), and vagal (CN X) cranial nerve (CN) relays. The NTS is an initial level of sensory convergence in the brainstem, and maintains a degree of functional specificity, whereby taste afferents are predominately situated in the rostral NTS (Halsell, Travers and Travers, 1993). Caudally, the NTS is organized into a viscerotopic map (Altschuler, 1989; Travagli, 2006), with modular domains representing different body regions in close proximity to one another (Paton, 1999), suggesting an early spatial organization of different interoceptive afferents. Nevertheless, evidence for functional integration in the NTS has been garnered from neuronal populations responsive to both lingual tactile and taste stimuli (Halsell, Travers and Travers, 1993). Multi-modal NTS responses have also been recorded

from thermo-gustatory (Lemon, Kang, and Li, 2016) and odor-taste stimuli (Escanilla, Victor and Di Lorenzo, 2015).

From the medulla interoceptive afferents ascend, targeting pre-autonomic nuclei (i.e. the parabrachial nucleus and periaqueductal gray), before terminating in the topographically organized ventromedial thalamic nucleus. Cranial afferents V, VII, IX and X synapse in the ventromedial basal (VMb) portion (Pritchard et al., 1986), while remaining interoceptive inputs synapse in the ventromedial posterior portion (VMpo) of the nucleus (Craig, Bushnell, Zhang, & Blomqvist, 1994). The VMb encoding preserves a dorsoventral topography of gustatory and visceral afferents, respectively; while VMpo encodes spinal and trigeminal laminar afferents in an anteroposterior manner, with the face and cervical spinal regions oriented anteriorly (Fig. 2). Thereby, VMb projections terminate in the granular anterior dorsal fundus of the insula (Idfa), and VMpo predominantly projects to the granular posterior dorsal fundus of the insula (Idfp) with an ancillary projection to area 3a, a region nestled within the sulcus of the primary somatosensory cortex, or S1 (Craig, 2014; Craig, 2002). For the purpose of this work, Idfa was further parcellated into a middle (Idfm) and anterior (dAIC) representation.

The thalamic nuclei receiving projections from deep spinal lamina V and VI (encoding haptic touch and proprioceptive information) are also topographically organized, whereby the ventroposterior medial (VPM) and lateral (VPL) nuclei receive afferents from the forelimbs and hindlimbs, respectively. VPM and VPL both project to area 3b of the primary somatosensory cortex. Their functional representations comprise the homunculus – first described in humans by Wilder Penfield (Penfield & Boldrey, 1937). The ventrocaudal portion of the mediodorsal (MDvc) thalamus receives proprioceptive as well as interoceptive projections and relays to the anterior cingulate cortex (ACC), an upstream cortical area reciprocally connected to the anterior insular cortex (AIC). Notably, spinothalamic lamina I terminals converge with deeper laminar projections in the intermediate ventroposterior (VPI) thalamic nucleus predominantly relaying vestibular information to the retro-insular (Ri) cortex, just posterior to the dorsal insular cortex (Brandt and Dietrerich, 1999). Such anatomical knowledge has played a vital role in developing this research and in the interpretation of functional results.

Based upon tract-tracing and electrophysiological recordings of the macaque thalamus (Craig, 2014; Pritchard et al., 1986), one might expect a functional encoding in the Primary

Interoceptive Cortex (PIC) that reflects the topographic innervation of sensory afferents. These afferents are specifically relayed to the granular dorsal fundus of the insula (Fig. 2). Here, both neuroimaging and electrophysiological methods were applied within one research program to uncover the organization of multiple functional responses both at the population level to examine the modularity of neuronal response profiles and at the network insular level (extending across all anatomical subdivisions). This research investigated the relationship between functional processing and anatomically distinct insular subregions.

It is thought, for both humans and non-human primates (e.g. *Macaca mulatta)*, that interoceptive inputs relayed to the insula are primarily organized in a foot-to-head topography (Brooks et al., 2005; Hua et al., 2005; Segerdahl et al., 2015), and extend from the posterior-to-anterior dorsal fundus (Craig, 2009; Evrard, 2018). Anterograde tract-tracing injections in the similarly organized VMpo have labeled Idfp and the dysgranular mound of the insular cortex (Craig, 2014). It is anterior to this body map that VMb afferents innervate the granular insula (Fig. 2).

Human gustatory literature suggests the encoding of taste occurs in the middle of the dorsal fundus (Idfm), at the junction between Idfa and Idfp, with a distinct representation extending

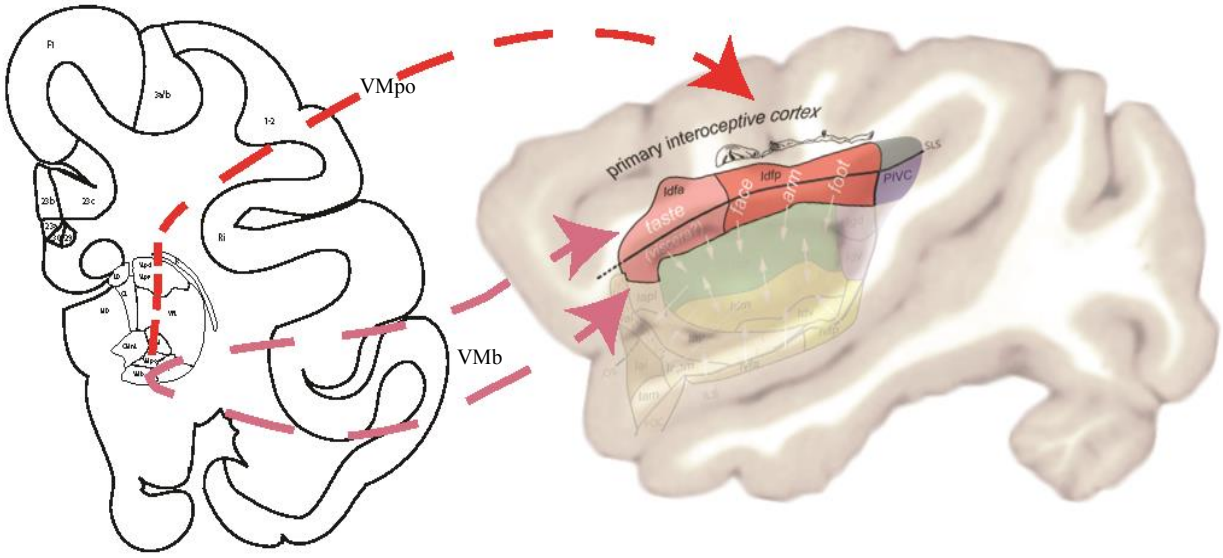

Fig. 2: Thalamo-insular connectivity and relay of afferent activity to the PIC. Sensory afferent relay by the ventromedial thalamus. The ventromedial basal (VMb) nucleus projects predominantly to the anterior half of the insular cortex (Idfa); the ventromedial posterior (VMpo) nucleus projects to the posterior dorsal fundus of the insula (Idfp). VMb projects gustatory afferents dorsally and visceral (vagal) afferents ventrally to the insular cortex. Contouring of coronal section done by Mark Byrne; insular cortex schematic adapted from Evrard (2018).

ventroanteriorly (Yeung et al., 2017). However, previous electrophysiology studies in macaques suggest that taste occupies the entire Idfa, leaving little residual substrate for the processing of other ongoing visceral activity. Further details and discussion on this topographic representation in macaques and how it compares to humans will be revealed throughout the next few chapters of this dissertation. Chapter 2, for instance, discusses how well the taste representation in macaque monkeys resembles that of the human representation and Chapter 4 presents maps of the somatotopic encoding of functional responses in the insula.

Although a gross topography is evident, there is indication from previous literature that taste and interoceptive responses (e.g. nociceptive, baroreceptive, and cardiac) share an anatomical substrate within the insular cortex. Such evidence garnered from rodent electrophysiology (Hanamori et al., 1998; Ogawa & Wang, 2002) and human functional magnetic resonance imaging (fMRI) studies (Avery et al., 2015, 2017) appear to highlight the mid-dorsal granular and dysgranular insula as potential substrates for multi-modal convergence within the insula. Given the parallels in functional neuroanatomy between these species and macaques, we predicted that a similar organization could be identified from this work. A more in-depth discussion on the implications of functional convergence with preserved modular domains is saved for Chapter 4 of this dissertation.

BUILDING UPON THE SENSES

Between humans and macaque monkeys the functional neuroanatomy of the insula is, to a large extent, homologous. However, a volumetric comparison of the insular cortex across primates has shown that the anterior insula grew disproportionately more in humans than in any other primate species (Bauernfeind et al., 2013), suggesting a new expansion and subdivision of this region in the human brain late in evolution. Coincidentally, a specific cell type was identified in the expanded anterior insula - the unique spindle-shaped von Economo Neuron (VEN) in the ventral agranular anterior insular cortex (vAIC), a demarcated cytoarchitectonic area otherwise known as the frontoinsula in humans (von Economo, 2009; von Economo, 1925). With that said, however, the macaque vAIC was also shown to possess the von Economo neuron (Evrard, Forro & Logothetis, 2012). This led to further discussion about the potential analogous functional capacity in macaques as based upon the anatomical homologs (Critchley & Seth, 2012). This cortical region harboring the VENs is activated during the processing of interoceptive and emotional feelings in humans

(Harrison et al., 2010; Bartels & Zeki, 2004; Craig, 2002). In patients suffering from a subtle loss of self-conscious emotions, VENs are selectively depleted (Kim et al., 2012). All of this evidence suggests a critical role for the vAIC and its VENs in substantiating the emotional self.

The unique role of the AIC has already been highlighted and evidence suggests this area is involved in the conscious evaluation of sensations and percepts, ultimately modulating one's emotional state and behavioral responses. Human neuroimaging research supports this argument with activations in the AIC related to the processing of happy voices (Johnstone, van Reekum, Oakes, & Davidson, 2006), seeing or making a smile (Hennenlotter et al., 2005), heartbeat awareness (Critchley et al., 2004), attention to heat pain (Brooks et al., 2002), and pleasant music (Koelsch et al., 2006)**.** Thus, it becomes evident that, in sentient beings, the AIC and its cross-species homolog is a key anatomical substrate for higher-order information processing. The AIC processes salient, interoceptive stimuli (Uddin, 2015) and related affective (Harrison et al., 2010) and motivational constructs (Wager & Barrett, 2017). Interestingly, dissociable large-scale networks, subserving affective experience and attention (Touroutoglou, Hollenbeck, Dickerson, 2012), are purportedly anchored in the right AIC. Moreover, the functional role of the AIC can be further subdivided into the dorsal and ventral aspects, whereby the dorsal AIC (dAIC) is more readily involved in cognition and the ventral AIC (vAIC) in affective experiences (Kurth, 2010; Mutschler, 2009; Small, 2010; Wager & Barrett, 2017). Further evidence to support the hypothesis that the AIC plays a key role in such functions is its connectivity to higher-order brain regions, namely the anterior cingulate (ACC), orbitofrontal (OFC), and prefrontal (PFC) cortices (Carmichael & Price, 1995).

SCIENTIFIC OBJECTIVES

I. Interotopy

The primary aim of this research was to investigate the underlying neuronal responses to interoceptive stimulation and to determine if a topographic map of the macaque insula could be produced by applying a pre-defined set of functional stimuli representing distinct interoceptive modalities (i.e., temperature, taste, visceral distention). Using fMRI, we examined the insula's responses to these interoceptive stimuli in the anesthetized macaque. After imaging, we recorded from the underlying neuronal populations during similar functional stimulation, using tetrode

recoding arrays, to characterize the responses and to capture the areal localization of specific sensory processing hubs. The data collected by this research provides valuable insight into the functional organization of the macaque insular cortex and serves to refine the working model illustrated by Evrard (2018).

II. Insulo-Insular Dynamics

We hypothesized that, by examining the processing of interoceptive inputs, we could garner the insight needed to further understand the functional organization across the different anatomical realms of the insular cortex. With the resolution afforded by our methodology, we examined the different connectivity profiles of the granular insular dorsal fundus with the more integrative dysgranular and agranular components. How functional information is processed in the insular cortex in conjunction with its intrinsic and extrinsic connectivity was probed using descriptive measures of statistical dependencies on modality-specific activation patterns.

III. Anterior Insular Cortex

Building upon the knowledge gained from this repertoire of data, a consideration was made as to the functional role of the AIC during interoceptive processing and how this region in macaques, as compared to humans, processes sensory information. In particular, the AIC relates expectancy and incoming sensory signals to estimate a prediction error, which it relays in top-down fashion to modulate autonomic nervous system activity (Barrett & Simmons, 2015; Seth, Suzuki, & Critchley, 2012). For example, the AIC estimates the probability of body damage to painful stimuli based upon the integration of sensory inputs as well as the prior representation of such constructs (Sharvit, Vuilleumier, Corradi-Dell'Acqua, 2019). Considering the principles of predictive coding, regions providing higher-order modulation do not require direct sensory input from the thalamus. However, some anatomical studies suggest an ancillary projection from VMb to the vAIC (Carmichael & Price, 1995). The notion of ancillary thalamic afferent projections to the agranular and dysgranular insula are reviewed and considered within the framework of this dissertation. To discern the underlying integrative nature of the AIC, a model for information relay within the insular cortex was derived and tested, at first using functional data where correlated activations were localized to the different anatomical subdivisions (see Chapter 3 for results and further discussion).

STATE OF THE ART

Previous literature implicates the insular cortex as the cortical terminus of ascending gustatory and interoceptive projections from the brainstem and spinal cord (Craig, 2002; Pritchard et al., 1986); while descending projections from the insula terminate in pre-autonomic and homeostatic brainstem nuclei (Chavez et al., 2018; Beckstead, Morse, & Norgren, 1980; Yasui et al., 1991). Understanding the anatomical organization of ascending and descending pathways puts into perspective how incoming functional information is encoded and subsequently relayed. Functional methods, such as fMRI and electrophysiology, help to elucidate the mechanism of information encoding. It is only by recognizing the relationship between structure and function that the clearest picture of the underlying neurological processes can be described and effectively outlined.

The knowledge of structural connectivity supports the functional findings highlighted in this dissertation and provides perspective on the topographic and integrative nature of the insula. We refine the concept of a somatotopographically organized insular cortex in the macaque monkey and provide empirical evidence that complement prior tract-tracing studies. The functional modalities employed in this research were intended to evoke interoceptive sensations and enable us to study the consequent functional responses in the brain. Chapters 2-3 devote themselves to the gustatory and visceral modalities studied in a series of fMRI experiments and the relevant experimental procedure for each stimulation is described there in further detail. Questions extending across the modalities applied in this research will be addressed in this dissertation. For example, how is the encoding of taste information related to the mid-dorsal and anterior insular cortex? What is the relationship of information processing between these areas? Does the AIC serve as an anatomical substrate for higher-order sensory processing, ultimately leading to emotional and behavioral outputs? How does the brain state (anesthetized vs. awake) influence sensory processing?

DYNAMIC BRAIN STATES

The brain is a unique organ, capable of entering many different physiological states. Morcos & Harvey (2016) have described multiple possible sequences of neural activity for the same event, thereby defining distinct cluster sequences. However, in terms of maintaining a consistent physiological state during data acquisition, stable anesthesia controls some level of respiratory and

cardiac variations over time. As Sellers, Bennett, Hutt, & Fröhlich (2013) acknowledged, anesthesia differentially modulates spontaneous network dynamics by cortical area and layer. Therefore, the most reliable paradigms of study are those that introduce an experimental manipulation to perturb the functional brain state in a controlled manner. By stabilizing as many physiological parameters as possible, we aimed to measure the endogenous changes specifically related to our stimulation paradigms. Further, sensory relay by the thalamus persists in the anesthetized state, whereby electrophysiology recordings of VMpo during morphine-induced anesthesia in macaque monkeys and interoceptive stimulation resulted in clear responses by the thalamic neurons (Craig, 2014). Further, stimulation of oral and perioral surfaces effectively drove neuronal responses in the VMb of macaques, despite the depressive effects of general anesthesia (Pritchard et al., 1986).

With this evidence, we were confident that the primary sensory relay pathway would remain rather intact under anesthetized conditions. However, it is at the level of higher-order processing that it becomes difficult to identify specific neuronal signatures. Take for instance, the variability of vAIC activity in individual subjects during gastrointestinal distention (Chapter 3). The inconsistent areal localization within this one region was enough to limit robust localization at the group-level. We must further consider the influence of the subject and the subject's brain state on activation in regions that possess such complex processes as perception and self-evaluation. Questions of arousal and how salient our applied stimuli actually were cannot be addressed by this work, but this dissertation does provide a basis for future studies in the awake, behaving state.

FUNCTIONAL MAGNETIC RESONANCE IMAGING

A method first pioneered at AT&T Bell Laboratories in New Jersey, U.S.A. using a 7 Tesla scanner to image not just the anatomy of the brain but also its biological function was successfully performed in the rat animal model (Ogawa, Lee, Kay, & Tank, 1990). One can imagine that MRI has exploded into the world of functional neuroscience. Since the time this dissertation work began, fMRI has been cited an average of 30,786 times per year (PubMed). Understandably, fMRI is an instructive technique that allows us to examine state-dependent changes in the brain at rest or during sensory and/or motoric events.

As fMRI expert Robert Turner would describe in his seminal lectures, the blood-oxygen-level-dependent (BOLD) signal measured by fMRI acts as a function of cortical profiling and, in some cases, helps to elucidate laminar cortical profiles at ultra-high magnetic fields (> 7 Tesla)

(Goense, Merkle, & Logothetis, 2012). Especially, given the correlation between BOLD responses and neural mechanisms, particularly local field potentials (LFPs) in the low (2-15 Hz) and high (40-80 Hz) frequency ranges (Schölvinck et al., 2010; Logothetis & Wandell, 2004; Logothetis et al., 2001), non-invasive fMRI is particularly common in neuroscience research.

The fMRI data collected for the outlined research program was done with two types of radio frequency (RF) receiver coils. The model that was utilized included an additional 8-channel coil array and custom-fit helmets for three subjects that allowed for parallel imaging and acceleration across both temporal and spatial domains. Additionally, all fMRI data collected went through a process of quality checks and images were assessed for distortions. Data used for analysis were calculated in the native brain space of each subject and normalized to a standardized atlas template (see Chapter 1 for normalization pipeline). Given the large count of subjects included in this work, data were averaged and analyzed at the group-level to minimize inconsistencies at the single-subject level and aid in the extrapolation of findings to the population as a whole.

ELECTROPHYSIOLOGY

Establishing regions-of-interest (ROIs) for interoceptive processing first by fMRI aided in electrophysiological recordings of the insula - a large cortical region with an approximate volume of 420 cm^3 (average dimensions: 8 x 24 x 22 mm^3). Such electrophysiology techniques afforded the opportunity to record multi-unit neuronal activity (MUA) from our regions-of-interest (ROIs). At the population level one may examine, as related to cellular morphology and functional encoding (Andrew and Craig, 2001), the different neuronal response profiles of modality-specific cell types: nociceptive (NS), gustatory, and heat-pinch-cold (HPC) cells, among others. We had the opportunity to sample bilaterally the extent of the insular cortex in four subjects that permitted not only the characterization of responses from the somatotopographically organized PIC and poly-modal dysgranular insula, but also provided concurrent recordings from the ventral agranular insula (the area harboring VENs), to study the responses of this region during sensory stimulation. And as hypothesized, but nevertheless surprising, there are cases where the vAIC area responds, with some latency, to interoceptive stimulation. These results are discussed further in the last chapter of this dissertation.

In order to determine the stereotaxic coordinates for electrode placement and tract-tracer injections, the insular cortex was drawn to-scale based upon each animal's high-resolution

anatomical scan. From these individual reconstructions, any necessary recording chambers and scaled models of the insular cortex were 3D-printed. Chamber implants and craniotomies provided a window into the brain, allowing us to enter with a micropipette for tract-tracing injections and also with recording (and stimulating) electrodes.

OVERVIEW

The dissertation at hand compiles a series of manuscripts that complement one another and portray the development of a group-level analysis pipeline for NHP neuroimaging and an in-depth study of specific interoceptive modalities, including stimulation of the taste and visceral pathways. Each sensory modality warrants its own investigation given the sheer number of animals included in this research, providing a strong statistical ground for analysis of functional networks at the population level. The final part of this dissertation is an overarching examination of the multi-modal functional maps, conducted from the perspective of relating structure and function. A dedicated approach to parcellate the insula, as based upon its known anatomical subdivisions, has aided in developing the working functional model, while regarding other regions-of-interest known to transmit and receive projections from this cortical region. What can be learned at the end of the day is that a gross sacral-to-cranial topography exists within the macaque insular cortex, one which is not just limited to the granular dorsal fundus but extends also to its dysgranular region; and the macaque indeed has a taste area more closely aligned with humans than previously believed. And whether the dysgranular insula is activated under direction by the ventromedial thalamus or serves as the first poly-modal integrator of interoceptive and non-interoceptive information is discussed further in this work, along with the relationship between these regions and the insula's agranular pole.

PART 1: FUNCTIONAL IMAGING DURING INTEROCEPTIVE STIMULATION

Interoceptive afferent fibers innervating all the tissues and organs of the body (from the skin to the bone) inform the brain about the ongoing physiological state of the body. The dorsal fundus of the insula or Primary Interoceptive Cortex (PIC) is the primary recipient of interoceptive sensory information from all areas of the body, including also specialized tissues and organs. At this level of functional processing, the insula can discriminate between different types of stimuli. The response patterns elicited by these stimuli were measured first by fMRI and later by electrophysiology to

create subject-based interotopic maps (Part 2). Neuroimaging (BOLD) data were collected during graded cooling and heating of the hand and foot, taste delivery, rectal distention (RD) and transcutaneous electrical stimulation of the auricular vagus nerve branch (ABVN). The functional representations were subsequently mapped onto the corresponding anatomical regions within the insular cortex, and as a whole, within the brain. Cutaneous thermal stimuli elicited activations in the posterior area of the dorsal fundus of the insula (Idfp), while activations related to taste stimuli were localized more anteriorly. Considering the gross insula innervation topography, the visceral distention activations are indicative of two ascending pathways for gastrointestinal information: one through the lateral spinothalamic pathway and another through the ascending vagal afferent pathway. Ultimately, we aimed to create a normalized functional map of each individual interoceptive modality to identify consistent activation patterns needed to illustrate a translational comparison between non-human and human neuroanatomical functional organization, while also considering conserved organizational properties from studies using the rodent model.

PART 2: INTEROTOPIC MAPS

The topographical organization of interoceptive information within the insula was examined using fMRI, electrophysiology and tract-tracing in the anesthetized macaque. Electrophysiological recordings (n = 4) confirmed this overall topography. Recordings in Idfp revealed a somatotopic organization in which the foot, hand, and face were represented from posterior to anterior. Neurons in Idfp responded either to noxious heat, pinch and cold (HPC cells), or were nociceptive-specific with responses to only noxious cold or pinch (NS cells). Recording in the mid-dorsal fundus of the insula (Idfm) revealed an extensive multi-sensory representation of the orofacial cavity, including taste. Recordings in the anterior portion of the dorsal fundus (dAIC) revealed spontaneous rhythmic activities potentially correlated with visceral processes (e.g. heart rate, respiration). Tracer injections in the dorsal fundus confirmed prior evidence for specific thalamocortical projections from the ventromedial nucleus of the thalamus. The present study supports the idea that the primate insula represents interoception in a manner that preserves the spinocranial topography and the encoding of interoceptive modalities (e.g. HPC and NS) along distinct labeled-lines throughout the neuraxis. This refined representation of internal bodily signals likely plays a crucial role in the homeostatically efficient shaping of cognitive processes by interoception, and provides the basis for the evolutionary emergence of embodied subjective feelings in the human anterior insula.

PART 3: FUNCTIONAL CONNECTIVITY

The PIC receives direct connections from the thalamic relay nuclei as described above, and is able to discriminate and identify different stimulus modalities (Bender et al., 2009; Rolls et al., 2004). From this primary cortical processing area, information is relayed further upstream, etching a sophisticated intra-insular organization, where sensory stimuli are represented across the dysgranular and agranular regions all the while incorporating multi-modal information from other sensory domains. It is at the level of multi-modal functional integration that incoming sensory information is evaluated at a higher-order and translated into percepts. To further study the intrinsic and extrinsic connectivity of the insula, fMRI time series data were examined across intra-insular regions as well as regions involved in processing interoceptive information at a more limbic or higher-order level.

A STEP FORWARD

The findings in this dissertation depict a select arrangement of interoceptive inputs within the macaque insula. The manner in which this information is organized may disclose how upstream regions integrate sensory information to form a conscious percept of the body's physiological state, contribute to emotional embodiment, and provide top-down influence on bodily function. The present work serves as a basis for mapping functional responses with more involved paradigms designed to assess the emotional and cognitive responses to interoceptive sensations in the awake, behaving state.

The insula plays a vital role in manifesting percepts and emotional constructs from interoceptive afferents, all the while integrating incoming signals across the realm of sensory modalities. In order to understand further the perception and sensation of sensory stimuli, we should consider agranular cortices, much like the vAIC region containing the VENs. On this premise, we acknowledge an integrative agranular and dysgranular insular cortex that serves to communicate information between high-order cortices and limbic centers (e.g., amygdala, hypothalamus).

The anterior insula, in particular, possesses a unique capability for higher-order processes, such as that needed for perception of oneself and one's current emotional state. The AIC integrates salient information to develop perceptual decisions, like executing the appropriate behavioral response to pain (Wiech et al., 2010). Disruptions in the insula's functional neuroanatomical

circuitry has led to multiple psychiatric disorders; for example, post-traumatic stress disorder, obsessive compulsive disorder (Nagai, Kishi & Kato, 2007), and schizophrenia (Wylie & Tregellas, 2010). There is still much to learn about emotions and their necessity for navigating social environments.

Our biological energy consumption serves to maintain a constant state of physiological stability (Cannon, 1929). This homeostatic process is crucial for survival and energy optimization (De Araujo, Geha, & Small, 2012); it also provides the biological basis for all subjective bodily and emotional feelings in humans (Craig, 2009). Sensations ultimately translate to emotions. Antonio Damasio, with his somatic marker hypothesis, expanded upon the classic James-Lange theory to include the ACC and AIC as regions involved in translating emotions from different somatic and physiological responses (Poppa & Bechara, 2018; Damasio & Carvalho, 2013; Cannon, 1931; James, 1884). Unlike the approach put forth by Cartesian dualism where there is an independent, dissociative relationship between body and mind; mind and body are concomitant, complementary systems.

One vital feeling is suffering, for it is the capacity to emotionally suffer which defines a sentient being. And, "what marks the transition from non-sentient to sentient beings? A model of increasing complexity based on evolution through natural selection (Lama, 2005)." It can be argued that those unable to possess such emotions are not sentient beings. However, this evolution of emotions may best be understood by relating the complexity of emotion to the anatomical regions involved in its manifestation.

There are different levels of emotions; the sophisticated ones arising cortically and those manifested by subcortical regions (i.e. the amygdala) that drive crucial behaviors for survival, such as, fleeing from a predator. The insula is a phylogenetically old cortex bordering the basal ganglia (Sudakov et al., 1971), a paralimbic region, which integrates poly-modal sensory activity with affective information from limbic centers (Adolfi et al., 2017; Evrard, Craig, Logothetis, 2014). However, the emotions arising from this cortex are more developed than subcortical regions, for example with love (Bartels & Zeki, 2004), empathy (Gu et al., 2012), and trust (Adolphs, 2002).

Progressing up the mammalian brain hierarchy, cortical structures appear to have enlarged. For instance, even though humans and macaques are closely related in terms of phylogeny, the human insular and prefrontal cortices (Elston et al., 2005) have largely expanded in volume, albeit

proportionately to other primates (Gabi et al., 2016), with the exception of the rostral insula (Bauernfeind et al., 2013). One reason for the disproportionate growth of the anterior insula (AIC) in humans may be to accommodate the growing importance of social skills for survival. Modern-society, as dominated by humans, demands such beings express highly sophisticated emotions to succeed in the complex interactions between conspecifics and with all realms of nature. The human insula was recently recognized as a highly evolved and organized cortical lobe with a crucial role in engendering human subjective feelings, and in providing a possible neurobiological substrate for human sentience (Craig, 2015).

Nevertheless, with a full understanding of the underlying basic principles of sensory information relay and organization, we can ascertain the underlying mechanisms of more complex neuroanatomical circuitry. Moving forward with this research, experiments should be conducted during the awake state to obtain a more accurate assessment of behavioral and physiological responsivity to interoceptive stimulation. It is expected that much of the PIC activation remains, even in awake subjects, however, an attentional shift may be placed upon any incoming perturbations and influence AIC connectivity patterns and the global networks tied to this region.

Furthermore, the responsivity of neuronal populations to multiple modalities deserves further consideration. Evidence exists for a labeled relay of individual interoceptive modalities (Craig, 2014; Mueller et al., 2005; Zhao et al., 2003), however, the degree to which neuronal populations respond preferentially may be indicative of the tuning of homeostatically-relevant stimuli and the weight given to different sensory components.

While fMRI affords the advantage of examining global brain networks, neuroimaging sequences, such as gradient-echo echo-planar imaging (EPI), are highly sensitive not just to metabolic changes related to neural activity but also to extravascular constituents, i.e. large draining veins (Lee, Silva, Ugurbil, & Kim, 1999). It is important to interpret fMRI results within the context of meticulously acquired data from the field of neuroanatomy and the emerging computerized endeavors of connectomics. We must consider the variability in neuroimaging data between single subjects has been examined in previous reports to localize the primary factors influencing variance. One major factor influencing the reproducibility of BOLD fluctuation amplitudes is inter-subject differences in hemodynamic response (Aguirre, Zarahn, & D'esposito, 1998) and early BOLD response amplitude (Hu, Le, & Ugurbil, 1997). An additional factor is the functional task itself. One

mechanism that is difficult to parse is the cognitive processing associated with a specific task. A recent study by Shulman & Rothman (2019) introduces a non-cognitive behavioral model to assess lower-level functional processes in the brain. Denoting the non-cognitive functional regions could help determine how regional hubs in the salient network process information below the level of cognitive evaluation. Incoming signals provide the brain with potentially salient information related to the body - vital to the maintenance of homeostasis. In those cases where bodily signals chronically evoke surprise, a dyshomeostatic state occurs, in which affected individuals have expressed symptoms of fatigue and depression (Stephan et al., 2016).

Lastly, functional methods with greater spatial and temporal resolution (e.g. laminar electrophysiology, *in vivo* fluorescent imaging, etc.) would undoubtedly complement the data presented in this dissertation and serve to validate a larger repertoire of other existing data. The brain is a complex organ, but such an astute and diligent integration of different methodologies will only help to further develop the basic principles of neuroscience and push the field forward. The future of neuroscience is now, we are in a technological revolution and the technology needed to gather essential data is developing every day. With each advance we are becoming more innovative and calculating in our applications of these basic principles of brain structure and function.

BIBLIOGRAPHY

Adolphs, R. (2002). Trust in the brain. *Nature Neuroscience*, *5*(3), 192–193. https://doi.org/10.1038/nn0302-192

Adolfi, F., Couto, B., Richter, F., Decety, J., Lopez, J., Sigman, M., … Ibáñez, A. (2017). Convergence of interoception, emotion, and social cognition: A twofold fMRI meta-analysis and lesion approach. *Cortex*, *88*, 124–142. https://doi.org/10.1016/j.cortex.2016.12.019

Aguirre, GK., Zarahn, E., & D'esposito, M. (1998). The Variability of Human, BOLD Hemodynamic Responses. *NeuroImage, 8,* 360-369.

Altschler, SM., Bao, X., Bieger, D., Hopkins, DA., Miselis, RR. (1989). Viscerotopic representation of the upper alimentary tract in the rat: Sensory ganglia and nuclei of the solitary and spinal trigeminal tracts. *J. Comp. Neurol., 283,* 248-268.

Andrew, D. and Craig, AD. (2001). Spinothalamic lamina I neurons selectively sensitive to histamine: a central neural pathway for itch. *Nature*, *4*(1), 72–77.

Avery, JA., Gotts, SJ., Kerr, KL., Burrows, K., Ingeholm, JE., Bodurka, J., … Kyle Simmons, W. (2017). Convergent gustatory and viscerosensory processing in the human dorsal mid-insula. *Human Brain Mapping*, *38*(4), 2150–2164. https://doi.org/10.1002/hbm.23510

Avery, JA., Kerr, KL., Ingeholm, JE., Burrows, K., Bodurka, J., & Simmons, WK. (2015). A common gustatory and interoceptive representation in the human mid-insula. *Hum Brain Mapping*, *36*(8), 2996–3006. https://doi.org/10.1002/hbm.22823

Barrett, L. F., & Simmons, W. K. (2015). Interoceptive predictions in the brain. *Nature Reviews Neuroscience*, *16*(7), 419–429. https://doi.org/10.1038/nrn3950

Bartels, A., & Zeki, S. (2004). The neural correlates of maternal and romantic love. *NeuroImage*, *21*(3), 1155–1166. https://doi.org/10.1016/j.neuroimage.2003.11.003

Bauernfeind, AL., de Sousa, AA., Avasthi, T., Dobson, SD., Raghanti, MA., Lewandowski, AH., … Sherwood, CC. (2013). A volumetric comparison of the insular cortex and its subregions in primates. *J Hum Evol*, *64*(4), 263–279. https://doi.org/10.1016/j.jhevol.2012.12.003

Beckstead, RM., Morse, JR., & Norgren, R. (1980). The nucleus of the solitary tract in the monkey: projections to the thalamus and brain stem nuclei. *The Journal of Comparative Neurology*, *190*(2b), 259–282. https://doi.org/10.1002/cne.901900205

Bender, G., Veldhuizen, M. G., Meltzer, JA., Gitelman, D. R., & Small, DM. (2009). Neural correlates of evaluative compared with passive tasting. *Eur J Neurosci*, *30*(2), 327–338. https://doi.org/10.1111/j.1460-9568.2009.06819.x

Bereiter, DA., Hirata, H., & Hu, JW. (2000). Trigeminal subnucleus caudalis: beyond homologies with the spinal dorsal horn. *Pain*, *88*(3), 221–224. https://doi.org/10.1016/S0304-3959(00)00434-6

Bonaz, B., Bazin, T., & Pellissier, S. (2018). The Vagus Nerve at the Interface of the Microbiota-Gut-Brain Axis. *Frontiers in Neuroscience*, *12*(49), 1–9. https://doi.org/10.3389/fnins.2018.00049

Brandt, T., & Dieterich, M. (1999). The Vestibular Cortex: Its Locations, Functions, and Disorders. *Annals of the New York Academy of Sciences*, *871,* 293–312. https://doi.org/10.1111/j.1749-6632.1999.tb09193.x

Brooks, JCW, Zambreanu, L., Godinez, A., Craig, AD., & Tracey, I. (2005). Somatotopic organisation of the human insula to painful heat studied with high resolution functional imaging. *NeuroImage*, *27*(1), 201–209.

https://doi.org/10.1016/j.neuroimage.2005.03.041

Brooks, Jonathan CW, Nurmikko, TJ., Bimson, WE., Singh, KD., & Roberts, N. (2002). fMRI of Thermal Pain: Effects of Stimulus Laterality and Attention. *NeuroImage, 15,* 293-301. https://doi.org/10.1006/nimg.2001.0974

Burton, H., & Jones, EG. (1976). The posterior thalamic region and its cortical projection in New World and Old World monkeys. *Journal of Comparative Neurology*, *168*(2), 249–301. https://doi.org/10.1002/cne.901680204

Cannon, WB. (1929). Organization for Physiological Homeostasis. *Physiological Reviews*, *9*(3), 399–431.

Cannon, WB. (1931). Again the James-Lange and the thalamic theories of emotion. *Psychological Review*, *38*(4), 281–295. https://doi.org/10.1037/h0072957

Carleton A, Accolla R, Simon, S. (2010). Coding in the mammalian gustatory system. *Trends Neurosci*, *33*(7), 326–334. https://doi.org/10.1016/j.tins.2010.04.002

Carmichael, ST., & Price, JL. (1995). Limbic connections of the orbital and medial prefrontal cortex in macaque monkeys. *J.Comp Neurol.*, *363*(4), 615–641. https://doi.org/10.1002/cne.903630408

Chavez, G., Saleh, TS., Horn FM., Evrard HC. (2018) Von Economo and Fork neuron projections to preautonomic nuclei in the macaque monkey. Poster, CIN-NIPS Symposium, 4-5 October.

Craig, AD. (2015). *How do you feel?* Princeton University Pres.

Craig, AD. (2014). Topographically Organized Projection to Posterior Insular Cortex from the Posterior Portion of the Ventral Medial Nucleus (VMpo) in the Long-tailed Macaque Monkey. *J Comp Neurol*, *522*(1), 36–63. https://doi.org/10.1016/j.pestbp.2011.02.012.Investigations

Craig, AD. (2009). How do you feel—now? The anterior insula and human awareness. *Nat Rev Neurosci*, *10*(1), 59–70. https://doi.org/10.1038/nrn2555

Craig, AD. (2004). Lamina I, but not Lamina V, Spinothalamic Neurons Exhibit Responses That Correspond With Burning Pain. *J Neurophysiol*, *92*. https://doi.org/10.1152/jn.00385.2004

Craig, AD. (2002). How do you feel? Interoception: the sense of the physiological condition of the body. *Nature Reviews Neuroscience*, *3*(August), 655–666. https://doi.org/10.1038/nrn894

Craig, AD., Bushnell, MC., Zhang, ET., & Blomqvist, A. (1994). A thalamic nucleus specific for pain and temperature sensation. *Nature*, *372*(6508), 770–773. https://doi.org/10.1038/372770a0

Critchley, H., & Seth, A. (2012). Will Studies of Macaque Insula Reveal the Neural Mechanisms of Self-Awareness? *Neuron*, *74*(3), 423–426. https://doi.org/10.1016/j.neuron.2012.04.012

Critchley, HD., Wiens, S., Rotshtein, P., Ohman, A., Dolan, R. J., Öhman, A., … Dolan, R. J. (2004). Neural systems supporting interoceptive awareness. *Nat Neurosci*, *7*(2), 189–195. https://doi.org/10.1038/nn1176

Dalai Lama, X. (2000). *The Meaning of Life: Buddhist Perspectives on Cause and Effect.* Oxford University Press.

Dalai Lama, X. (2005). *The universe in a single atom : the convergence of science and spirituality*. Morgan Road Books.

Damasio, A., & Carvalho, GB. (2013). The nature of feelings: evolutionary and neurobiological origins. *Nature Reviews. Neuroscience*, *14*(2), 143–152. https://doi.org/10.1038/nrn3403

De Araujo, IE., Geha, P., & Small, DM. (2012). Orosensory and homeostatic functions of the insular taste cortex. *Chemosensory Perception*, *5*(1), 64–79. https://doi.org/10.1007/s12078-012-9117-9

Elston, GN., Benavides-Piccione, R., Elston, A., Zietsch, B., Defelipe, J., Manger, P., … Kaas, J. H. (2005). Specializations of the Granular Prefrontal Cortex of Primates: Implications for Cognitive Processing. https://doi.org/10.1002/ar.a.20278

Escanilla, O. D., Victor, J. D., & Lorenzo, P. M. Di. (2015). Odor-Taste Convergence in the Nucleus of the Solitary Tract of the Awake Freely Licking Rat. https://doi.org/10.1523/JNEUROSCI.3526-14.2015

Evrard, HC. (2018). Von Economo and fork neurons in the monkey insula, implications for evolution of cognition. *Current Opinion in Behavioral Sciences*, *21*, 182–190. https://doi.org/10.1016/j.cobeha.2018.05.006

Evrard, HC., Logothetis, NK., & Craig, AD. (2014). Modular architectonic organization of the insula in the macaque monkey. *Journal of Comparative Neurology*, *522*(1), 64–97. https://doi.org/10.1002/cne.23436

Evrard, HC, Forro, T., Logothetis, NK. (2012). Von Economo Neurons in the Anterior Insula of the Macaque Monkey. *Neuron*, *74*(3), 482–489. https://doi.org/10.1007/s00429-010-0265-x

Farb, NAS., Segal, ZV., & Anderson, AK. (2013). Attentional modulation of primary interoceptive and exteroceptive cortices. *Cerebral Cortex*, *23*(1), 114–126. https://doi.org/10.1093/cercor/bhr385

Fukushima, H., Tanaka, Y., & Myowa, M. (2018). Temporal Matching between Interoception and Exteroception: Electrophysiological Responses in a Heartbeat Discrimination Task. *Journal of Psychophysiology*, (June). https://doi.org/10.1027/0269-8803/a000224

Gabi, M., Neves, K., Masseron, C., Ribeiro, PFM., Ventura-Antunes, L., Torres, L., … Buckner, R. L. (2016). No relative expansion of the number of prefrontal neurons in primate and human evolution. *PNAS*, *113*(34), 9617–9622. https://doi.org/10.1073/pnas.1610178113

Galizia, CG., & Lledo, P. (2013). *Neurosciences*. Springer.

Garfinkel, SN., & Critchley, HD. (2013). Interoception, emotion and brain: new insights link internal physiology to social behaviour. Commentary on:: "Anterior insular cortex mediates bodily sensibility and social anxiety" by Terasawa et al. (2012). *Social Cognitive and Affective Neuroscience*, *8*(3), 231–234. https://doi.org/10.1093/scan/nss140

Goense, J., Merkle, H., & Logothetis, NK. (2012). High-Resolution fMRI Reveals Laminar Differences in Neurovascular Coupling between Positive and Negative BOLD Responses. *Neuron*, *76*(3), 629–639. https://doi.org/10.1016/j.neuron.2012.09.019

Gu, X., Gao, Z., Wang, X., Liu, X., Knight, RT., Hof, PR., & Fan, J. (2012). Anterior insular cortex is necessary for empathetic pain perception. *Brain*, *135*(9), 2726–2735. https://doi.org/10.1093/brain/aws199

Halsell, CB., Travers, JB., Travers, SP. (1993). Gustatory and tactile stimulation of the posterior tongue activate overlapping but distinctive regions within the nucleus of the solitary tract. *Brain Research, 632*(1-2), 161-173.

Han, ZS., Zhang, ET., & Craig, AD. (1998). Nociceptive and thermoreceptive lamina I neurons are anatomically distinct. *Nature Neuroscience*, *1*(3), 218–225. https://doi.org/10.1038/665

Harrison, NA., Gray, MA., Gianaros, PJ., & Critchley, HD. (2010). The embodiment of emotional feelings in the brain. *The Journal of Neuroscience, 30*(38), 12878–12884. https://doi.org/10.1523/JNEUROSCI.1725-10.2010

Haupt, P., Jänig, W., & Kohler, W. (1983). Response pattern of visceral afferent fibres, supplying the colon, upon chemical and mechanical stimuli. *Pflügers Archiv European Journal of Physiology*, *398*(1), 41–47. https://doi.org/10.1007/BF00584711

Hennenlotter, A., Schroeder, U., Erhard, P., Castrop, F., Haslinger, B., Stoecker, D., … Ceballos-Baumann, A. O.

(2005). A common neural basis for receptive and expressive communication of pleasant facial affect. *NeuroImage*, *26*(2), 581–591. https://doi.org/10.1016/J.NEUROIMAGE.2005.01.057

Hu, X., Le, TH., & Ugurbil, K. (1997). Evaluation of the early response in fMRI in individual subjects using short stimulus duration. *Magnetic Resonance in Medicine*, *37*(6), 877–884.

Hua lH., Strigo, IA., Baxter, LC., Johnson, SC., & Craig, AD. (2005). Anteroposterior somatotopy of innocuous cooling activation focus in human dorsal posterior insular cortex. *Am J Physiol Regul Integr Comp Physiol*, *289*(2), R319–R325. https://doi.org/10.1152/ajpregu.00123.2005

James, W. (1884). What is an emotion? *Mind*, *9*(34), 188–205.

Johnstone, T., van Reekum, CM., Oakes, TR., & Davidson, RJ. (2006). The voice of emotion: an FMRI study of neural responses to angry and happy vocal expressions. *Social Cognitive and Affective Neuroscience*, *1*(3), 242–249. https://doi.org/10.1093/scan/nsl027

Kim, EJ., Sidhu, M., Gaus, SE., Huang, EJ., Hof, PR., Miller, BL., … Seeley, WW. (2012). Selective frontoinsular von economo neuron and fork cell loss in early behavioral variant frontotemporal dementia. *Cerebral Cortex*, *22*(2), 251–259. https://doi.org/10.1093/cercor/bhr004

Koelsch, S., Fritz, T., Yves Cramon, D., Mü ller, K., & Friederici, AD. (2006). Investigating Emotion With Music: An fMRI Study. *Hum Brain Mapp*, *27*, 239–250. https://doi.org/10.1002/hbm.20180

Kurth, F., Zilles, K., Fox, P. T., Laird, AR., & Eickhoff, SB. (2010). A link between the systems: functional differentiation and integration within the human insula revealed by meta-analysis. *Brain Structure and Function*, 1–16. https://doi.org/10.1007/s00429-010-0255-z

Lee, SP., Silva, AC., Ugurbil, K., & Kim, SG. (1999). Diffusion-Weighted Spin-Echo fMRI at 9.4 T: Microvascular/Tissue Contribution to BOLD Signal Changes. *Magnetic Resonance in Medicine, 42*(5), 919-928.

Lemon, C. H., Kang, Y., & Li, J. (2016). Separate functions for responses to oral temperature in thermo-gustatory and trigeminal neurons. *Chemical Senses*, *41*(5), 457–471. https://doi.org/10.1093/chemse/bjw022

Logothetis, NK., & Wandell, BA. (2004). Interpreting the BOLD signal. *Annu Rev Physiol*, *66*, 735–769. https://doi.org/10.1146/annurev.physiol.66.082602.092845

Logothetis, NK., Pauls, J., Augath, M., Trinath, T., & Oeltermann, A. (2001). Neurophysiological Investigation of the Basis of the fMRI Signal. *Nature*, *412*, 150–157.

Marciani, L., Pfeiffer, J. C., Hort, J., Head, K., Bush, D., Taylor, AJ., … Gowland, PA. (2006). Improved methods for fMRI studies of combined taste and aroma stimuli. *Journal of Neuroscience Methods*, *158*(2), 186–194. https://doi.org/10.1016/J.JNEUMETH.2006.05.035

Mayer, EA. (2011). Gut feelings: the emerging biology of gut-brain communication. *Nature Reviews Neuroscience*, *12*(8), 453–466. https://doi.org/10.1038/nrn3071

Morcos, AS., & Harvey, CD. (2016). History-dependent variability in population dynamics during evidence accumulation in cortex. *Nature Neuroscience*, *19*(12), 1672–1681. https://doi.org/10.1038/nn.4403

Mueller, KL., Hoon, MA., Erlenbach, I., Chandrashekar, J., Zuker, CS., & Ryba, NJP. (2005). The receptors and coding logic for bitter taste. *Nature*, *434*(7030), 225–229. https://doi.org/10.1038/nature03352

Mutschler, I., Wieckhorst, B., Kowalevski, S., Derix, J., Wentlandt, J., Schulze-Bonhage, A., & Ball, T. (2009). Functional organization of the human anterior insular cortex. *Neuroscience Letters*, *457*(2), 66–70. https://doi.org/10.1016/j.neulet.2009.03.101

Nagai, M., Kishi, K., & Kato, S. (2007). Insular cortex and neuropsychiatric disorders: A review of recent literature. *European Psychiatry*, *22*(6), 387–394. https://doi.org/10.1016/j.eurpsy.2007.02.006

Ogawa, S., Lee, TM., Kay, AR., & Tank, DW. (1990). Brain magnetic resonance imaging with contrast dependent on blood oxygenation. *Proc. NatI. Acad. Sci. USA, 87*(24) 9868-9872.

Ozaki, N., & Gebhart, GF. (2001). Characterization of mechanosensitive splanchnic nerve afferent fibers innervating the rat stomach. *Am J Physiol Gastrointest Liver Physiol*, *281*(6), G1449-59. https://doi.org/10.1152/ajpgi.2001.281.6.G1449

Paton, JFR., Li, YW., Kasparov, S. (1999). Reflex response and convergence of pharyngoesophageal and peripheral chemoreceptors in the nucleus of the solitary tract. *Neuroscience, 93*(1), 143-154.

Penfield, W., & Boldrey, E. (1937). Somatic Motor and Sensory Representation in Man. *Brain: A Journal of Neurology*, *60,* 389–443. https://doi.org/10.1093/brain/60.4.389

Poppa, T., & Bechara, A. (2018). The somatic marker hypothesis: revisiting the role of the 'body-loop' in decision-making. *Current Opinion in Behavioral Sciences*, *19*, 61–66. https://doi.org/10.1016/j.cobeha.2017.10.007

Pritchard, TC., Hamilton, RB., Morse, JR., & Norgren, R. (1986). Projections from thalamic gustatory and lingual areas in the monkey, Macaca fascicularis. *Journal of Comparative Neurology*, *244*(2), 213–228. https://doi.org/10.1002/cne.902440208

Rolls, ET. (2004). Smell, taste, texture, and temperature multimodal representations in the brain, and their relevance to the control of appetite. *Nutr Rev*, *62*(11 Pt 2), S193-204; discussion S224-41. https://doi.org/10.1111/j.1753-4887.2004.tb00099.x

Schölvinck, ML., Maier, A., Ye, F. Q., Duyn, JH., & Leopold, DA. (2010). Neural basis of global resting-state fMRI activity. *Proc. Natl. Acad. Sci. U.S.A., 107*(22), 10238-43. https://doi.org/10.1073/pnas.0913110107

Segerdahl, AR., Mezue, M., Okell, TW., Farrar, JT., & Tracey, I. (2015). The dorsal posterior insula subserves a fundamental role in human pain. *Nature Neuroscience*, *18*(4), 499–500. https://doi.org/10.1038/nn.3969

Sellers, KK., Bennett, DV., Hutt, A., & Fröhlich, F. (2013). Anesthesia differentially modulates spontaneous network dynamics by cortical area and layer. *Journal of Neurophysiology*, *110*(12), 2739–2751. https://doi.org/10.1152/jn.00404.2013

Seth, AK., Suzuki, K., & Critchley, HD. (2012). An Interoceptive Predictive Coding Model of Conscious Presence. *Frontiers in Psychology*, *2*, 395. https://doi.org/10.3389/fpsyg.2011.00395

Sharvit, G., Vuilleumier, P., & Acqua, CC. (2019). Sensory-specific predictive models in the human anterior insula. *F1000Research*, (February). https://doi.org/10.12688/f1000research.17961.1

Shulman, RG., & Rothman, DL. (2019). A Non-cognitive Behavioral Model for Interpreting Functional Neuroimaging Studies. *Frontiers in Human Neuroscience*, *13*, 28. https://doi.org/10.3389/fnhum.2019.00028

Small, DM. (2010). Taste representation in the human insula. *Brain Struct Funct*, *214*(5–6), 551–561. https://doi.org/10.1007/s00429-010-0266-9

Stephan, KE., Lae, W., Manjaly, ZM., Mathys, CD., E Weber, LA., Paliwal, S., … Petzschner, FH. (2016). Allostatic Self-efficacy: A Metacognitive Theory of Dyshomeostasis-Induced Fatigue and Depression. *Frontiers in Human Neuroscience | Www.Frontiersin.Org*, *10*, 550. https://doi.org/10.3389/fnhum.2016.00550

Sudakov, K., MacLean, PD., Reeves, A., Marino R. (1971). Unit Study of Exteroceptive Inputs to Claustrocortex

in Awake, Sitting, Squirrel Monkey. *Brain Research*, *28*, 19–34.

Sugiura, Y., Terui, N., & Hosoya, Y. (1989). Difference in distribution of central terminals between visceral and somatic unmyelinated (C) primary afferent fibers. *Journal of Neurophysiology*, *62*(4), 834–840. https://doi.org/10.1016/S0163-7258(03)00060-3

Suzuki, K., Garfinkel, SN., Critchley, HD., & Seth, AK. (2013). Multisensory integration across exteroceptive and interoceptive domains modulates self-experience in the rubber-hand illusion. *Neuropsychologia*, *51*(13), 2909–2917. https://doi.org/10.1016/j.neuropsychologia.2013.08.014

Touroutoglou, A., Hollenbeck, M., Dickerson, BC., Feldman Barret, L. (2012). Dissociable large-scale networks anchored in the right anterior insula subserve affective experience and attention. *Neuroimage*, *60*(4), 1947–1958. https://doi.org/10.1016/j.pestbp.2011.02.012.Investigations

Travagli, RA., Hermann, GE., Browning, KN., Rogers, RC. (2006). Brainstem circuits regulating gastric function. *Ann. Rev. Physiol. 68,* 279-305.

Tsakiris, M. & De Preester, H. (2018). *The Interoceptive Mind: from Homeostasis to Awareness*. Oxford University Press.

Uddin, LQ. (2015). Salience processing and insular cortical function and dysfunction. *Nature Reviews Neuroscience, 16,* 55-61. https://doi.org/10.1038/nrn3857

von Economo, C. (2009). *Cellular structure of the human cerebral cortex*. (K. Translated by L.C. Triarhou, Ed.). Basel.

von Economo C. (1925). *Die Cytoarchitectonik der Hirnrinde des erwachsenen Menschen*. Springer.

Wager, TD., & Feldman Barrett, L. (2017). From affect to control: Functional specialization of the insula in motivation and regulation. *BioRxiv*, 102368. https://doi.org/10.1101/102368

Wiech, K., Lin, C.-S., Brodersen, KH., Bingel, U., Ploner, M., & Tracey, I. (2010). Behavioral/Systems/Cognitive Anterior Insula Integrates Information about Salience into Perceptual Decisions about Pain. https://doi.org/10.1523/JNEUROSCI.2087-10.2010

Wylie, KP., & Tregellas, JR. (2010). The role of the insula in schizophrenia. *Schizophrenia Research*, *123*(2–3), 93–104. https://doi.org/10.1016/j.schres.2010.08.027

Yasui, Y., Breder, CD., Saper, CB., & Cechetto, DF. (1991). Autonomic Responses and Efferent Pathways from the Insular Cortex in the Rat. *Journal of Comparative Neurology*, *303*, 355–374. https://doi.org/10.1002/cne.903030303

Zhao, GQ., Zhang, Y., Hoon, MA., Chandrashekar, J., Erlenbach, I., Ryba, NP., & Zuker, CS. (2003). The Receptors for Mammalian Sweet and Umami Taste. *Cell*, *115*(3), 255–266. http://doi.org/10.1016/S0092-8674(03)00844-4

DECLARATION OF CONTRIBUTIONS

Hartig, R.[1,2,3], Murayama, Y.[3], Evrard, HC[1,3]. (2019). Normalizing Group-Level Primate Neuroimaging Results. Manuscript.

[1] Functional and Comparative Neuroanatomy Laboratory, Werner Reichardt Center for Integrative Neuroscience, Tübingen, Germany, [2] IMPRS for Cognitive and Systems Neuroscience, Tübingen, Germany, [3] Department of Physiology of Cognitive Processes, Max Planck Institute for Biological Cybernetics, Tübingen, Germany

Author contributions: Developed, performed analyses, wrote and edited manuscript: RH; Developed code and programming: YM; Initiated, reviewed and drew anatomical parcellations, contributed to and edited manuscript: HCE.

Hartig, R.[1,2,3], Balla, D.[3], Logothetis, NK.[3], Evrard, HC.[1,3] (2019). The Non-Human Primate Cortical Taste Representation. Manuscript.

[1] Functional and Comparative Neuroanatomy Laboratory, Werner Reichardt Center for Integrative Neuroscience, Tübingen, Germany, [2] IMPRS for Cognitive and Systems Neuroscience, Tübingen, Germany, [3] Department of Physiology of Cognitive Processes, Max Planck Institute for Biological Cybernetics, Tübingen, Germany

Author contributions: Conceived, initiated, developed and performed experiments: RH; Developed image acquisition sequences and performed signal quality assessment: DB; Performed analyses: RH; Wrote and edited manuscript: RH; Conceived and supervised the study, reviewed and edited manuscript: HCE; Reviewed manuscript and provided material support: NLK.

Hartig, R.[1,2,3], Karimi, A.[4], Steudel, T.[3], Logothetis, NK.[3], Evrard, HC[1,3]. (2019). BOLD Correlates of Rectal Distention in the Anesthetized Macaque. Manuscript.

[1] Functional and Comparative Neuroanatomy Laboratory, Werner Reichardt Center for Integrative Neuroscience, Tübingen, Germany, [2] IMPRS for Cognitive and Systems Neuroscience, Tübingen, Germany, [3] Department of Physiology of Cognitive Processes, Max Planck Institute for Biological Cybernetics, Tübingen, Germany, [4] Department of Connectomics, Max Planck Institute for Brain Research, Frankfurt, Germany

Author contributions: Conceived, initiated & supervised the study: HCE; Conceived, developed and performed experiments: RH; Technical and imaging assistance: TS; Performed analyses: RH and AK; Wrote and edited manuscript: RH; Reviewed and edited manuscript: HCE; Reviewed manuscript and provided material support: NLK.

Hartig, R.[1,2,3], Vedoveli, A.[3], Werner, J.[3], Oeltermann, A.[3], Krampe, E.[3], Logothetis, NK.[3], Evrard, HC[1,3]. (2019). The Insular Cortex's Interotopic Map. Manuscript.

[1] Functional and Comparative Neuroanatomy Laboratory, Werner Reichardt Center for Integrative Neuroscience, Tübingen, Germany, [2] IMPRS for Cognitive and Systems Neuroscience, Tübingen, Germany, [3] Department of Physiology of Cognitive Processes, Max Planck Institute for Biological Cybernetics, Tübingen, Germany

Author contributions: Conceived, initiated, developed & performed experiments: RH and HCE; Provided theoretical input, technical and mechanical assistance: JW, AO and EK. Performed analyses: RH and AV; Wrote and edited manuscript: RH, AV and HCE; Reviewed manuscript and provided material support: NLK.

Parts of this thesis work were presented at the following external seminars & conferences:

External talks by the candidate:

Mapping Gustatory & Interceptive Responses in the Primate Brain. Interoception vs. Exteroception Symposium. 41st Annual AChemS Meeting. Bonita Springs, Florida, U.S.A. 17. April 2018.

Sensory Input: from the Body to the Insular Cortex. 19th Annual Conference of Junior Neuroscientists of Tübingen. Schramberg, Germany. 26. September 2018.

Gustation, Interoception and the Insular Cortex. Cornell University, School of Medicine. New York, New York, U.S.A. 20. April 2018.

fMRI Measurement During Transcutaneous Vagus Nerve Stimulation in Primates. Psychiatry & Psychotherapy Department Colloquium. Tübingen, Germany. 17. January 2018.

Neuroanatomical and Functional Localization of Sensory Taste Processing in Primates. 19th Annual Conference of Junior Neuroscientists of Tübingen. Schramberg, Germany. 25. October 2016.

Conference poster presentations:

fMRI and Electrophysiological Mapping of Sensory Afferent Activity in the Macaque Insular Cortex. Society for Neuroscience Conference. San Diego, CA, U.S.A. 3. November 2018.

Localizing Interoceptive Responses via fMRI and Electrophysiology in the Anesthetized Macaque. Federation of European Neuroscience Societies (FENS). Berlin, Germany. 8. July. 2018.

The Insula and Bodily Processing: An examination of Gustation and Rectal Distention in the Anesthetized Macaque. 40th Annual AChemS Meeting. Bonita Springs, Florida, U.S.A. 19. April 2018.

Functional Mapping of Insular Cortex Activity Using Gustatory and Interoceptive Stimuli. Primate Neurobiology Meeting. Tübingen, Germany. 13. March. 2018.

Functional Mapping of Insular Cortex Activity Using Gustatory and Interoceptive Stimuli. Society for Neuroscience Conference. Washington D.C., U.S.A. 14. November. 2017.

Measurement of Transcutaneous Vagus Nerve Stimulation in the Anesthetized Macaque by Ultra-High Field fMRI. 18th Annual Conference of Junior Neuroscientists of Tübingen. Schramberg, Germany. 17. October. 2017.

Topographic Mapping of the Primate Primary Interoceptive Cortex. Belgian Society for Neuroscience. Ghent, Belgium. 22. May 2017.

Taste Processing in the Primate Brain. The 6th Joint CIN (Tübingen, Germany) – NIPS (National Institute for Physiological Sciences, Japan) Symposium. Tübingen, Germany. 11. October 2016.

1. NORMALIZING PRIMATE NEUROIMAGING RESULTS

ABSTRACT

It is standard practice in human research to normalize neuroimaging data. Typically, this normalization is done between an individual's native brain structure and that of a template (e.g. MNI template). However, this standard practice is not as streamlined for neuroimaging data of other species (e.g. non-human primates, or NHPs). While structural templates exist for NHPs, which include atlases of parcellated anatomical regions, the analysis software used to normalize these data are, at times, insufficient. In recent years, one atlas produced by Saleem & Logothetis was digitized by Reveley and colleagues at the National Institute of Health (NIH). There, researchers morphed a high-resolution ex-vivo brain scan to the original anatomical scan of D99, the animal used to create the Saleem & Logothetis atlas of the macaque monkey cerebral cortex. From this higher-resolution quality, the atlas' structural components could be overlaid onto an isotropic voxel resolution of 250 μm^3. The current work has tested the applicability of open-source code provided by NIH to perform normalizations using AFNI, a Linux-based neuroimaging analysis software, and outlines requisite code to stream-line the normalization process using additional Matlab-based programming functions to construct a reliable operating procedure for non-human primate normalization with accuracy as high as 1 mm^3 for unsmoothed functional images. The process was tested with normalization to the D99 template. In addition, while the current NHP atlases cover mainly the cerebral cortex, we used here both the Saleem & Logothetis atlas as well as an upgraded atlas including digital subcortical parcellations.

KEYWORDS

Neuroimaging, normalization, non-linear warping, non-human primates, multi-subject analysis

INTRODUCTION

Within the field of neuroscience many different animal models are available to study the basic principles of neuronal function. One such valuable model is the macaque monkey, a non-human primate (NHP), which exhibits a conserved functional neuroanatomy that largely parallels humans. NHP research is crucial to the development of knowledge about the brain as well as for developing new vaccines and treatments for pathologies afflicting humans. With that said, this precious animal model is used only when no other alternative exists and the number of NHPs used in research is limited to responsibly reduce the overall number of animals used in science.

For this reason, many studies examining neuronal properties use only a small number of animals, usually two, but sometimes a few more. Nevertheless, it is often that data, whether electrophysiology (Buckmaster & Amaral, 2001; Scott & Plata-Salamán, 1999), *in vivo* calcium imaging (Heider et al., 2010; Li et al., 2017), or functional magnetic resonance imaging (fMRI), collected with these animals are portrayed individually. Some efforts have been made with neuroimaging to normalize results in an average or standardized space (Fox et al., 2015; Mantini et al., 2012). The current work establishes a protocol and operating procedure for normalizing NHP fMRI data. From an overarching study that included 10 macaque monkeys, a pipeline was tested across cases to examine the validity and reproducibility of data standardization to a set of brain templates commonly used in NHP imaging, using corresponding atlases for either mainly the cerebral cortex (Saleem & Logothetis, 2007) or both the cerebral cortex and the subcortex (Paxinos, Petrides and Evrard, *in preparation*).

A variety of calculations were tested to optimize this pipeline. Once the optimal transformation parameters were configured, the results were applied to fMRI data. Subsequently, a univariate analysis was conducted using images coregistered to each animal's normalized anatomical scan. Data reported here were normalized to the D99 template (Saleem & Logothetis, 2007).

To validate these results, we applied the normalization procedure to functional data sets collected during the presentation of a visual stimulus known previously (Logothetis et al., 2010) to elicit robust activation of the lateral geniculate nucleus (LGN) of the thalamus. Thus, normalized functional activation maps were compared to the results in native space. The idea being that when the LGN is activated, such activation retains anatomical precision throughout the entire coregistration and normalization pipeline. Data quality checks were performed to compare the native

anatomical regions to that of the atlas. Here, we present an outline of the workflow to execute the normalization procedure. From these results one can determine the accuracy of the method used to transform fMRI data into standardized space.

MATERIALS & METHODS

Subjects

This study employed 10 rhesus macaque monkeys (*Macaca mulatta*; 6 females; average weight: 8.63 kg). Animals were treated according to the guidelines of the European Parliament and Council Directive 2010/63/EU on the protection of animals used for experimental and other scientific purposes. Our protocol was approved by the local German authorities.

Anesthesia

Before commencing an experiment, animals were pre-sedated with glycopyrrolate (Robinul, 0.01 mg/kg, i.m., anticholinergic) and ketamine (15 mg/kg, i.m., dissociative anesthetic). After transport to the experimental setup, they were anesthetized with sequential injections of fentanyl (3 µg/kg, i.v., analgesic), thiopental (5 mg/kg, i.v., hypnotic), and succinylcholine chloride (3 mg/kg, i.v., muscle relaxant). They were then intubated and ventilated (24 strokes/min) throughout the procedure, using 100% oxygen during preparation, and 21% oxygen during functional data acquisition. The anesthesia parameters had previously been optimized for imaging BOLD signal changes and recording neuronal activity (Logothetis et al., 2012). After intubation, the anesthesia was maintained using a combination of remifentanil (1-3 µg/kg/min, analgesic and anesthetic) and mivacurium chloride (5-7 mg/kg/h, muscle relaxant). The physiological state of the animal was continuously monitored using infrared pulse oximetry (Nonin Medical Inc., Plymouth, MN, USA), electrocardiography (ECG), thermometry, and sphygmomanometry. A rectal thermometer continuously measured body temperature, which was regulated using a water-heating pad to maintain a body temperature within normal physiological range (38.3 – 38.8 °C). In order to attain physiological values optimal for fMRI, body temperature was maintained within this range, and end-tidal CO_2 and oxygen saturation were kept constant at 33 mmHg and over 95%, respectively. Acidosis was prevented by the administration of lactated Ringer's solution with 2.5% glucose, infused at 10 ml/kg/h, and intravascular volume was maintained by the additional administration of colloids (hydroxyethyl starch, 20-30 ml over 1-2 minutes or 20 ml/kg/h).

Image Acquisition

Neuroimaging data were acquired using a 7 Tesla vertical Nuclear Magnetic Resonance (NMR) scanner (Bruker, Billerica, MA, U.S.A.) and Paravision (versions 5 & 6). Whole-brain functional scans were acquired with multi-shot gradient-echo echo planar imaging (GE-EPI; 1x1 mm^2 in-plane resolution; flip angle: 53°; TR/TE: 2000/19 ms; 20 axial slices) when using the quadrature coil, and with GRAPPA-accelerated parallel imaging (0.85x0.85 mm^2 in-plane resolution; flip angle: 53°; TR/TE: 1000/18 ms, 18 axial slices) when using the phased-array helmets. Slice volumes were acquired in contiguous sections. Both scan sequences had the same matrix size (128x128), field-of-view (FOV; 96x96 mm^2) and slice thickness (2 mm). During each experiment, a T2-weighted Rapid Imaging with Refocused Echoes (RARE) scan was collected to image the native structural space (FOV: 96x96 mm^2; matrix size: 256x256; 8 segments; flip angle: 8°; TR/TE: 4000-6500/25-48 msec; 40 slices). A three-dimensional anatomical scan was acquired for each subject using a T1-weighted modified driven equilibrium Fourier transform scan (MDEFT; FOV: 128x128 mm^2; matrix size: 256x256; 4 segments; flip angle: 20°; TR/TE: 15/4.5 msec; 136 slices).

Image Pre-Processing

Acquired data were converted from Bruker file format to an SPM-readable file format (.nii or .hdr/.img). Functional volumes were manually examined for ghosting and signal dropout artifacts using MRIcro (version: 1.40). Individual volumes that exhibited artifacts were extracted from the time series; runs were excluded if more than 5% of frames exhibited artifacts. The resulting functional data were realigned using SPM12 (Statistical Parametric Mapping; Wellcome Department of Imaging Neuroscience, London, UK) to obtain 6 rigid-body transformation parameters, and then coregistered to each subject's native anatomical (RARE) scan. Data were smoothed using a 2 mm FWHM Gaussian kernel. A visual examination of the coregistration was done before modeling functional images in native space.

Image Normalization

To normalize an individual's MDEFT to a high-resolution digital surrogate of the D99 atlas (Saleem & Logothetis, 2007), we used AFNI (Cox, 1996), a Linux-based software, in combination with open-source scripts developed by Reveley et al. (2016). Their script calls upon standard AFNI functions: @Align_Centers, @3DAllineate (linear transformation), and @auto_warp (nonlinear transformation), which we applied for data normalization. In an attempt to optimize the result of

normalized T2-weighted images, we modified the *lpa* and *gridlist* parameters (see Parameter Definition Box for details). The results were visually examined, and upon failing to meet the criteria of anatomical alignment to the D99 template, we implemented additional steps to complete the normalization process.

We resliced and applied an affine transformation to align each individual's RARE scan to the normalized MDEFT image in template space and applied the resulting transformation matrix to all functional scans (already coregistered to the native RARE) using SPM12 (Wellcome Trust Centre, London, UK). The RARE scan was then warped using an in-house MATLAB (Version 2017b, MathWorks, U.S.A.) function for nonlinear transformations. The resulting deformation matrix was applied to the functional images. The EPIs were smoothed using a 2 mm FWHM Gaussian kernel. At each step, the spatial alignment was checked by direct visual examination. An analysis of the resulting spatial disparity between functional images and template revealed a +/- 2 mm spatial arrangement difference. Figure 1 portrays a schematic of the normalization pipeline.

Functional Paradigm

We presented a 2.5 Hz rotating checkerboard visual stimulus during a 10 minute EPI scan, whereby 300 volumes (600 for helmet-acquired data) were collected. The flicker stimulus was presented for 4 sec preceded by an 8 sec OFF period and followed by a longer 18 sec OFF period to

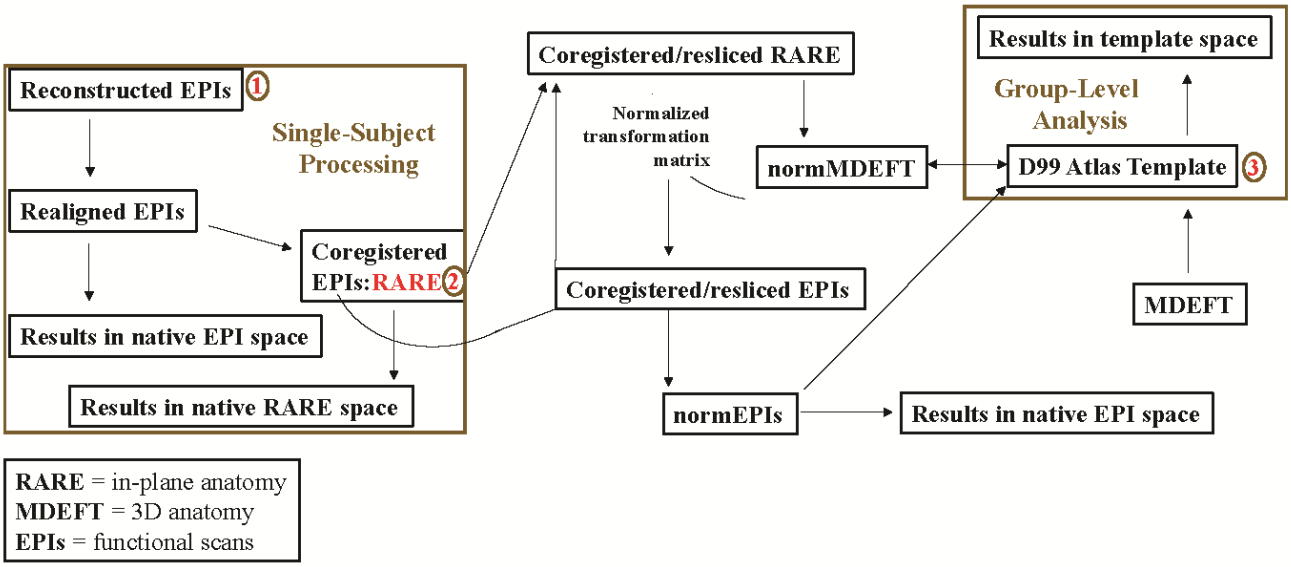

Fig. 1: Schematic outlining the coregistration to normalization pipeline.

allow the return of BOLD signal to baseline. The paradigm applied here was previously reported by Logothetis et al. (2010).

Functional Data Modeling

Functional data were analyzed using a General Linear Model (GLM). The rigid-body transformation parameters were included as regressors in the univariate model and the event-related responses correlated to the visual stimulus presentation and the baseline periods were modeled for each trial onset. The average data for each subject were compared using a T-contrast. The results reported here are at the single-subject level, with representative functional data overlaid onto the D99 template.

RESULTS

Our dataset was subjected to the normalization procedure as outlined by Reveley et al. (2016), where the high-resolution (3D) anatomical scan (MDEFT) of each individual was first normalized to the D99 template (Fig. 6a) with near perfect accuracy. However, the coregistration of the subject's 2D anatomical scan (RARE) to the subject's normalized MDEFT using the pipeline was not sufficient (Fig. 2). Therefore, a tweaking of the AFNI function for nonlinear warping (@auto_warp) was conducted in an attempt to achieve better results (Fig. 3).

The script published by Reveley et al. (2016) was altered by adjusting certain input parameters, namely the local Pearson correlation (*lpa*) and the *gridlist* (see Parameter Definition Box for a list of modifiable parameters). Figure 3 outlines the results from this code modification, and from these results, an additional route was explored to obtain a more optimal coregistration of an individual's anatomical scan (RARE) to the normalized MDEFT. The resulting transformation

Parameter Definitions:

-lpa % local Pearson correlation Ab

-gridlist % alternate specification of the patch grid sizes used in the warp optimization process

-qblur % specifies 3dQwarp blurs for base and source volumes

-qworkhard % sets the two values for finer control of 3dQwarp function

-qw_opts % save the inverse warp and do extra padding

-pblur % FWHM smoothing

-noneg % ignores negative values acquired during alignment as a result of interpolation artifacts

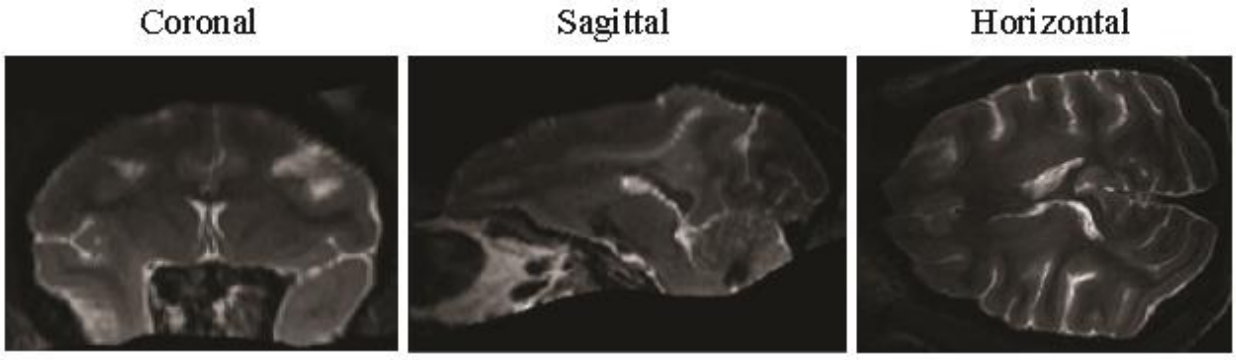

Fig. 2. The result of coregistering the subject's 2D anatomical scan to its normalized high-resolution (3D) anatomical scan using the processing pipeline of Reveley et al. (2016). Data shown for Case A09.

matrix was subsequently applied to all functional images in alignment with the individual's coregistered RARE scan.

To obtain an accurate coregistration and normalization, we developed the mreg2d_gui (Fig. 4), which uses a locally linear local-weighted mean approach to warp the RARE scan to the normalized MDEFT. Before coregistration, the RARE was linearly translated to the atlas space and the transformation was applied to all relevant functional (EPI) scans. A validation test was conducted using the functional data collected during the visual stimulus paradigm, one which has previously shown to reliably activate the lateral geniculate nucleus (LGN) by Logothetis and colleagues (2010). Figure 5 highlights our result in a representative case, whereby the functional activation was anatomically localized to the LGN.

- **Fig. 3:** To improve the results obtained from the Reveley et al. (2016) pipeline, the *gridlist* and *lpa* parameters were modified. In (b) and (c) the nonlinear warping function was modified, whereby the lpa parameter was excluded. Top panels in (a) and (c) were provided by David Balla.

Original line of code: *auto_warp.py -base $base -affine_input_xmat ID -qworkhard 0 2*

a

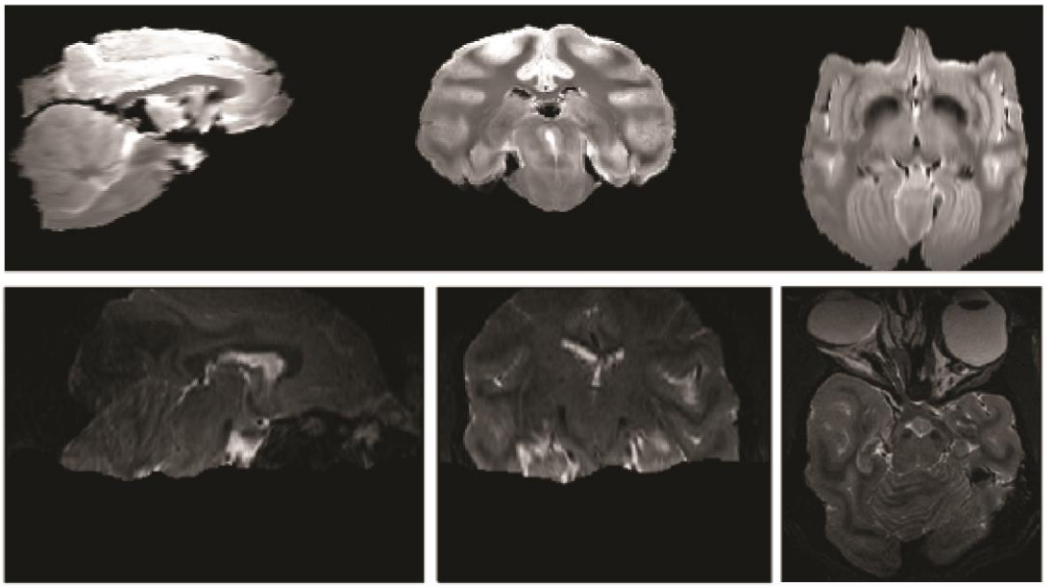

Modification 1: *auto_warp.py -base $base -affine_input_xmat ID -output_dir WARP -input $source -qblur 2 -1 -qworkhard 0 0 -qw_opts -pblur 0.05 0.05 -noneg -lpa -gridlist '1D: 0 51 11'*

b

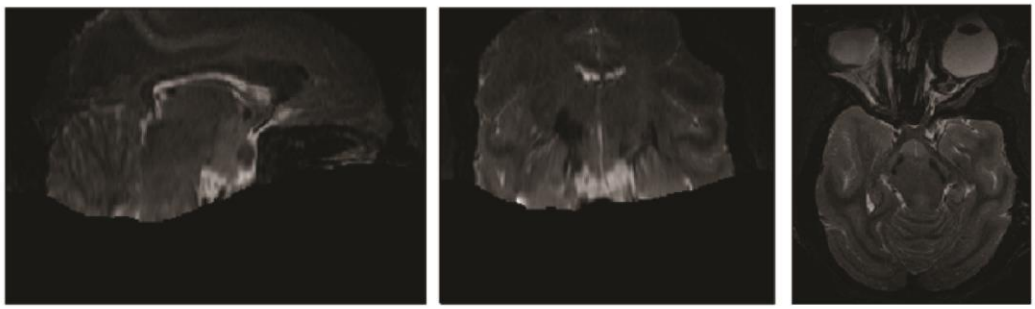

Modification 2: *auto_warp.py -base $base -affine_input_xmat ID -output_dir WARP -input $source -qblur 2 -1 -qworkhard 0 0 -qw_opts -pblur 0.05 0.05 -noneg -gridlist '1D: 0 51 11'*

c

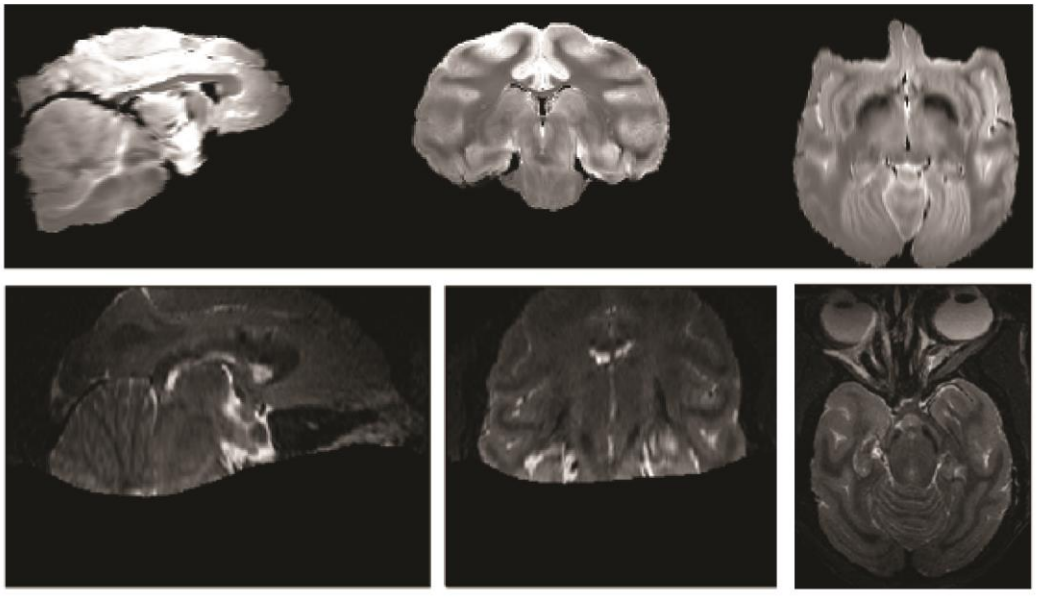

Modification 3: *auto_warp.py -base $base -affine_input_xmat ID -output_dir WARP -input $source -qblur 2 -1 -qworkhard 0 0 -qw_opts -pblur 0.05 0.05 -noneg -gridlist '1D: 0 51 25 15 11'*

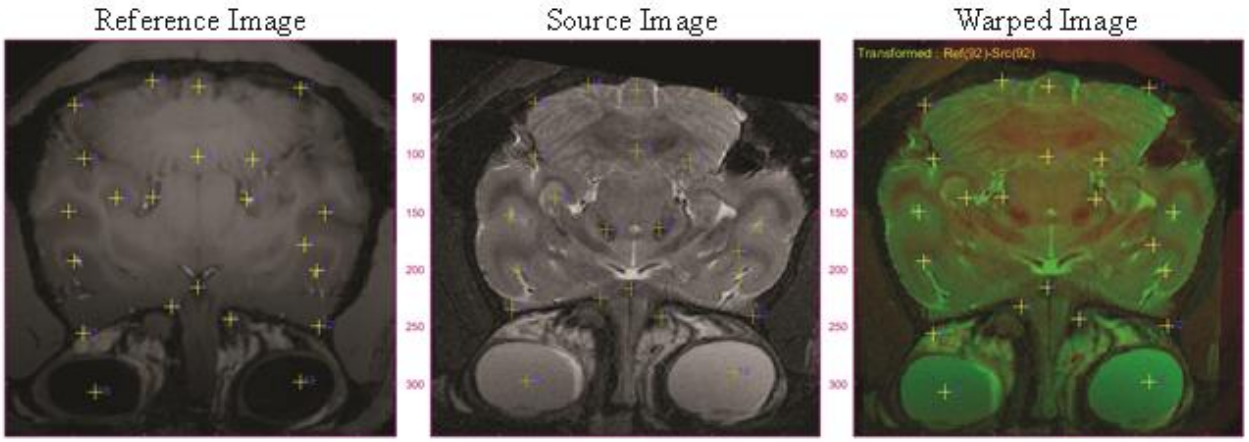

Fig. 4: The GUI interface for placing the anatomical landmarks on an individual's normalized MDEFT (Reference Image) and coregistered RARE scan (Source Image). The right panel illustrates the Warped Image as a result of placing the fiducial points. For each slice, 15-20 points were placed.

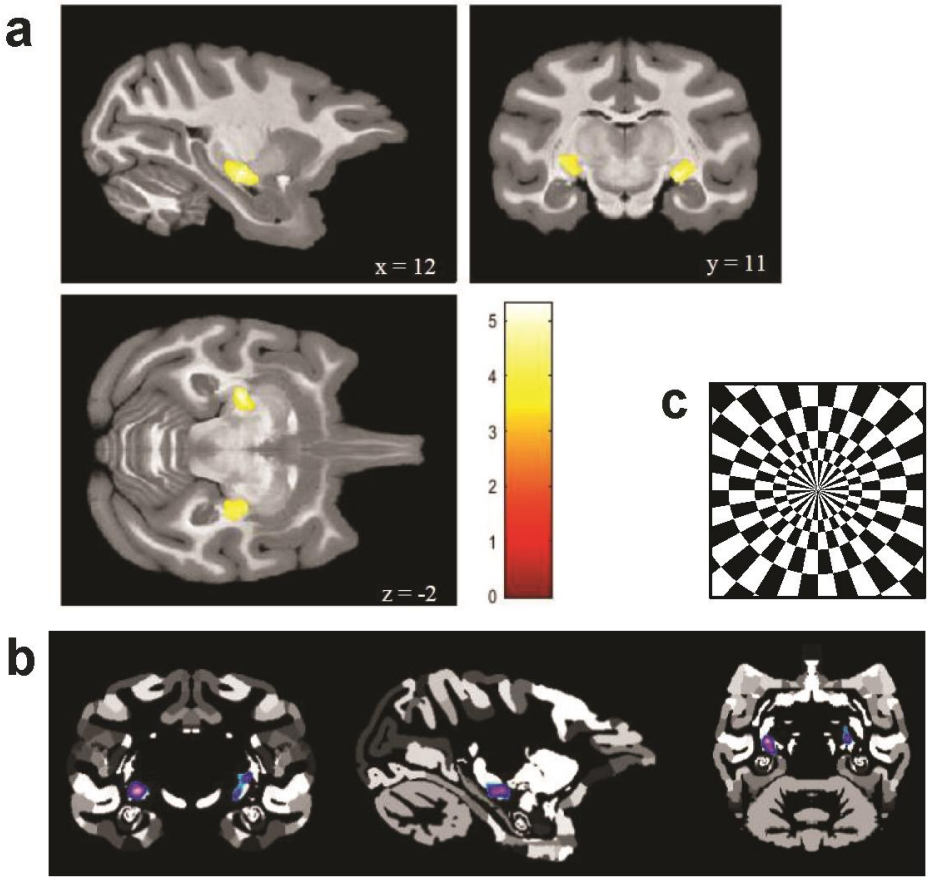

Fig. 5: Presentation of a (**c**) checkboard stimulus at 2.5 Hz flickering frequency elicited robust activation of the sensory thalamic relay nucleus, or lateral geniculate nucleus (LGN). Functional activation for one checkboard session overlaid onto the (**a**) D99 template and (**b**) corresponding atlas.

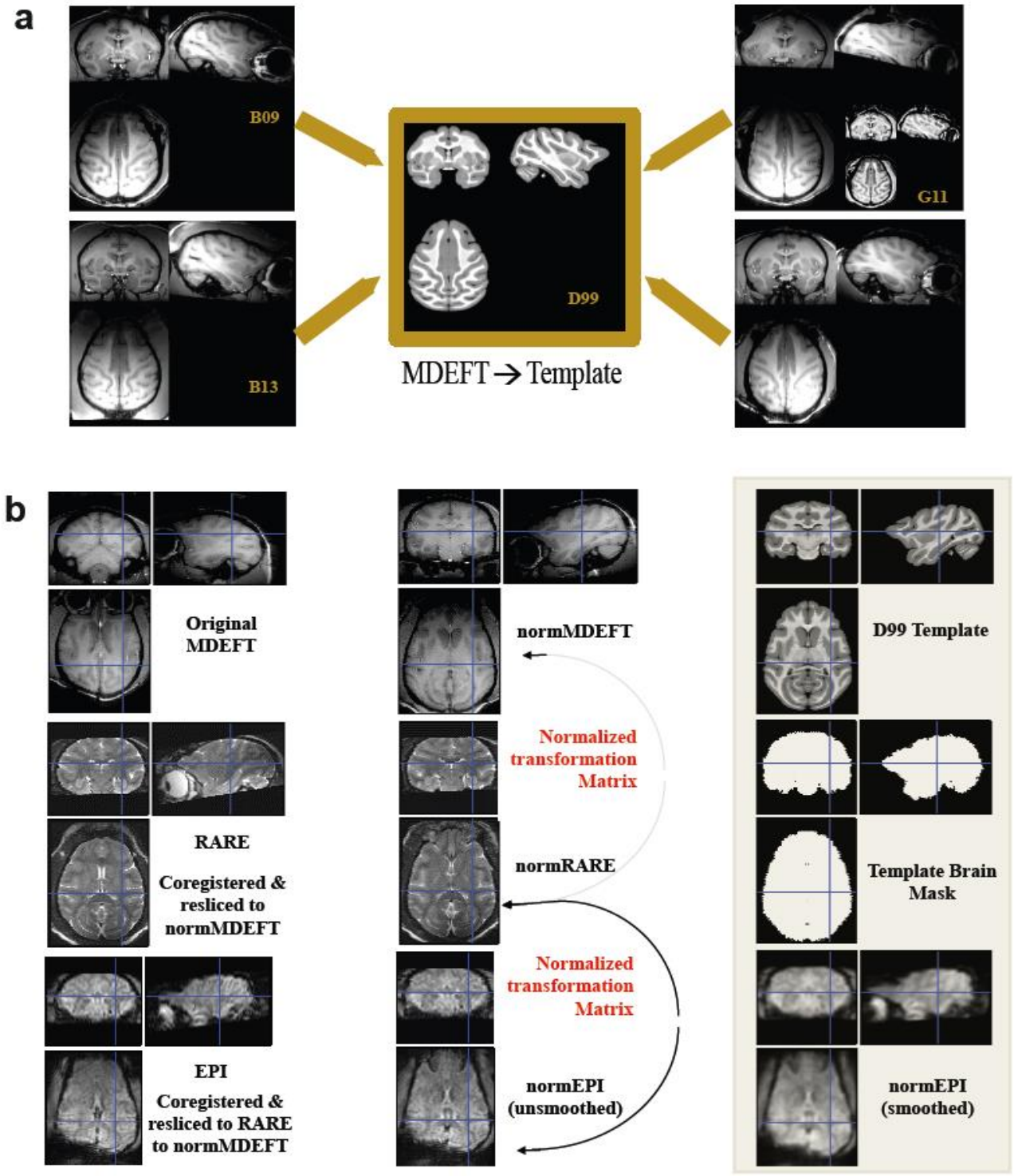

Fig 6: The normalization pipeline is a non-linear process, divided into two parts: (**a**) Part 1: the transformation from an individual MDEFT to the high-resolution D99 surrogate brain (Reveley et al., 2016); and (**b**) Part 2: the process of normalization using the deformation field, or transformation matrix, and individual's 2D anatomical (RARE) scan to normalized functional scans. Representative images are shown here from one animal.

DISCUSSION

We have executed the normalization procedure as outlined by Reveley et al., (2016) and have shown where the normalization algorithm excels and the drawbacks of some of the requisite AFNI functions. We found that the spatial coherence between the 2D and 3D anatomical scans was unsatisfactory. The specific combination of such AFNI functions did not seem to provide adequate results for 2D to 3D anatomical coregistration. This may because our 2D structural scan is T2-weighted and the algorithm cost function previously established was not optimized for T2-weighted images. As is, the Reveley et al. (2016) method does not prove useful for the entire coregistration-normalization procedure, especially when the structural image is not T1-weighted. Either the cost function must be optimized or another method should be implemented to achieve desirable results.

By combining fully and semi-automated programming functions, we show that a reliable normalization of fMRI may be obtained. The processing pipeline highlighted in this report serves to instruct and direct fellow researchers, so that they may easily apply the technique to their own data sets. With an accurate normalization of data, functional activation maps may be interpreted reliably as according to a standardized template. We normalized our data to the D99 atlas (Saleem & Logothetis, 2007); however, in theory any atlas may be used simply by exchanging the relevant image files.

The methodology employed to obtain a reliable normalization calls upon both AFNI and Matlab programming software. It is recommended to execute the normalization procedure using a Linux-based operating system, however, a Linux virtual machine will also suffice. The code for the AFNI portion was made publicly available by Reveley and colleagues (2016). The GUI for placing fiducial points and creating the transformation matrix is made available upon publication.

Our normalization procedure is applicable for any type of functional sequence applied during magnetic resonance imaging. The accuracy of the result is user-dependent, therefore, an a priori knowledge of the contrast difference between T1- and T2-weighted images will aid in delimiting the anatomical areas analogous between scans. One of the advantages of this pipeline is the manual intervention for quality assessment, so that the calculated result may be evaluated by checking the spatial coherence between multiple cortical and subcortical brains regions.

Overall, a streamlined normalization pipeline will promote the reporting of neuroimaging results in standardized space. With that accomplished, significant foci of activation can be translated

and compared across studies and research groups. Such reporting of results in common space will ultimately make way for cross-study comparisons and meta-analyses.

ACKNOWLEDGMENTS

This work was supported by the Werner Reichardt Centre for Integrative Neuroscience (CIN) at the Eberhard Karls University of Tübingen (CIN is an Excellence Cluster funded by the Deutsche Forschungsgemeinschaft [DFG] within the framework of the Excellence Initiative EXC 307) and by the Max Planck Society. We acknowledge support by the Deutsche Forschungsgemeinschaft and Open Access Publishing Fund of University of Tübingen for the cost of publication.

CONFLICT OF INTEREST STATEMENT

The author declares having no personal, professional or financial relationships that could potentially be construed as a conflict of interest.

REFERENCES

Fox, A., Oler, JA.,, Shackman, AJ., Shelton, SE., Raveendran, M., McKay, DR., Converse, AK., Alexander, A., Davidson, RJ., Blangero, J., Rogers, J., and N. H. K. (2015). Intergenerational neural mediators of early-life anxious temperament. *PNAS*, *112*(29), 9118–9122. https://doi.org/10.1073/pnas.1508593112

Buckmaster, PS., & Amaral, DG. (2001). Intracellular recording and labeling of mossy cells and proximal CA3 pyramidal cells in macaque monkeys. *The Journal of Comparative Neurology*, *430*(2), 264–281.

Cox, RW. (1996). AFNI: Software for Analysis and Visualization of Functional Magnetic Resonance Neuroimages. *Computers and Biomedical Research*, *29,* 162-173.

Heider, B., Nathanson, JL., Isacoff, EY., Callaway, EM., & Siegel, RM. (2010). Two-Photon Imaging of Calcium in Virally Transfected Striate Cortical Neurons of Behaving Monkey. *PLoS ONE*, *5*(11), e13829. https://doi.org/10.1371/journal.pone.0013829

Li, M., Liu, F., Jiang, H., Lee, TS., & Tang, S. (2017). Long-Term Two-Photon Imaging in Awake Macaque Monkey. *Neuron*, *93*(5), 1049-1057.e3. https://doi.org/10.1016/J.NEURON.2017.01.027

Logothetis, NK., Eschenko, O., Murayama, Y., Augath, M., Steudel, T., Evrard, HC., … Oeltermann, A. (2012). Hippocampal-cortical interaction during periods of subcortical silence. *Nature*, *491*(7425), 547–553. https://doi.org/10.1038/nature11618

Logothetis, NK., Augath, M., Murayama, Y., Rauch, A., Sultan, F., Goense, J., … Merkle, H. (2010). The effects of electrical microstimulation on cortical signal propagation. *Nature Neuroscience*, *13*(10), 1283–1291. https://doi.org/10.1038/nn.2631

Mantini, D., Hasson, U., Betti, V., Perrucci, M. G., Romani, G. L., Corbetta, M., … Vanduffel, W. (2012). Interspecies activity correlations reveal functional correspondence between monkey and human brain areas. *Nature Methods*, *9*(3), 277–282. https://doi.org/10.1038/nmeth.1868

Paxinos, G., Petrides, M., Evrard, HC. (in preparation). *The Rhesus Monkey Brain in Stereotaxic Coordinates 4th Ed.*. Elsevier.

Reveley, C., Gruslys, A., Ye, FQ., Glen, D., Samaha, J., E. Russ, B., … Saleem, KS. (2016). Three-Dimensional Digital Template Atlas of the Macaque Brain. *Cerebral Cortex*, 1–15. https://doi.org/10.1093/cercor/bhw248

Saleem, KS., Logothetis, NK. (2007). *Atlas of the Rhesus Monkey Brain*. Academic Press.

Scott, TR., & Plata-Salamán, CR. (1999). Taste in the monkey cortex. *Physiology and Behavior*, *67*(4), 489–511. https://doi.org/10.1016/S0031-9384(99)00115-8

2. THE NON-HUMAN PRIMATE CORTICAL TASTE REPRESENTATION

ABSTRACT

The insular cortex receives sensory afferent inputs from the entire body, including the mouth and the gastrointestinal tract. For this reason, insular cortex function has been implicated in the homeostatic regulation of feeding, digestion and bodily processing. Here, novel taste delivery systems were tested and implemented to localize the primary taste area in humans and macaques. Tastant stimuli at different concentrations were evaluated first by human psychophysical testing; then, in several ultra-high field fMRI experiments with the anesthetized macaque, we presented a refined selection of tastants during BOLD measurements. We found that the insula was consistently activated, specifically the mid-insula dorsal fundus (Idfm) and dorsal anterior insular cortex (dAIC) in macaque monkeys. These areas of activation were compared to the human functional homologs and also to data collected from an awake macaque to study the existence of a common gustatory area. The localization of the common gustatory area was investigated in a translative manner to determine the degree of homology between primate species. From this approach, it was found that the dual-representation localized in the anesthetized macaque extended to humans and to the awake state.

KEYWORDS

Taste, gustation, non-human primates, insula, neuroimaging, sensory processing

INTRODUCTION

The mouth serves as a bridge between the external world and the body, taking in essential nutrients and vitamins, while also creating a rich tasting experience. Oral receptors relay sensory information about ingested contents to the insular cortex - the primary cortical center for gustatory information processing. It has been contested as to whether the representation of gustatory information in the non-human primate (NHP) insular cortex reflects that of humans. Therefore, we

examined the functional responses of the insular cortex to the application of different taste stimuli with the intention of localizing the primary taste area in macaque monkeys by functional magnetic resonance imaging (fMRI).

Prior neuroimaging studies in humans have shown that a Primary Gustatory Area (PGA) exists within the insular cortex, particularly situated in the anterior portion of the Primary Interoceptive Cortex (PIC). The PIC represents interoceptive information somatotopographically along a posteroanterior gradient, reflecting a foot-to-head representation of the body. For instance, the hindlimb, forelimb, face and visceral afferents are represented successively in the PIC (Bjornsdotter et al., 2009; Brooks et al., 2005; Hua et al., 2005; Segerdahl et al., 2015), with taste afferents being represented in the mid-dorsal insular fundus (Veldhuizen et al., 2007; Zald, 2009; Small, 2010).

In humans, the cortical region lying rostral to the mid-dorsal fundus is not specifically gustatory and does not appear to contain a specific primary sensory representation; instead, it preferentially harbors highly sophisticated activities related to emotion and cognition (Craig, 2009; Critchley et al., 2004; Kurth et al., 2010). Prior electrophysiology studies in macaques have hinted that the PIC, including the gustatory region, occupies the entire rostrocaudal extent of the insular dorsal fundus, with taste processing at the anterior front (Hirata, Nakamura, Ifuku, & Ogawa, 2005; Pritchard et al., 1986; Scott et al., 1986; Verhagen et al., 2004; Yaxley, 1988). In contrast to human imaging studies, these electrophysiological studies suggest that monkeys do not have a non-gustatory area in the dorsal anterior insula (dAIC). So far, all prior NHP electrophysiological studies examined taste at one or another anteroposterior level, however, none of these studies concurrently examined the entire anteroposterior extent. By fMRI, we were able to image the extent of the insular cortex (region-of-interest ~10-15 mm along the sagittal plane) to better uncover the spatial organization across this distance.

We implemented a custom-made non-invasive gustolingual stimulator to activate taste cells embedded within the tongue's papillae (e.g. circumvallate, foliate and fungiform). The design of this gustolingual stimulator was modeled from gustometers used in previous research on mammalian taste processing (Heck, Persaud, & DeSimone, 1989; Kobayakawa et al., 1996; Reilly, 1994). To compare the activated regions related to taste processing across species, we first collected a small data set with humans. Then, with a reference for taste localization in humans, we went on to ascertain the PGA in NHPs. Additionally, by employing human psychophysics, we had the opportunity to tune our tastant concentrations and select a detectable concentration as well as an amount that was

below the level of perceptual detection. These high- and low-intensity stimuli were translated from the human to the macaque.

We analyzed the resulting activations in the human and NHP insular cortex, also including one awake macaque as further validation, to draw upon the conclusion that the representation of taste in the insular cortex is more similar than previously believed. The restriction of the taste area to discretely localized regions in the macaque insula suggest that the fundal area anterior to the taste area in monkeys may share an evolutionary origin and neuroanatomical functional organization with humans. Most importantly, the existence of a non-gustatory area in NHPs offers potential to examine the functional anatomical nature of a cortical region that plays such a crucial role in integrating sensory information and translating activity into higher-order behavioral and cognitive responses (Craig, 2009).

MATERIALS & METHODS

Ethical Approval

The Ethics Commission at the University of Tuebingen (Germany) approved our human research protocol. Human participants signed a waiver of consent to participate in experiments. Our work with macaque monkeys was carried out with the permission of the local German authorities. Animals were handled according to the guidelines of the European Parliament and Council Directive 2010/63/EU on the protection of animals used for experimental and other scientific purposes.

Anesthesia

Before commencing an experiment, animals were pre-sedated with glycopyrrolate (Robinul, 0.01 mg/kg, i.m., anticholinergic) and ketamine (15 mg/kg, i.m., dissociative anesthetic). After transport to the experimental setup, they were anesthetized with sequential injections of fentanyl (3 μg/kg, i.v., analgesic), thiopental (5 mg/kg, i.v., hypnotic), and succinylcholine chloride (3 mg/kg, i.v., muscle relaxant). They were then intubated and ventilated (24 strokes/min) throughout the procedure, using 100% oxygen during preparation, and 21% oxygen during functional data acquisition. The anesthesia parameters had previously been optimized for imaging BOLD signal changes and recording neuronal activity (Logothetis et al., 2012). After intubation, the anesthesia was maintained using a combination of remifentanil (1-3 μg/kg/min, analgesic and anesthetic) and mivacurium chloride (5-7 mg/kg/h, muscle relaxant). The physiological state of the animal was continuously monitored using infrared pulse oximetry (Nonin Medical Inc., Plymouth,

MN, USA), electrocardiography (ECG), thermometry, and sphygmomanometry. A rectal thermometer continuously measured body temperature, which was regulated using a water-heating pad to maintain a body temperature within normal physiological range (38.3 – 38.8 °C). In order to attain physiological values optimal for fMRI, body temperature was maintained at 38-39ºC, and end-tidal CO_2 and oxygen saturation were kept constant at 33 mmHg and over 95%, respectively. Acidosis was prevented by the administration of lactated Ringer's solution with 2.5% glucose, infused at 10 ml/kg /h, and intravascular volume was maintained by the additional administration of colloids (hydroxyethyl starch, 20-30 ml over 1-2 minutes or 20 ml/kg/h).

Taste Stimulus Preparation

A modest stock concentration was configured for each taste quality as based upon previous literature (Arvidson & Friberg, 1980; Schoenfeld et al., 2004; Ogawa et al., 2005; Bender et al., 2009; Chen et al., 2011). Stock concentrations were as follows: NaCl (salt, 0.9 M), sucrose (sweet, 0.5 M), citric acid (sour, 80 mM), quinine (bitter, 4 mM), and monosodium glutamate (MSG; umami 0.06 M). Serial dilutions of the stock concentration were applied during behavioral tests in humans. A high and low intensity concentration was configured for each tastant applied during fMRI (i.e. sweet, salt and sour).

This study used artificial saliva (AS), a tasteless solution that mimics the concentration of saliva. A 12.5% dilution of AS (stock: 25 mM KCl, 2.5 mM NaHCO3) in dH20 was used as the rinse and the base for taste solutions. In comparison to previous experiments, the 12.5% dilution was perceived as most tasteless, especially compared to rinses with water (Veldhuizen et al., 2007).

Tastant Delivery Devices

ssGLS. Our MR-compatible suction-sealed gustolingual stimulation (ssGLS) was built by the mechanical workshop at the Max Planck Institute for Biological Cybernetics. The design was modeled from a lingual device used to record translingual epithelial currents of ionic taste compounds at the lingual and cranial nerve levels in humans (Feldman et al., 2003) and rodents (Heck, Persaud & Desimone, 1989). This stimulation method eliminated artifacts caused by swallowing, moving liquid around the oral cavity, and tongue movements by maintaining constant contact with the lingual surface.

The ssGLS was applied to the dorsal anterior lingual surface. The surface area of the tongue under the inner chamber (depth: 0.75 mm; diameter: 13 mm) was the primary location for tastant delivery. Fluid flowed into the ssGLS via the central port of the inner chamber and circulated until

exiting via the outflow port within the inner ring. This outflow port carried fluid to a solution-collecting container. The outer chamber functioned as a vacuum seal, which when strong enough, would bring fluid from the inner chamber to the outer chamber. This would not disrupt the constant flow of solution into the inner chamber, and an intermediate fluid collector was placed along the vacuum line to clear fluid from the outer chamber (Fig. 1c).

Additionally, cotton was placed in the cheek pouches to collect accumulating saliva. Taking this measure helped to eliminate the swallowing reflex and to prevent build-up of liquid in the mouth. Furthermore, ssGLS users chose whether to stick their tongue out or to keep it inside during experimentation, whichever way was most comfortable. During each testing session further efforts were made to maximize one's comfort, such as, implementing an external support system for the ssGLS.

The pressure within the system created the suction seal necessary to maintain contact with the tongue. Pressure exerted by the vacuum system (Knf Neuberger, Type N816.3KN.18; Type N035.1.2AN.18) was adapted during preliminary tests to find a comfortable working level (600 – 800 mbar) for the device and the user. Considering the mechanical impact of the ssGLS on the lingual surface, the amount of pressure exerted at this level was monitored within the system by a manometer (located at the central opening of the infusion aggregating port, Fig. 1c) via a fiber optic sensor (OPS.320.20138, Soliton Laser- und Messtechnik GmbH, München). The manometer was connected to an extension cable manufactured for Opsens fiber optic sensors (OPS.320.40010, Soliton Laser- und Messtechnik GmbH, München). The cable was connected to a single channel pressure-reading device, PicoSens (LIS- P1-N-62SC), also manufactured by Opsens. The sampling rate for this channel system was 50 Hz. Pressure data were recorded by a computer running SoftSens (2012) and saved as a text file.

Solution temperature also influences taste perception (Green & Frankmann, 1987); therefore, the liquid temperature within the ssGLS was recorded via a fiber optic thermosensor (OPS.320.20103, Soliton Laser- und Messtechnik GmbH, München). The temperature sensor was connected to an independent port of the infusion aggregator (Fig. 1c) and bridged via extension cable (OPS.320.40010, Soliton Laser- und Messtechnik GmbH, München) to a multi-channel signal conditioner provided by the same company. Temperature data were sampled at 50 Hz with a $\pm$ 0.3^{o}C total system accuracy. Data were recorded by SoftSens (2012) and saved as a text file.

PSFS. We designed a custom Peripheral Suction Fluid Stimulator (PSFS; Fig 1d), which is comprised of a basin supporting the underbelly of the tongue. A funnel at the external portion of

the basin facilitated the removal of infused liquid by vacuum suction. Liquid infusions entered the mouth via an infusion line embedded within the mouthpiece used to fix the jaw and head during scanning.

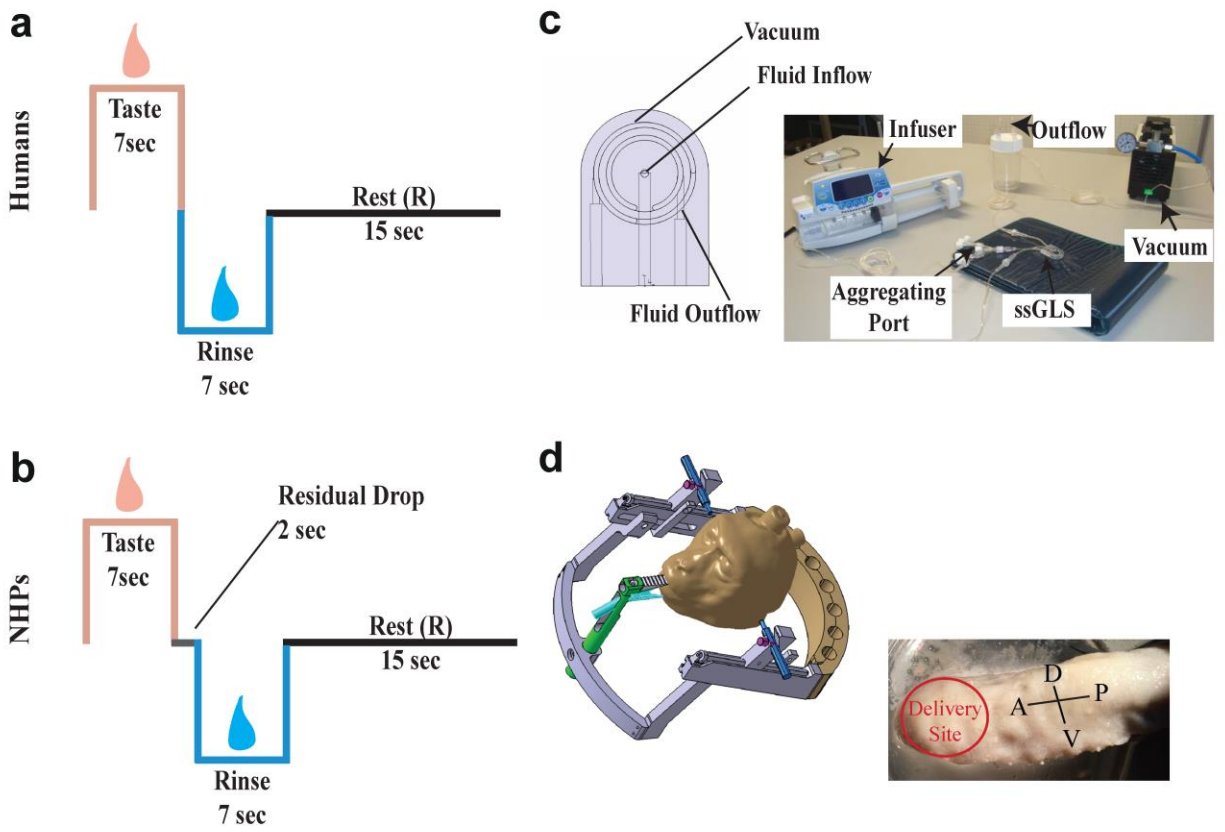

Fig. 1: The (**a**) human and (**b**) macaque taste paradigms. The (**c**) annotated ssGLS design and system of infusion aggregation and circulation within the inner ring for fluid inflow and outer ring for maintaining the vacuum suction seal. (**d**) Schematic of the head-fixed PSFS system and target delivery site for taste stimulation.

Behavioral Measurements

Qualitative Ratings. Eight healthy participants (4 female; average age: 23) volunteered to take part in this study. Qualitative ratings were made based upon the application of five taste qualities (i.e., sour, sweet, salt, umami and bitter). A series of tastants along a concentration gradient were tested during a task measuring stimulus intensity and pleasantness. During this task, solution pairs of different concentration (same taste quality) were consecutively presented to the participant. They were asked to note which one had the greatest intensity and to rate the intensity and pleasantness of each taste. Solutions were presented twice: the first randomly, and the second, in pairs of least and greatest concentration intensity, eliminating effects of strong intensity taste on the perception of relatively weaker stimuli during the second presentation. Ratings were averaged over the two presentations for each solution. We employed a labeled line scaling method to rate the stimuli, as it is quantifiable and includes ratiometric properties to help eliminate perceptual ceiling effects (Lawless, Horne & Spiers, 2000). Scoring was based upon the Labeled Magnitude Scale (LMS) and Labeled Hedonic Scale (LHS), semantic scales of stimulus intensity and pleasantness, respectively, characterized by quasi-logarithmic spacing of its verbal labels (Green et al., 1996). Using this scale, subjective responses were recorded in a proportionate manner. Subjects were instructed to place a mark along the scale where they felt best evaluated their perception of taste intensity (LMS) and pleasantness (LHS). Intensity and pleasantness ratings were quantified from the spatial location of points along the respective scales, each scale totaled 135 mm in length. These ratings were normalized across subjects. An example of the LMS is shown in Figure 2b.

Participants were allowed to sip filtered water in between each testing pair, however, this was only necessary when the taste stimulus concentration was high, i.e. stock salt taste solution. For each test, approximately 0.2 mL of solution were dropped onto the anterior lingual surface using a 0.5 mL plastic micropipette. Participants were instructed to evaluate the taste quality based upon the immediate sensation. Four sampling points were tested for each taste quality (25%, 50%, 75% and 100% of the stock concentration).

The average intensity and pleasantness ratings of the taste qualities between subjects were analyzed using a repeated measures analysis of variance (rANOVA) to detect the overall differences in perceived intensity and pleasantness ratings. Five tastants were compared with 4 concentration levels using SPSS (Version 22). If the assumption of sphericity was violated, the Greenhouse

Geisser values were reported. A Bonferroni correction was applied to adjust for multiple comparisons

2AFC Task. To determine the sensitivity and thresholds for taste detection, we implemented a yes/no signal detection (2-choice alternative forced choice, 2AFC) task during the application of a refined concentration order of salt and sweet tastants (Fig. 2c). These stimuli were presented to subjects (n = 8, 4 female; average age: 23) with and without application of the ssGLS. Participants were instructed to say *yes* or *no* depending on whether they detected taste.

For taste detection without ssGLS, 7 sampling points were used (20 trials/sampling point), and with ssGLS application 5 sampling points were used (20 trials/sampling point). The decrease in sampling points was simply because of a mechanical limitation imposed by the number of infusion pumps used for the experiment. Each testing session took 45 ± 15 minutes.

In the first testing session, stimuli were presented without the ssGLS via direct application to the anterior lingual surface. For each trial, approximately 0.2 mL of solution were dropped onto the anterior tongue surface using a 0.5 mL plastic micropipette. Participants were allowed to sip filtered water when they felt the need to rinse the oral cavity. On a separate day, subjects returned for the second testing session, whereby the yes/no detection task was administered again during ssGLS application.

After data collection, the probability of taste detection was calculated for each sampling point tested. Then, with the MATLab Toolbox psignifit (Wichmann & Hill, Oxford University), data were fit to a probability distribution function. The probability of taste detection was fit to the psychometric function (Fründ, Haenel, & Wichmann, 2011). The normally free parameter lambda (lapse rate) was set equal to 0. Gamma was set to the probability of detecting taste during catch trials (0 mM in 12.5% AS). A bootstrap simulation was performed with 4999 iterations. After these simulations, the thresholds and slopes were calculated by maximum-likelihood estimation.

Data collected without the ssGLS were modeled with a Weibull function to describe the distribution of detection rates in statistical terms. Overall, the outputs from this function provided individual threshold values for taste detection. The analysis procedure was duplicated for data collected with the ssGLS. The absolute threshold was determined by the probability of detection (either 0.5 or 0.82). Concentrations below and above the detection threshold were transferred to neuroimaging experiments with humans and macaques.

fMRI Experiments

Human. All fMRI experiments were conducted using a 3 Tesla Siemens Prisma (Erlangen, Germany) at the Max Planck Institute for Biological Cybernetics. Five healthy volunteers (2 female; average age: 23), whom had already participated in the yes/no detection task with and without the ssGLS, participated in the neuroimaging session. The session included diffusion tensor imaging (not shown here), resting-state and fMRI scans. During fMRI scans, taste stimuli above (suprathreshold) and below (subthreshold) the level of perceptual taste detection were applied. Before scanning, the solutions were run through the ssGLS in a mock experiment to help acclimate participants to the set-up and confirm that taste could still be detected during infusion of suprathreshold concentrations. Data were collected with the ssGLS (passive tasting condition) while participants fixated on a black cross presented on a screen with gray background. During each experiment, participants were given earplugs and told to remain still while in the scanner. For safe operation of the MR scanner, items composed of ferromagnetic material (e.g. vacuum and recording computer) were placed on a table outside the scanner room.

Taste stimuli were delivered via the ssGLS, positioned in the same location as during the yes/no detection task. Tastants were prepared at two concentrations: a subthreshold concentration (15mM sweet and 25mM salt) and a suprathreshold concentration that was 25% greater than the participant's detection threshold. Syringe pumps (Fresenius-Kabi, Frankfurt, Germany) were set to inject a 0.7 mL bolus at a constant pressure of 300 mmHg from a 60 mL syringe (inner diameter 26.43 mm). Independent pumps controlled the infusions of tastant and rinse syringes. Each taste and rinse infusion lasted 3 sec with an additional 4 sec circulation period within the inner chamber before exiting (total length: 7 sec). Rinse cycles occurred after each tastant infusion and additionally served to negate the effects of stimulus habituation (Veldhuizen, Bender, Constable, & Small, 2007). The experimental paradigm (Fig. 1a) included a 15 sec wait period between trials. Each participant underwent 8 runs of sweet and salt tastants (4 runs per taste quality). The order of taste quality presentation was counterbalanced across subjects. The functional blocks were 4 min for humans (9 taste trials).

Macaque. Nine healthy macaque monkeys (4 females; average weight: 9.83 kg) participated in anesthetized fMRI experiments, where one of which was used for a piloting session to test the taste delivery system. Anesthetized data were acquired using a 7 Tesla vertical Nuclear Magnetic Resonance (NMR) scanner (Bruker, Billerica, MA, U.S.A.). One healthy female macaque was included during awake fMRI using a vertical 4.7 Tesla scanner (Bruker, Billerica, MA, U.S.A.).

Once positioned in a custom-designed MR-compatible chair, anesthetized animals had their legs wrapped from toe to pelvis to prevent venostasis. All physiological monitoring sensors (noted above) were secured with medical tape and the torso and arms were snugly wrapped in towels to maintain temperature and prevent obstruction of blood flow and airways. The head of the animal was immobilized using fitted ear bars and mouthpiece. For some anesthetized experiments, a visual flicker was administered during inter-trial rest periods to validate BOLD levels online. This particular stimulus was employed as it had previously been used as a robust marker of sensory activation in the subcortex and cortex (Logothetis et al., 2010).

For macaque monkeys, high (H) and low (I) intensity concentrations of sour (H: 0.08 M, L: 1.25 mM), sweet (H: 0.5 M, L: 15 mM) and salt (H: 0.8 M, L: 25 mM, only in anesthetized experiments) tastants were prepared as configured from human behavioral data. Liquid infusions were delivered via syringe pumps (Aladdin-1000, World Precision Instruments), programmed to operate at the same flow rate (17 mL/min) as the Fresenius pumps and to infuse the same amount of liquid during each infusion period. The syringes were also the same type and size as those used in human experiments. Following an initial rinse infusion (1 mL), the paradigm began with a 7 sec infusion duration, followed by a 2 sec delay period to capture residual drips from the delivery spout, before the rinse cycle began. This paradigm replicated that from humans with the exception of the residual drop period (Fig. 1b). Each functional scan sequence was 8 min in total with 15 trials of pseudo-randomized presentations of high and low intensity tastants. In a typical experiment, there were 8 sessions per taste quality recorded; however, constraints were placed upon the number of sessions, depending on the subject's stability and BOLD response under anesthesia as well as time allocated to run independent fMRI scans employing other stimulus sets (e.g. visceral distention), which were included as part of a broader project to map multi-modal interoceptive responses.

For awake fMRI experiments, only the sweet and sour high-intensity concentrations were administered. As the animal passively received and swallowed the infusion contents, appetitive stimuli promoted motivation to continue the taste task. Thus, in one scan session both sweet and sour high-intensity stimuli were administered. During this time, a camera within the scanner allowed experimenters to observe the subject's behavior during infusion periods. While the stimulation paradigm remained the same as in anesthetized experiments, the flow rate was decreased to 8 mL/min to ensure the volumetric amount was sufficient for activating the taste pathway, but not enough to bring about satiety and a lack of interest in the tastants.

Image Acquisition

Human. Using the Siemens 64-channel head coil, whole-brain volumes were acquired using a 4-band multi-shot gradient-echo Echo Planar Imaging (EPI) sequence (in-plane resolution: 2.67 mm^2; slice thickness: 2 mm; TR/TE 870/30 msec; 56 axial slices; flip angle: 57°; matrix: 96 x 96; field-of-view (FOV): 192 mm). Slice volumes were acquired in contiguous sections. A T1-weighted MP-RAGE scan was acquired for each subject (1 mm^2 isotropic voxel resolution; TR/TE: 2000/3 msec; 192 axial slices; flip angle: 9°; matrix: 96 x 96; FOV: 192 mm).

Macaque. Whole-brain functional scans were acquired with a multi-shot gradient-echo EPI sequence (GE-EPI; 1x1 mm^2 in-plane resolution; flip angle: 53°; TR/TE: 2000/19 ms; 20 axial slices) when using the quadrature coil, and with GRAPPA-accelerated parallel imaging (0.85 x 0.85 mm^2 in-plane resolution; flip angle: 53°; TR/TE: 1000/18 ms, 18 axial slices) when using the phased-array coil helmets. Slice volumes were acquired in contiguous sections. Both scan sequences had the same matrix size (128x128), field-of-view (FOV; 96x96 mm^2) and slice thickness (2 mm).

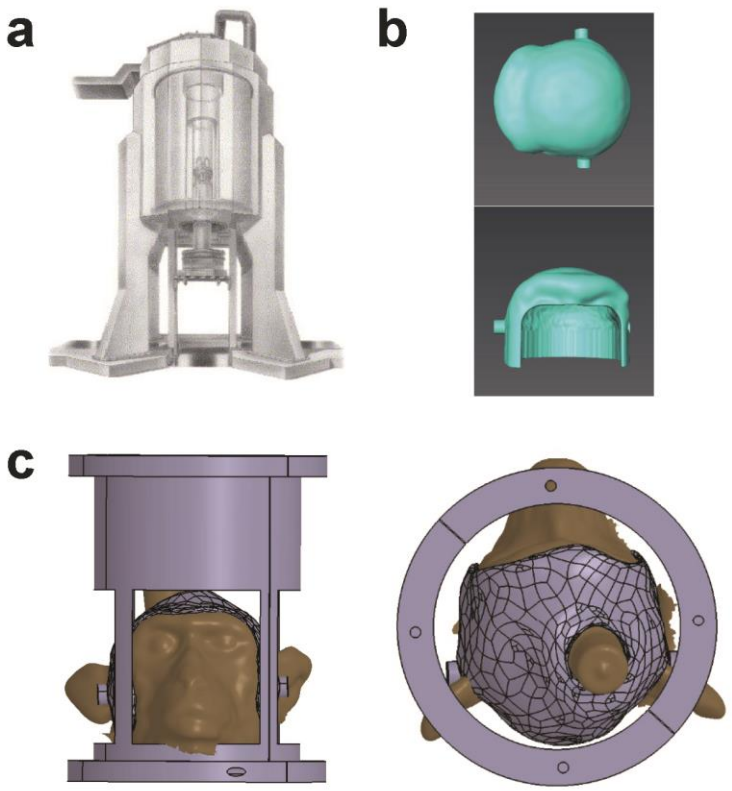

Fig. 2: The (a) 7 Tesla vertical scanner; (b) the custom-designed helmet for imaging with phased-array coil elements; (c) the positioning of the head within the receiver and transmitter coils. Images courtesy of the Department of Physiology of Cognitive Process, Max Planck Institute for Biological Cybernetics (Tübingen, Germany).

During each experiment, a T2-weighted Rapid Imaging with Refocused Echoes (RARE) scan was collected to image the native structural space (FOV: 96x96 mm^2; matrix size: 256x256; 8 segments; flip angle: 8°; TR/TE: 4000-6500/25-48 msec; 40 slices). A three-dimensional anatomical scan was acquired for each subject using a T1-weighted modified driven equilibrium Fourier transform scan (MDEFT; FOV: 128x128 mm^2; matrix size: 256x256; 4 segments; flip angle: 20°; TR/TE: 15/4.5 msec; 136 slices).

Image Pre-Processing and Normalization

Human data were converted from DICOMs to NIfTI images and macaque data were converted from the Bruker file format to an SPM-readable file format (.nii or .hdr/.img). Functional volumes were manually examined for ghosting and signal dropout artifacts using MRIcro (version: 1.40). Individual volumes that exhibited artifacts were extracted from the time series; runs were excluded if more than 5% of frames exhibited artifacts. The resulting functional data were realigned using SPM12 (Statistical Parametric Mapping; Wellcome Department of Imaging Neuroscience, London, UK) to obtain 6 rigid-body transformation parameters, and then coregistered to each subject's native anatomical scan. A visual examination of the coregistration was done before normalization. As the data were collected using multi-shot EPI sequences with low TR, data were not slice-time corrected.

Human data were normalized to the MNI template and macaque data were normalized to a high-resolution digital surrogate of the D99 atlas (Saleem & Logothetis, 2007). For the macaque data, we used AFNI (Cox, 1996) in combination with open-source scripts developed by Reveley and colleagues (2016). Each animal's native 2D anatomical scan was linearly aligned to the normalized MDEFT and subsequently warped using an in-house MATLAB (Version 2017b, MathWorks, U.S.A.) function for nonlinear transformations. The resulting transformation matrix was applied to the functional images (already coregistered to the native RARE scan).

At each step, the spatial alignment was checked manually during visual examination. An analysis of the resulting spatial disparity between functional images and template was below that of the smoothing kernel applied. Human and macaque data were smoothed using 8 mm and 2 mm FWHM Gaussian kernels, respectively.

Univariate fMRI Analysis

All runs collected within one session (day of experimentation) for each subject were concatenated. The measured BOLD data were modeled by an event-related univariate General

Linear Model (GLM) using SPM12. Each infusion event and its temporal derivative was modeled separately and convolved with the canonical hemodynamic response function. Six parameters obtained by rigid-body head motion correction were included in the model. The data were high-pass filtered with a cutoff of 128 sec and a first-degree autocorrelative model was included to correct for aliasing. GLM parameter estimates (β-weights) were subjected to a *t*-test ($p = 0.05$, corrected for false positives using FDR-correction). Inferences were made on whole-brain activity minimizing the circularity of results (Kriegeskorte et al., 2009).

Functional activation maps were made by contrasting the rinse activity from the taste activity. To test for any confounding or repeating influence of the rinse on taste activity, a control experiment was conducted (n = 2, 15 taste scans), whereby the subthreshold solution was replaced with AS, so that each subthreshold trial would result in AS followed by AS. These rinse periods were then used in the contrast against suprathreshold taste to cross-check the activation patterns to the standard paradigm.

For the macaque data, a non-parametric (permutation) multi-subject *t*-test was independently calculated for each condition using the scaled individual contrast maps derived at the single-subject level. Nonparametric testing was employed here as it been shown, with sufficient effect size, to trump parametric tests at the group-level (Eklund, Nichols, & Knutsson, 2016). Analysis was conducted using SnPM (Nichols & Holmes, 2001). An equal number of runs across experimental sessions were included, and the analysis was repeated using different sets of scans to test for robustness. The group-level analysis underwent 500 permutations and the resulting significant effects were mapped onto the template brain.

A parametric multi-subject analysis was performed on the human data (with n = 5 subjects, the number of sessions was not fit to perform a non-parametric analysis). Normalized functional scans were concatenated across subjects and a second-level GLM was calculated. The resulting *t*-contrast maps were overlaid onto the MNI template.

RESULTS

We developed and implemented a novel taste delivery system suitable for studies in humans and macaques. We analyzed the different effects of taste quality on human perception; the ratings for intensity and pleasantness were compared across types of tastants. The stimuli applied were further evaluated by a yes/no taste detection task and these participants were invited to return for an fMRI experiment.

Qualitative Taste Ratings

The average pleasantness and intensity ratings (mean) and standard deviation were calculated for each sampling point. Mauchly's test indicated that the sphericity assumption was violated for intensity rating data (W = 0.172, p = 0.08). There was no significant main factor of tastant ($F(1.09, 7.6) = 0.31, p = 0.61$), concentration ($F(1.57, 11) = 1.3, p = 0.3$), or for the interaction between tastants and concentration ($F(12, 84) = 1.11$, p = 0.34). As it was found that salty and umami taste qualities had the largest distributions in taste ratings, a post hoc test was conducted for these tastants and the four stimulus concentrations. Pairwise comparisons revealed a significant difference between the weakest and strongest salt concentrations ($F(3, 21) = 1.17$, p = 0.05, partial eta-squared = 0.75). There was no difference between the other three salt concentrations. The post hoc test for umami revealed no significant differences ($F(3, 21) = 0.7$, p = 0.56). The pleasantness data did not violate the sphericity assumption. There was no significant main factor of tastant ($F(4, 28) = 0.31$, p = 0.87), or concentration ($F(3, 21) = 1.3$, p = 0.3). However, the interaction between them was significant ($F(12, 84) = 1.11$, p = 0.04), indicating differences between the pleasantness ratings for the sampling points of different tastants.

From these tests, we received feedback about the different effect taste qualities had on the location of taste stimulation. For example, bitter and umami had a more noticeable effect in the posterior oral cavity as opposed to the anterior. For this reason, subsequent tests focused on sweet, salt and sour tastants. The graphical results of evaluated sweet, salt and sour taste intensity for the 25-100% stock dilution series are shown in Figure 2a. We expanded upon our four initial sampling points (e.g. 100%, 75%, 50% and 25%) to offer a more refined dilution series (Fig. 2c) in the signal detection task.

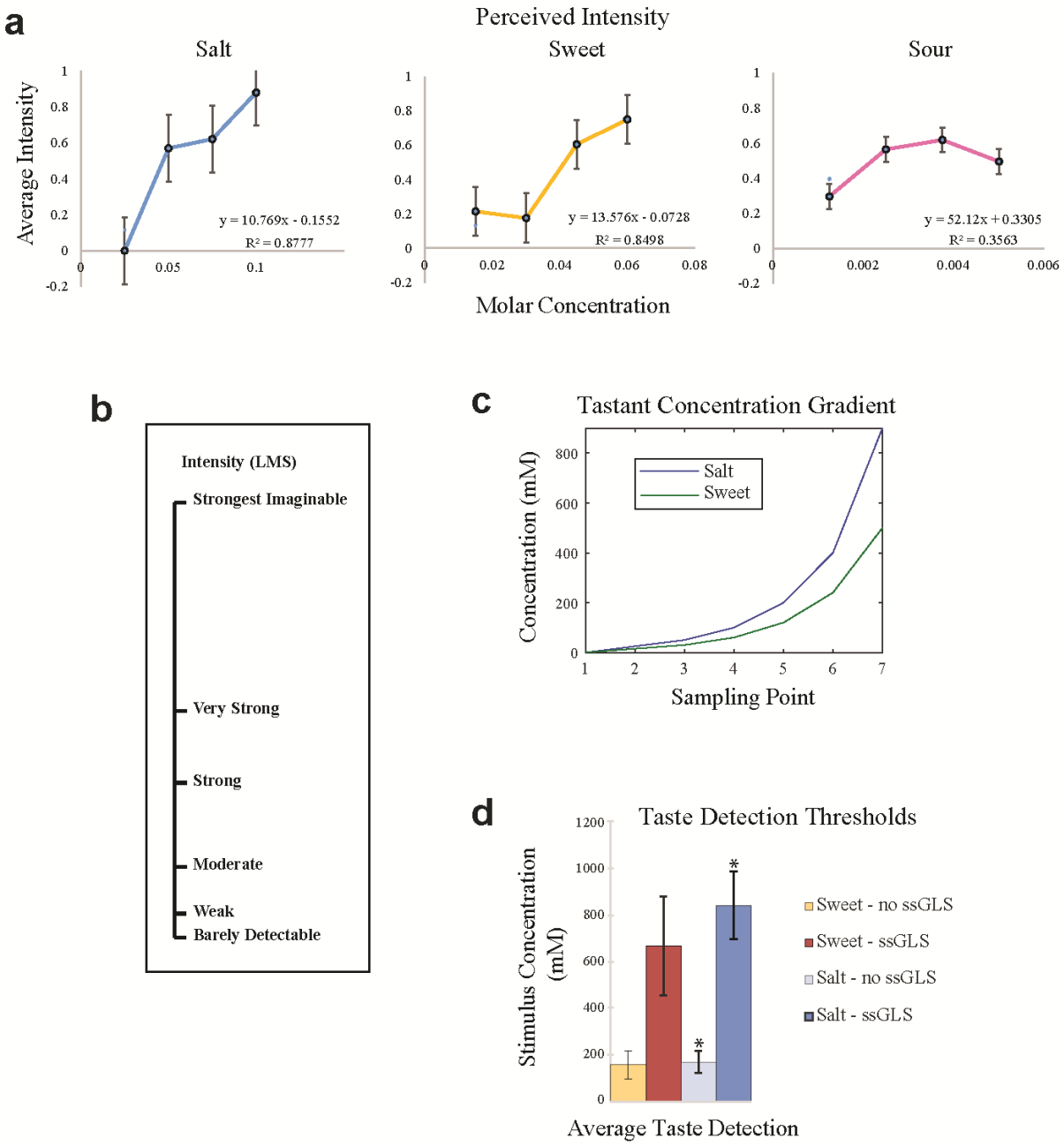

Fig. 3: The (**a**) normalized average intensity across subjects (n = 8) for salt, sweet and sour tastants. (**b**) The Labeled Magnitude Scale (LMS), as designed by Green et al. (1996), used for evaluating tastant intensity. (**c**) The sampling concentrations used in the yes/no signal detection task with and without the ssGLS. (**d**) Average taste detection threshold (n = 8) for sweet and salt tastants with and without use of the ssGLS in terms of stimulus concentration (mM). A two-way ANOVA revealed a significant difference between groups ($F(3, 24) = 6.74$, $p = 0.002$), and when conducting a test for multiple comparisons, a significant difference was found between salt taste detection with and without the ssGLS.

Signal Detection Task

We determined the absolute threshold and level of individual sensitivity to different sweet and salt tastants in a 2AFC task for signal detection. We sampled 7 concentrations for each tastant without ssGLS and modeled the functions for individual taste detection thresholds. We tested each sampling point 20 times during the threshold detection experiments. However, this number is not a fixed parameter. The number of trials is largely dependent upon the level of noise in the experimental set-up and on the internal level of sensory perception. With 20 trials, there was enough time to sufficiently test sweet and salt tastants in one behavioral session without evoking fatigue by the observer.

The salt concentration range (0-200 mM) tested without the ssGLS found an average detection threshold of 33.23 mM (std = 13.38). For sweet, the average detection threshold for a concentration range of 0 - 240 mM was 33.83 mM (std = 17.65). The average sensitivity was 24.62 and 31.09 for sweet and salt tastants, respectively. The salt concentration range (0-200 mM) tested with the ssGLS found an average detection threshold of 101.95 mM (std = 11.54); the average detection threshold for sweet over the concentration range 0–240 mM was 54.65 mM (std = 9.36). The average sensitivity was 20.86 and 46.62 for sweet and salt solutions, respectively.

Neuroimaging Results

Human participants were scanned under passive testing conditions (no perceptual responses recorded in the scanner) with sweet and salt stimulus delivery via the ssGLS. The results (Fig. 4) replicated the mid-dorsal insular taste activation reported previously in humans (Veldhuizen et al., 2007; Zald, 2009; Small, 2010). In addition to this activated region, another area more anteriorly was activated (Fig. 6, human panel).

Each macaque used for anesthetized experiments (n = 8) underwent an average of 2 scan sessions, resulting in 17 total fMRI experiments. Given the longer period of scanning time in anesthetized experiments, we tested not only sweet and salt tastants in the macaque but also sour tastants. A total of 349 fMRI runs (scans) were collected, with an average of 8 scans per taste quality. It was originally intended to directly transfer the ssGLS to the 7 Tesla set-up, however, it was found that the suction seal could not be maintained given the curvature of the macaque lingual surface. As this aspect is crucial to prevent uncontrolled fluid leakage into the oral cavity another stimulus delivery system was built and implemented. The resulting set-up was the PSFS (Fig. 1d).

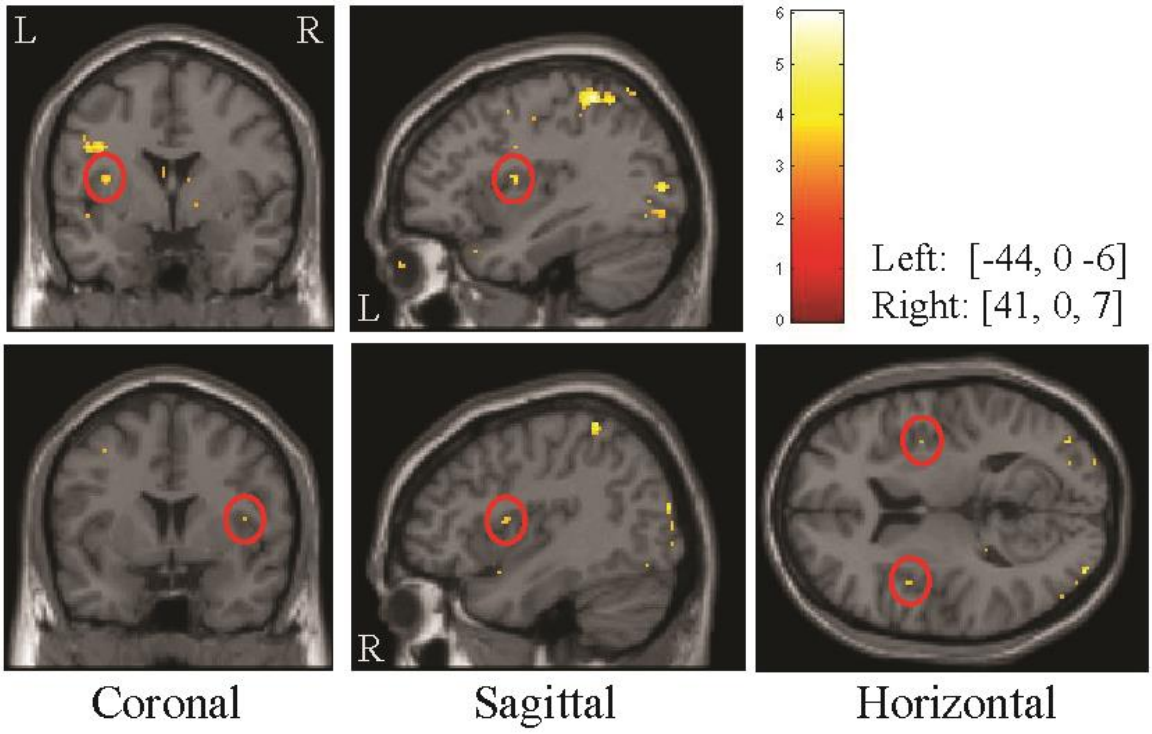

Fig. 4: Representation of the Primary Gustatory Area (PGA) in humans. Functional MRI taste data from one human participant. Eight blocks of taste stimulation, half with sweet and the other half with salt tastants. During each stimulation block the subject experienced 9 trials of sub- or supra-threshold taste stimulation.

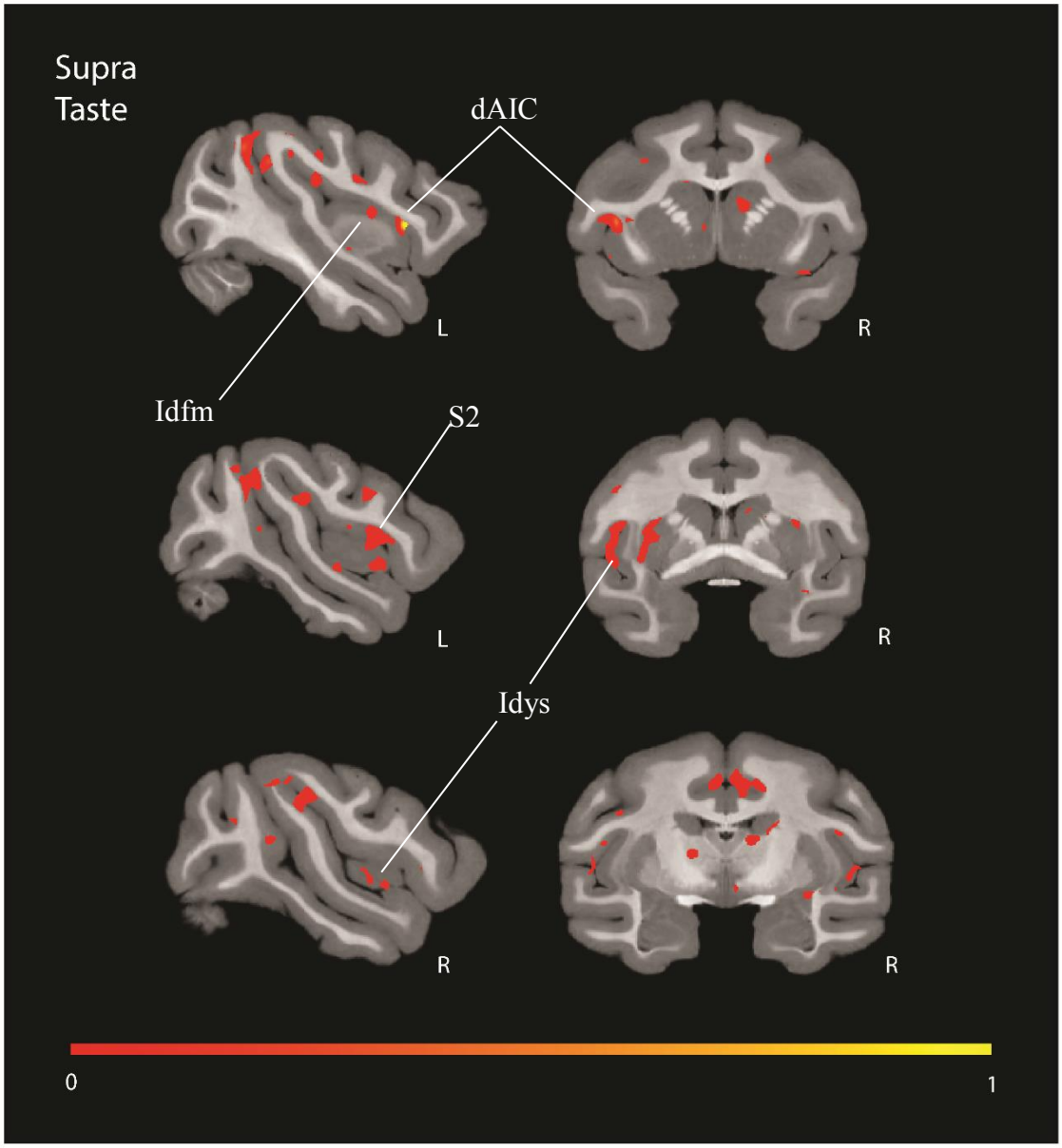

Fig. 5: Representation of the Primary Gustatory Area (PGA) in macaque monkeys as determined by analysis of the high-intensity taste concentrations. Functional MRI data normalized at the group-level. Activations in the dAIC, Idfm, S2 and Idys are highlighted.

The group-level results for high-intensity taste are shown in Figure 5. The same mid-insular activation in the dorsal fundus was seen as well as a discretely localized activation in dAIC. Significant activations in the striatum, S2, and ventral dysgranular insula ($p = 0.05$, FDR-corrected) were also noted. In most cases, the ventral extent of the fMRI slice acquisition excluded medullar nuclei.

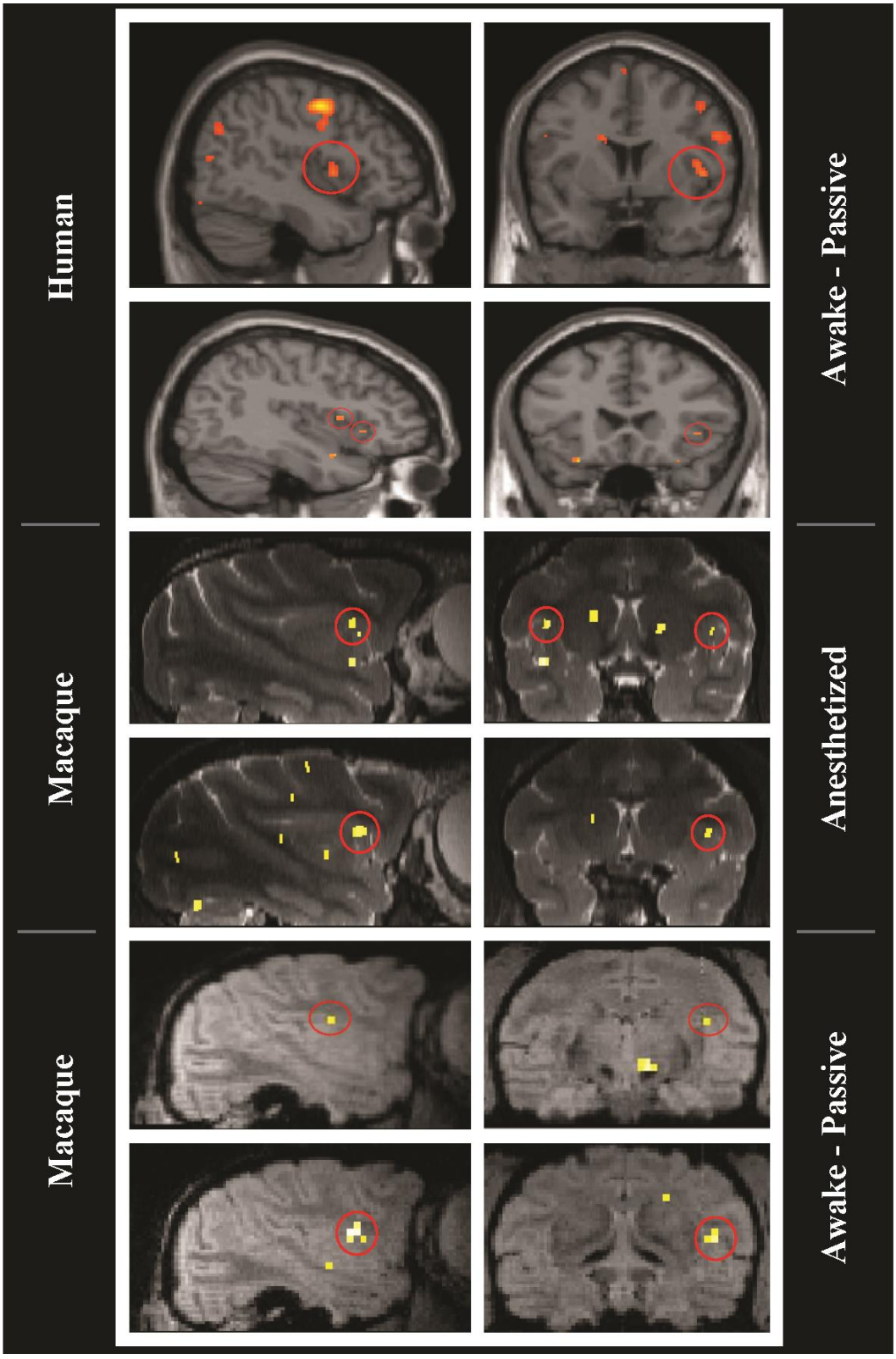

Fig. 6: Comparative portrayal of the middle and anterior activations of the insular dorsal fundus (circled in red) for humans and macaques. The top segment represents the group-level (n = 5) results from passive high- and low-intensity salt and sweet taste processing in humans; the middle segment represents results from high- and low-intensity salt taste processing in the anesthetized macaque (Case K07); the bottom segment depicts passive high-intensity sour and sweet taste processing in the awake macaque (Case B10).

To compare the results in the anesthetized macaque to the primary taste representation in humans, we also scanned an awake macaque to provide a functional bridge between the anesthetized and awake state. Data from all three conditions are shown in Figure 6 to illustrate the coherence in taste localization across species and state.

DISCUSSION

In order to localize the primary taste area in primates, we first designed a way to activate the afferent pathway. As the taste pathway is well described (Carleton, Accolla, & Simon, 2010; Pritchard et al., 1986), we maintained predictions of specific areal activation in regions known to receive and relay incoming taste information. We collected psychophysical data from human participants to refine our stimulus concentrations and functional paradigm. We collected behavioral data on taste perception with our taste delivery system (ssGLS) and tested the working system during fMRI in humans. We confirmed a localization of the human primary taste area consistent with previously reported literature (Small, 2010; Veldhuizen et al., 2007; Zald, Hagen & Pardo, 2002) and optimized the delivery apparatus to suit studies in the anesthetized macaque.

To have data collected from both humans and macaques in one overarching study aided the translative comparison of homologous regions. From a previous study, Kadohisa and colleagues used subjective responses to taste stimuli in humans to better interpret neuronal representations elucidated by awake macaque electrophysiology in the amygdala, insular and orbitofrontal cortices (Kadohisa, Rolls & Verhagen, 2005). By confirming detection of high-intensity tastants in humans, we could make the assumption that these stimuli would be strong enough to drive activation in the anesthetized state.

We translated known supra- and sub-threshold taste concentrations from humans to macaques, and were able to measure the activation in the PGA. Based upon these results, we formulated valid inferences on the boundaries of taste processing in the insular cortex and on the existence of a non-gustatory area rostral to the PGA in macaques. Strikingly, in both species a dual-representation exists, one which is substantiated by prior tract-tracing studies (Pritchard et al., 1986). While a dual-representation of taste in the dorsal fundus of the insula is apparent in Idfm and dAIC, we also observed fairly consistent activation of the ventral dysgranular insula and the secondary somatosensory area (S2). Activation of these regions could indicate second-order sensory processing and upstream relay of basic taste information in the cortex.

It is known that subjects report differences in taste perception depending on the area of lingual stimulation (Zald, Hagen & Pardo, 2002), therefore, it was an objective to remain consistent throughout experimentation in stimulation location. We learned by testing that there is a large range of individual levels of sensory taste perception. Individual evaluations of taste intensity and pleasantness helped to understand these perceptual effects, all the while refining the 2-choice alternative force choice (2AFC) paradigm.

From our studies, we also found that salt solutions were easier to detect than sweet solutions. However, we must still take into account that participants have their own criterion for detection and different stimulus sensitivities. From our detection task, we measured absolute thresholds for taste perception. Conversely, if we sought to measure relative thresholds we could implement a 2AFC task for taste discrimination. Nevertheless, we were able to determine the absolute thresholds for detection and the information necessary for running an informed fMRI experiment.

The scientific objective of the investigations into the human PGA with the ssGLS was to provide a point of reference or comparison to examine whether the monkey PGA covers the entire anterior half of the insular dorsal fundus, as suggested by prior electrophysiology studies (Hirata, Nakamura, Ifuku, & Ogawa, 2005; Pritchard et al., 1986; Scott et al., 1986; Verhagen et al., 2004; Yaxley, 1988), or whether the taste region was more discretely localized within the insular cortex. The restriction of the PGA to the mid-dorsal fundus in monkeys would suggest that the fundal area anterior to the PGA may share an evolutionary origin and anatomo-functional organization with humans. Most importantly, the existence of a non-gustatory area in macaque monkeys would offer a unique opportunity to examine, in the laboratory, the nature of a brain region that maintains such a crucial role in human subjective feelings and sentience.

A previous study using in vivo 2-photon calcium imaging to map cortical fields in the rat insula discovered discretely labeled neuronal lines, or cortical “hot spots,” receptive to all taste qualities within the rat insular cortex (Chen et al., 2012). In an attempt to study the extent of gustatory processing in the PIC, we found variations in functional localizations, but the variations were not more than that seen at the single-subject level. As the number of subjects that took part in the human fMRI task was quite low, differential effects between taste qualities was not discernible. However, further analysis of the potential for gustotopic encoding in the macaque could be done on our data set using a multi-variate pattern analysis (Chikazoe, Lee, Kriegeskorte, & Anderson, 2019) or modeling of the organization of the neuronal encoding (Avery, et al., 2019).

The tongue is topographically innervated by gustatory and trigeminal cranial nerves, carrying multi-modal information from the taste buds to the brainstem and into the cortex (Lemon, Kang, and Li, 2016; Mueller et al., 2005). While there is some degree of labeled-line encoding, gustation is an integrative sense that bridges the realms of taste, texture, and temperature (Roper, 2007; Verhagen, Kadohisa & Rolls, 2004). The responses of these afferent fibers reflect a chemical difference in the taste and flavor of food and drink. Gustation is vital to controlling the quantity of food intake (Oliveira-Maia, Roberts, Simon, & Nicolelis, 2011) and food motivation (Holsen et al., 2005). This basic need to acquire metabolic nutrients and energy is present in both human and non-human species. Hence, the similarity in cortical taste representation between humans and macaques supports the notion that the underlying organization of a vital biological function is conserved across primate species.

ACKNOWLEDGMENTS

Dr. Frederico Azevedo is acknowledged for his assistance with awake macaque fMRI experiments. This work was supported by the Werner Reichardt Centre for Integrative Neuroscience (CIN) at the Eberhard Karls University of Tübingen (CIN is an Excellence Cluster funded by the Deutsche Forschungsgemeinschaft [DFG] within the framework of the Excellence Initiative EXC 307) and by the Max Planck Society. We acknowledge support by the Deutsche Forschungsgemeinschaft and Open Access Publishing Fund of University of Tübingen for the cost of publication.

CONFLICT OF INTEREST STATEMENT

The author declares having no personal, professional or financial relationships that could potentially be construed as a conflict of interest.

REFERENCES

Arvidson, K. & Friberg, U. (1980). Human Taste: Response and Taste Bud Number in Fungiform Papillae. *Science*, *209*(15), 807–808. https://doi.org/10.1126/science.7403846

Avery, JA., Lie AG., Ingeholm JE, Riddell, CD., Gotts SJ., M. A. (2019). Taste Quality Representation in the Human Brain. *BioRxiv*. Retrieved from https://www.biorxiv.org/content/biorxiv/early/2019/08/06/726711.full.pdf

Bender, G., Veldhuizen, MG., Meltzer, JA., Gitelman, DR., & Small, DM. (2009). Neural correlates of evaluative compared with passive tasting. *Eur J Neurosci*, *30*(2), 327–338. https://doi.org/10.1111/j.1460-9568.2009.06819.x

Bjornsdotter, M., Loken, L., Olausson, H., Vallbo, A., Wessberg, J. (2009). Somatotopic organization of gentle touch processing in the posterior insular cortex. *Journal of Neuroscience*, *29*(29), 9314–9320. https://doi.org/10.1523/JNEUROSCI.0400-09.2009

Brooks, JCW, Zambreanu, L., Godinez, A., Craig, AD., & Tracey, I. (2005). Somatotopic organisation of the human insula to painful heat studied with high resolution functional imaging. *NeuroImage*, *27*(1), 201–209. https://doi.org/10.1016/j.neuroimage.2005.03.041

Carleton A, Accolla R, Simon, S. (2010). Coding in the mammalian gustatory system. *Trends Neurosci*, *33*(7), 326–334. https://doi.org/10.1016/j.tins.2010.04.002

Chikazoe, J., Lee, DH., Kriegeskorte, N., & Anderson, AK. (2019). Distinct representations of basic taste qualities in human gustatory cortex. *Nature Communications*, *10*(1), 1048. https://doi.org/10.1038/s41467-019-08857-z

Craig, AD. (2009). How do you feel — now? The anterior insula and human awareness. *Nature Reviews Neuroscience*, *10*(1), 59–70. https://doi.org/10.1038/nrn2555

Critchley, HD., Wiens, S., Rotshtein, P., Ohman, A., Dolan, R. J., Öhman, A., … Dolan, RJ. (2004). Neural systems supporting interoceptive awareness. *Nat Neurosci*, *7*(2), 189–195. https://doi.org/10.1038/nn1176

Eklund, A., Nichols, TE., & Knutsson, H. (2016). Cluster failure: Why fMRI inferences for spatial extent have inflated false-positive rates. *Proceedings of the National Academy of Sciences*, *113*(28), 7900-7905. https://doi.org/10.1073/pnas.1602413113

Feldman, GM., Mogyorosi, A., Heck, GL., DeSimone, JA., Santos, CR., Clary, RA., & Lyall, V. (2003). Salt-evoked lingual surface potential in humans. *J Neurophysiol*, *90*(3), 2060–2064. https://doi.org/10.1152/jn.00158.2003

Fründ, I., Haenel, NV., & Wichmann, FA. (2011). Inference for psychometric functions in the presence of nonstationary behavior. *Journal of Vision*, *11*(6), 16. https://doi.org/10.1167/11.6.16

Green BG Cowart B, Shaffer G, Rankin K, Higgins J. (1996). Evaluating the "Labeled Magnitude Scale" for Measuring Sensations of Taste and Smell. *Oxford University Press*, *21*(3), 323–334. https://doi.org/10.1093/chemse/21.3.323

Heck, GL., Persaud, KC., & DeSimone, JA. (1989). Direct measurement of translingual epithelial NaCl and KCl currents during the chorda tympani taste response. *Biophysical Journal*, *55*(5), 843–857. https://doi.org/10.1016/S0006-3495(89)82884-X

Hirata, S., Nakamura, T., Ifuku, H., & Ogawa, H. (2005). Gustatory coding in the precentral extension of area 3 in Japanese macaque monkeys; comparison with area G. *Exp Brain Res*, *165*(4), 435–446. https://doi.org/10.1007/s00221-005-2321-y

Holsen, LM., Zarcone, JR., Thompson, TI., Brooks, WM., Anderson, MF., Ahluwalia, JS., … Savage, CR. (2005). Neural mechanisms underlying food motivation in children and adolescents. *Neuroimage*, *27*(3), 669–676. https://doi.org/10.1016/j.neuroimage.2005.04.043

Hua lH., Strigo, IA., Baxter, LC., Johnson, SC., & Craig, AD. (2005). Anteroposterior somatotopy of innocuous

cooling activation focus in human dorsal posterior insular cortex. *Am J Physiol Regul Integr Comp Physiol*, *289*(2), R319–R325. https://doi.org/10.1152/ajpregu.00123.2005

Kadohisa, M., Rolls, ET., & Verhagen, JV. (2004). Orbitofrontal cortex: Neuronal representation of oral temperature and capsaicin in addition to taste and texture. *Neuroscience*, *127*(1), 207–221. https://doi.org/10.1016/j.neuroscience.2004.04.037

Kobayakawa T Saito S, Ayabe-Kanamura S, Kikuchi Y, Yamaguchi Y, Ogawa H, Takeda T. (1996). Trial measurements of gustatory-evoked magnetic fields. *Visualization of Information Processing in the Human Brain: Recent Advances in MEG and Functional MRI*, *EEG Suppl.*, *47,* 133–141.

Kriegeskorte, N., Simmons, WK., Bellgowan, PSF., & Baker, CI. (2009). Circular analysis in systems neuroscience: the dangers of double dipping. *Nature Neuroscience*, *12*(5), 535–540. https://doi.org/10.1038/nn.2303

Kurth, F., Zilles, K., Fox, PT., Laird, AR., & Eickhoff, SB. (2010). A link between the systems: functional differentiation and integration within the human insula revealed by meta-analysis. *Brain Structure and Function*, 1–16. https://doi.org/10.1007/s00429-010-0255-z

Lawless HT, Horne, J., Spiers, W. (2000). Contrast and Range Effects for Category, Magnitude and Labeled Magnitude Scales in Judgements of Sweetness Intensity. *Chem Senses*, *25*(1), 85–92.

Logothetis, NK., Eschenko, O., Murayama, Y., Augath, M., Steudel, T., Evrard, HC., … Oeltermann, A. (2012). Hippocampal-cortical interaction during periods of subcortical silence. *Nature*, *491*(7425), 547–553. https://doi.org/10.1038/nature11618

Logothetis, NK., Augath, M., Murayama, Y., Rauch, A., Sultan, F., Goense, J., … Merkle, H. (2010). The effects of electrical microstimulation on cortical signal propagation. *Nature Neuroscience*, *13*(10), 1283–1291. https://doi.org/10.1038/nn.2631

Mueller, KL., Hoon, MA., Erlenbach, I., Chandrashekar, J., Zuker, CS., & Ryba, NJP. (2005). The receptors and coding logic for bitter taste. *Nature*, *434*(7030), 225–229. https://doi.org/10.1038/nature03352

Nichols, TE., & Holmes, AP. (2002). Nonparametric permutation tests for functional neuroimaging: A primer with examples. *Human Brain Mapping*, *15*(1), 1–25. https://doi.org/10.1002/hbm.1058

O'Doherty, J., Francis, S., Bowtell, R., McGlone, F. (2001). Representation of pleasant and aversive taste in the human brain. *Journal of Neurophysiology*, *85*(3), 1315–1321. https://doi.org/Thesis_references-Converted #291

Ogawa, H., Wakita, M., Hasegawa, K., Kobayakawa, T., Sakai, N., Hirai, T., … Saito, S. (2005). Functional MRI detection of activation in the primary gustatory cortices in humans. *Chem Senses*, *30*(7), 583–592. https://doi.org/10.1093/chemse/bji052

Oliveira-Maia, AJ., Roberts, CD., Simon, SA., & Nicolelis, MAL. (2011). Gustatory and reward brain circuits in the control of food intake. *Advances and Technical Standards in Neurosurgery*, *36*, 31–59. https://doi.org/10.1007/978-3-7091-0179-7_3

Pritchard, TC., Hamilton, RB., Morse, JR., & Norgren, R. (1986). Projections from thalamic gustatory and lingual areas in the monkey, Macaca fascicularis. *Journal of Comparative Neurology*, *244*(2), 213–228. https://doi.org/10.1002/cne.902440208

Reilly S, Norgren, R., Pritchard, TC. (1994). A New Gustometer for Testing Taste Discrimination in the Monkey. *Physiology & Behavior*, *55*(3), 401–406.

Reveley, C., Gruslys, A., Ye, FQ., Glen, D., Samaha, J., E. Russ, B., … Saleem, KS. (2016). Three-Dimensional Digital Template Atlas of the Macaque Brain. *Cerebral Cortex*, 1–15. https://doi.org/10.1093/cercor/bhw248

Roper, SD. (2007). Signal transuction and information processing in mammalian taste buds. *Pfugers Arch. Eur. J. Physiol., 454*(5), 759-776. https://doi.org/10.1007/s00424-007-0247-x

Saleem, KS., Logothetis, NK. (2007). *Atlas of the Rhesus Monkey Brain*. Academic Press.

Schoenfeld, MA., Neuer, G., Tempelmann, C., Schüßler, K., Noesselt, T., Hopf, J. M., & Heinze, H. J. (2004). Functional magnetic resonance tomography correlates of taste perception in the human primary taste cortex. *Neuroscience*, *127*(2), 347–353. https://doi.org/10.1016/j.neuroscience.2004.05.024

Scott, TR., Yaxley, S., Sienkiewicz, ZJ., Rolls, ET. (1986). Gustatory responses in frontal opercular cortex of the alert cynomolgus monkey. *Journal of Neurophysiology*, *56*(3), 876–890.

Segerdahl, AR., Mezue, M., Okell, TW., Farrar, JT., & Tracey, I. (2015). The dorsal posterior insula subserves a fundamental role in human pain. *Nature Neuroscience*, *18*(4), 499–500. https://doi.org/10.1038/nn.3969

Small, DM. (2010). Taste representation in the human insula. *Brain Struct Funct*, *214*(5–6), 551–561. https://doi.org/10.1007/s00429-010-0266-9

Veldhuizen, MG., Bender, G., Constable, RT., Small, DM. (2007). Trying to detect taste in a tasteless solution: Modulation of early gustatory cortex by attention to taste. *Chemical Senses*, *32*(6), 569–581. https://doi.org/10.1093/chemse/bjm025

Verhagen, JV, Kadohisa, M., Rolls, ET. (2004). Primate Insular/Opercular Taste Cortex: Neuronal Representations of the Viscosity, Fat Texture, Grittiness, Temperature and Taste of Foods. *Journal of Neurophysiology*, *92*(3), 1685–1699. https://doi.org/10.1152/jn.00321.2004

Chen, X., Gabitto, M., Peng, Y., Ryba, NH., Zuker, CS. (2011). A Gustotopic Map of Taste Qualities in the Mammalian Brain. *Science*, *333*, 1262–1266.

Yaxley S, Rolls, ET., Sienkiewicz, ZJ. (1988). The Responsiveness of Neurons in the Insular Gustatory cortex of the Macaque Monkey is Independent of Hunger. *Physiology & Behavior*, *42*, 223–229.

Zald DH, Hagen, MC., Pardo JV. (2002). Neural Correlates of Tasting Concentrated Quinine and Sugar Solutions. *Journal of Neurophysiology*, *87*(2), 1068–1075. https://doi.org/10.1152/jn.00358.2001.

3. BOLD CORRELATES OF RECTAL DISTENTION IN THE ANESTHETIZED MACAQUE

ABSTRACT

The insular cortex is a brain region responsible for the processing of bodily sensations and autonomic functions. Insular activity is, in many ways, correlated with the autonomic nervous system, including parasympathetic control over digestion and the detection of salient visceral activity. To study the role of the insular cortex during interoceptive processes, we employed stimulation of the lower gastrointestinal tract to perturb ongoing autonomic processing. Using ultra-high field fMRI in the anesthetized macaque, we measured the resulting brain activity in subcortical and cortical processing hubs related specifically to a Rectal Distention (RD) paradigm. The resulting functional activations in the periaqueductal gray (PAG), insula, hypothalamus, retro-insular (Ri) cortex, mid-cingulate cortex (MCC), and superior frontal gyrus (SFG) reflect the processing of sensory information from the viscera by the homeostatic afferent network and the activation of emotional arousal centers. Such results exhibit, for the first time, the BOLD correlates of RD in the macaque monkey, highlighting brain function related to visceral processing and the topographic localization within the insula's Primary Interoceptive Cortex (PIC).

KEYWORDS

Viscera, rectal distention, autonomic nervous system, non-human primates, insula, gastrointestinal (GI) tract

INTRODUCTION

The physiological processes supporting visceral activity occur within an integrated network of autonomic nervous system activity and bottom-up signaling by visceral afferents to the cortex. This network supports the body-brain axis and provides a basis for emotional embodiment and higher-order aspects of cognitive processing (Tillisch & Mayer, 2016). In turn, the cortex modulates visceral activity, whether directly or indirectly, with regards to one's emotional (Cannon, 1929;

Mayer, 2011) and physiological state (James, 1884). To further understand the functional neuroanatomical basis for brain-gut interactions, our work studied the relationship between subcortical and cortical processing during controlled changes in autonomic nervous system (ANS) activity.

Visceral processes, such as, slow-wave oscillations produced by the pacemaker cells of the gastrointestinal (GI) tract (Mayer, 2011), are relayed by unmyelinated and thinly myelinated (Aδ) afferent fibers, which link the enteric nervous system to the CNS (Sanders, Koh, & Ward, 2006). Given the types of innervating fibers, two possible ascending streams relay GI information, that through the spinal cord (spinothalamic tract) and that by the vagus nerve. The innervating fibers relay to autonomic brainstem nuclei - the nucleus tractus solitarius (NTS) and the dorsal vagal complex (Carabotti et al., 2015; Mayer, 2011), and then to the insular cortex, via the ventromedial thalamus (Gwyn, Leslie, & Hopkins, 1985; Mayer, Naliboff, & Craig, 2006). The ventromedial thalamus can be subdivided into a posterior (VMpo) and basal (VMb) portion, whereby spinothalamic and vagal (including cranial) afferents are respectively relayed.

The dorsal fundus of the insular cortex is commonly referred to as the Primary Interoceptive Cortex (PIC), given its predominant reception of visceral (vagal, trigeminal and spinothalamic lamina I) afferents and the processing of information related to the body's physiological state, or interoception. Such information includes cutaneous temperature (Craig, et al., 2000), pain (Craig, 2004), and itch (Andrew and Craig, 2001). These homeostatic afferents form an interotopic sensory representation, organized from foot-to-head along the posteroanterior axis of the insular cortex (Craig, 2015), whereby spinal afferents from VMpo are represented more posteriorly than vagal afferents from VMb.

Previous research in humans, using functional magnetic resonance imaging (fMRI), has largely studied how abnormal processing of visceral sensation differs from healthy controls. In the case of irritable bowel syndrome (IBS), it has been evidenced that alterations in reflexive and perceptual responses leads to symptoms of visceral pain (Mayer et al., 2006). Studies using fMRI have found that, in healthy individuals, distention of the rectum leads to increased activity in the ventromedial thalamus and insula (Mayer et al., 2006) as well as the retro-insula (Tillisch & Mayer, 2016). In comparison to normal viscerosensory relay to the CNS, studies where the sensation was perceived as emotionally salient, additionally activated limbic structures and the midbrain (Larsson et al., 2012).

While the extent of which the CNS controls and regulates visceral (i.e., gastrointestinal) processes remains unclear, it appears that cytoarchitectonically distinct insular regions may subserve different sensory and motoric processes (Mayer et al., 2006; Song et al., 2006; Yuan et al., 2003). The general framework of insular processing is that the dorsal granular aspects (i.e. the PIC) receive sensory input from the thalamus and relay this information anteriorly to the agranular aspect via the central dysgranular insular cortex, ultimately leading to a re-representation of sensory information with a gradient incorporating affective valance and emotional constructs reflecting the perceived sensation in coordination with the anterior insula (Evrard, 2018; Jezzini et al., 2015; Menon & Uddin, 2010; Craig, 2009). The ventral anterior insular cortex (vAIC) is a major constituent of the emotional arousal network and is reciprocally connected not only to limbic structures but also to high-order cortical regions supporting the awareness of sensations and emotional states, such as, the orbitofrontal cortex and anterior cingulate cortex (Adolfi et al., 2017; Führer, Zysset, & Stumvoll, 2008; Rolls, Grabenhorst, & Parris, 2008). With this, the interaction between viscera and cortex could support a "gut-feeling" mediated by emotional awareness. The localization of feelings to specific parts of the body has been reported previously by (Nummenmaa et al., 2014), with, for example, warm emotions (e.g., fear and anxiety) localized to the body's core and cool emotions (e.g., sadness and depression) localized to the limbs.

Here, we aimed to acquire data that could be used to assess, within the context of functional processing, the anatomical link, as previously outlined in animal models (Aziz et al., 2000; Bernhardt & Singer, 2012; Rubio et al., 2015), between viscera and cortex. To examine the brain activity correlated with rectal distention, we introduced an inflatable balloon to distend the rectum during imaging of the blood-oxygen-level-dependent (BOLD) contrast by fMRI in the anesthetized *Macaca mulatta*. A subsequent calculation of BOLD activity underlying the stimulus conditions (*Rest*, intraluminal balloon *Inflation* and *Deflation*) identified several areas responsive to rectal distention within the homeostatic afferent and emotional arousal networks, including the insula, cingulate cortex and hypothalamus. Further, the intra-insular connectivity was analyzed to parse the relationship of functional processing across the different cytoarchitectonic realms of the insular cortex.

MATERIALS AND METHODS

Subjects

This study employed 10 rhesus macaque monkeys (*Macaca mulatta*; 6 females; average weight: 8.36 kg). Animals were treated according to the guidelines of the European Parliament and Council Directive 2010/63/EU on the protection of animals used for experimental and other scientific purposes. Our protocol (KY/13) was approved by the local German authorities.

Anesthesia

Before commencing an experiment, animals were pre-sedated with glycopyrrolate (Robinul, 0.01 mg/kg, i.m., anticholinergic) and ketamine (15 mg/kg, i.m., dissociative anesthetic). After transport to the experimental setup, they were anesthetized with sequential injections of fentanyl (3 μg/kg, i.v., analgesic), thiopental (5 mg/kg, i.v., hypnotic), and succinylcholine chloride (3 mg/kg, i.v., muscle relaxant). They were then intubated and ventilated (24 strokes/min) throughout the procedure, using 100% oxygen during preparation, and 21% oxygen during functional data acquisition. The anesthesia parameters had previously been optimized for imaging BOLD signal changes and recording neuronal activity (Logothetis et al., 2012). After intubation, the anesthesia was maintained using a combination of remifentanil (1-3 μg/kg/min, analgesic and anesthetic) and mivacurium chloride (5-7 mg/kg/h, muscle relaxant). The physiological state of the animal was continuously monitored using infrared pulse oximetry (Nonin Medical Inc., Plymouth, MN, USA), electrocardiography (ECG), thermometry, and sphygmomanometry. A rectal thermometer continuously measured body temperature, which was regulated using a water-heating pad to maintain a body temperature within normal physiological range (38.3 – 38.8 °C). In order to attain physiological values optimal for fMRI, body temperature was maintained at 38-39ºC, and end-tidal CO_2 and oxygen saturation were kept constant at 33 mmHg and over 95%, respectively. Acidosis was prevented by the administration of lactated Ringer's solution with 2.5% glucose, infused at 10 ml/kg /h, and intravascular volume was maintained by the additional administration of colloids (hydroxyethyl starch, 20-30ml over 1-2 minutes or 20 ml/kg/h). Once positioned in a custom-designed MR-compatible chair, anesthetized animals were had their legs wrapped from toe to pelvis to prevent venostasis. All physiological monitoring sensors (noted above) were secured with medical tape and the torso and arms were snugly wrapped in towels to maintain temperature and prevent obstruction of blood flow and airways.

Electrogastrogram

In an independent anesthetized recording experiment (n = 3; 3 female) without fMRI, a 3-channel electrogastrogram (EGG) was placed in triangular formation over the naval region of the macaque as depicted in Figure 5a. The three leads used were the same type of leads as used for recording the ECG. Recorded signals were relayed to an in-house 32-channel preamplifier and Alpha Omega multi-channel processor (Alpha Omega Engineering, Nazareth, Israel). Signals were digitized at 20.83 kHz with 16-bit resolution (National Instruments, Austin, TX, U.S.A.).

The EGG signal was used to determine the representative peak frequency during our opiate-based anesthesia protocol. The traces was low-pass filtered and resampled before performing a fast Fourier transformation to examine the underlying frequencies. The parameters for filtering and the method for identifying the representative peak frequency were employed as previously reported (Richter et al , 2016; Rebollo et al., 2018).

Stimulus Preparation

Animals were placed into a head-fixed frame fit with a two-channel MRI receiver-transmitter coil and a biocompatible balloon with infinite compliance until a maximum volume of 100 mL (inflated width: 5 cm) was compressed, lubricated with Vaseline©, and introduced into the rectum. Since an assessment of perceived sensation and pain could not be made in an anesthetized animal; the volumetric amount was set to a level adequate to evoke an observable distention of the rectum as confirmed by sonographic visualization, the range was similar across animals (mean: 0.025 mm^3 at 20 mmHg). An internal manometer placed within the balloon tubing measured the mechanical pressure associated with air pressure inside the balloon, ranging from -25 – 25 mmHg (Fig. 1, top).

The distal opening of the catheter was attached to a 3-port stopcock connecting a manometer (Soliton Laser- und Messtechnik GmbH, München), to continuously measure the pressure within the balloon, and extension tubing (total length: 5.5 m), which connected to the barostat pump (Distender II; G&J Electronics Inc, Toronto, Ontario, Canada) a safe distance away from the MRI magnet (Mugie et al., 2015). The barostat controlled the inflation and deflation of the balloon with air, and continuously monitored the volume and pressure inside the balloon. Once in place, the balloon unfolded by slowly injecting air under controlled pressure (<20 mmHg) and was then completely deflated. The rectal distention (RD) paradigm (depicted in Fig. 1, bottom) included

three conditions: Inflation (I), Deflation (D) and Rest (R), whereby period I consisted of a 4 sec graded increase in pressure, followed by a 6 sec sustained increase in intraluminal pressure (rectal balloon inflation), then by a graded 4 sec period over which the balloon was deflated. The inter-stimulus trial period was between 16 - 36 seconds. This amounted to 15 - 20 trials per session (in 10 minute runs) and an average of 6 sessions per experiment.

Image Acquisition

Neuroimaging data were acquired using a 7 Tesla vertical Nuclear Magnetic Resonance (NMR) scanner (Bruker, Billerica, MA, U.S.A.). Whole-brain functional scans were acquired with multi-shot gradient-echo echo planar imaging (GE-EPI; 1x1 mm^2 in-plane resolution; flip angle: 53°; TR/TE: 2000/19 ms; 20 axial slices) when using the quadrature coil, and with GRAPPA-accelerated parallel imaging (0.85x0.85 mm^2 in-plane resolution; flip angle: 53°; TR/TE: 1000/18 ms, 18 axial slices) when using the phased-array helmets. Slice volumes were acquired in contiguous sections. Both scan sequences had the same matrix size (128x128), field-of-view (FOV; 96x96 mm^2) and slice thickness (2 mm). Within one experimental session GE-EPI scans were collected for the RD study and, in pseudo-randomized order, GE-EPI scans before and/or after the RD scans were

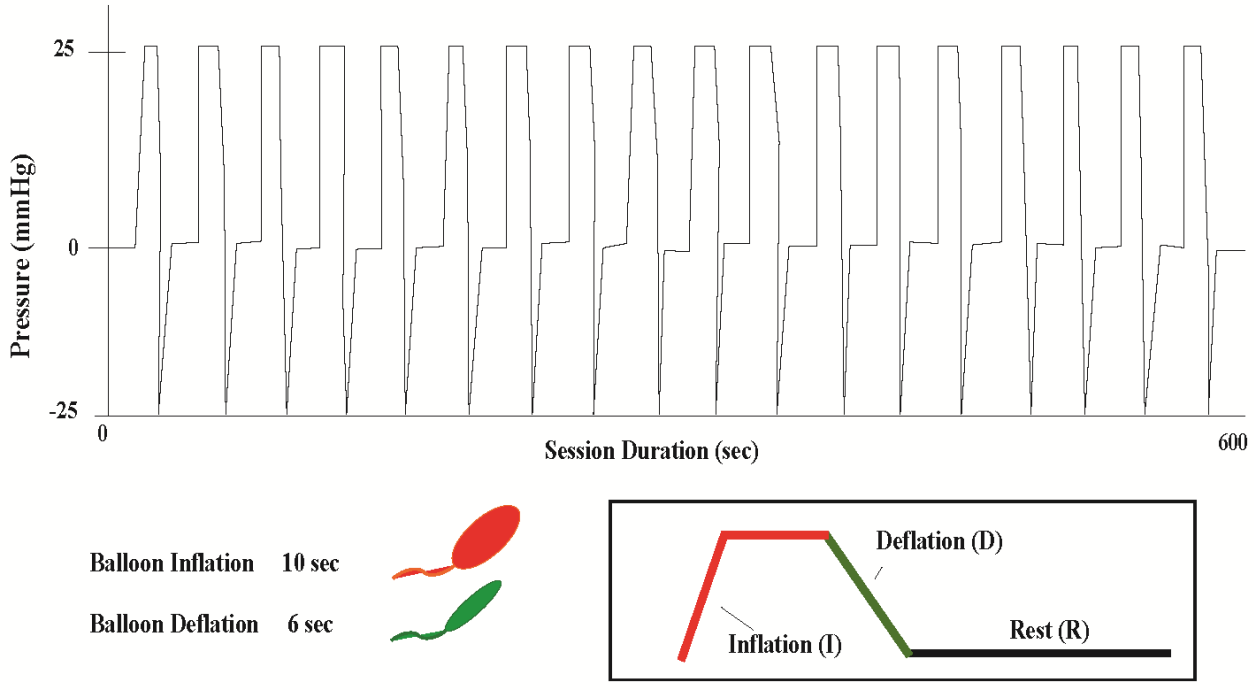

Fig. 1: Example of a 600 sec manometer recording from a single rectal distention (RD) session. During one complete functional scan 15-20 trials of balloon inflation and deflation were sequenced with an inter-stimulus interval (ISI) of 16 – 36 sec.

run with the application of other sensory stimulus types (e.g. taste, visual, cutaneous temperature), as part of a broader project to map multi-modal functional responses to interoceptive stimuli.

During each experiment, a T2-weighted Rapid Imaging with Refocused Echoes (RARE) scan was collected to image the native structural space (FOV: 96x96 mm^2; matrix size: 256x256; 8 segments; flip angle: 8°; TR/TE: 4000-6500/25-48 msec; 40 slices). A three-dimensional anatomical scan was acquired for each subject using a T1-weighted modified driven equilibrium Fourier transform scan (MDEFT; FOV: 128x128 mm^2; matrix size: 256x256; 4 segments; flip angle: 20°; TR/TE: 15/4.5 msec; 136 slices).

Image Pre-Processing and Normalization

Acquired data were converted from Bruker file format to an SPM-readable file format (.nii or .hdr/.img). Functional volumes were manually examined for ghosting and signal dropout artifacts using MRIcro (version: 1.40). Individual volumes that exhibited artifacts were extracted from the time series; runs were excluded if more than 5% of frames exhibited artifacts. The resulting functional data were realigned using SPM12 (Statistical Parametric Mapping; Wellcome Department of Imaging Neuroscience, London, UK) to obtain 6 rigid-body transformation parameters, and then coregistered to each subject's native anatomical (RARE) scan. A visual examination of the coregistration was done before normalization.

An individual's MDEFT was normalized to a high-resolution digital surrogate of the D99 atlas (Saleem & Logothetis, 2007) using AFNI (Cox, 1996) and open-source code (Reveley et al., 2016). The results were visually examined for each case. Each subject's native 2D anatomical (RARE) scan was linearly aligned to the normalized MDEFT and subsequently warped using an in-house MATLAB (Version 2017b, MathWorks, U.S.A.) function for nonlinear transformations. The resulting transformation matrix was applied to the functional images (already coregistered to the native RARE) and smoothed using a 2 mm FWHM Gaussian kernel. At each step, the spatial alignment was checked manually during visual examination. An analysis of the resulting spatial disparity between functional images and template was below that of the applied smoothing kernel. All analysis of single-subject data were made on the normalized (multi-step) EPIs.

Modeling BOLD Responses to Visceral Distention

Single-subject analysis. All runs (scans) collected within one session (day of experimentation) for each monkey were concatenated. The measured BOLD data were modeled by

an event-related univariate General Linear Model (GLM) using SPM12. Each condition (I, D and R) and its temporal derivative was modeled separately and convolved with the canonical hemodynamic response function. Induced visceral pressure, as derived from the manometer recordings, during balloon inflation and deflation was modeled as a covariate regressor in the GLM. Additionally, six parameters obtained by rigid-body head motion correction were included in the model. The data were high-pass filtered with a cutoff of 128 sec and a first-degree autocorrelative model was included to correct for aliasing. GLM parameter estimates (β-weights) were subjected to a *t*-test ($p = 0.05$, corrected for false positives using FWE and FDR correction (depending on the signal-to-noise in the individual data sets) to examine differential BOLD activity. Inferences were made on whole-brain activity minimizing the circularity of results (Kriegeskorte et al., 2009).

Multi-subject (group-level) analysis. Using the same number of scans per experimental session, a non-parametric (permutation) multi-subject t-test was independently calculated for each condition using the scaled individual contrast maps derived at the single-subject level. Nonparametric testing was employed here as it had been shown to trump parametric tests at the group-level (Eklund et al., 2016). Analysis was conducted using two toolboxes: SnPM (Nichols & Holmes, 2001) and LIPSIA (Lohmann et al., 2001), whereby similar results were obtained with both packages. SnPM results are shown in this report. As some experimental sessions had more runs, the analysis was repeated using different sets of scans to test for robustness. Significant differences across paradigm conditions were mapped onto the D99 template brain for the group-level and single-subject level.

Functional Connectivity

ROIs. We examined the BOLD correlates of rectal distention across anatomically distinct regions of the insular cortex, subdivided (Fig. 3a) as per previously reported cyto- and myelo-architectural evidence (Evrard et al., 2014). To examine the underlying functional connectivity, we correlated the group average BOLD time-series between *a priori* defined brain regions, implicated in previous reports of visceral stimulation: the amygdala, cingulate and insular cortices, S1/S2 (post-central gyrus), periaqueductal gray (PAG), ventral striatum, thalamus, and prefrontal cortex (Tillisch & Mayer, 2016), as well as visual cortices (Pigarev, 1994; Pigarev, Almirall, & Pigareva, 2008). We calculated the average normalized band-pass filtered ($0.008 < f < 0.25$ Hz) BOLD signal from regions-of-interest (ROI) over each trial period. These averages represent the deconvolved BOLD

plotted with the standard error of the mean (SEM). A grand mean of each session average was calculated and the resulting trial epoch activity was plotted.

Pearson's Correlation. To examine the relationship between different cortical and subcortical regions, the Pearson's R correlation coefficient was used to calculate the coherence of the average normalized band-pass filtered BOLD signal between different ROIs. To ensure the independence of the ROI analysis from selective analysis, data were split into odd and even runs (Kriegeskorte et al., 2009).

Partial Correlations. This analysis was conducted to test the hypothesis of sensory information re-representation across the different anatomical realms of the insular cortex. Therefore, the average normalized band-pass filtered BOLD signal from bilateral insular subregions (Idfm, Idfp, Idys, vAIC and dAIC) was used to calculate he pairwise partial (conditional) correlation of these regions as a measure of their functional connectivity.

Here, the partial correlation measured the linear relationship between the BOLD signal time-series of two cortical regions with the effects of the remaining regions removed. This abolished confounding effects of insular subregions on each other. We then used the partial correlation connectivity matrix to build a graph of connectivity between insular subregions. To build this graph, we only used correlations that were significantly different from zero (Student's t-distribution test, $\alpha = 0.05$, Bonferroni's correction for 56 comparisons).

RESULTS

We used 7 Tesla fMRI to investigate the BOLD correlates of rectal distention and normalized our results to extrapolate the corresponding activations to the population-level. A total of 129 10 min fMRI runs (scans) were collected, with an average of 12 scans per animal. Two fMRI experiments were subsequently excluded either because of a mechanical or technical default relating to the stimulus paradigm or to the NMR signal transmitter coil.

The group-level activity related to both the Inflation and Deflation periods (Fig. 2) revealed predominant activation in the left insular cortex (as compared to the right), as well as activation in the superior frontal gyrus (SFG), sub-genual anterior cingulate cortex, midcingulate cortex, ventral striatum, hypothalamus, PAG, and V2/V3 ($p = 0.05$, FWE-corrected). Activation of the ventromedial (VM) thalamus was evident from this analysis at a lower threshold for false positive correction ($p = 0.01$, FWE-corrected). A further look at the cross-correlation of VM thalamic activity with cortical and subcortical structures revealed overall low functional connectivity (< 0.5) with

most structures, except for the right VM thalamus and right PAG and the left VM thalamus with the left globus pallidus (Supplement 1).

At the individual-level, significant insular activations occupied the dAIC, Idfm, Idfp, Idys and vAIC (Supplement 2), these same areas were activated at the group level, with the exception of dAIC (Fig. 2). The intra-insular activations were examined further within the context of

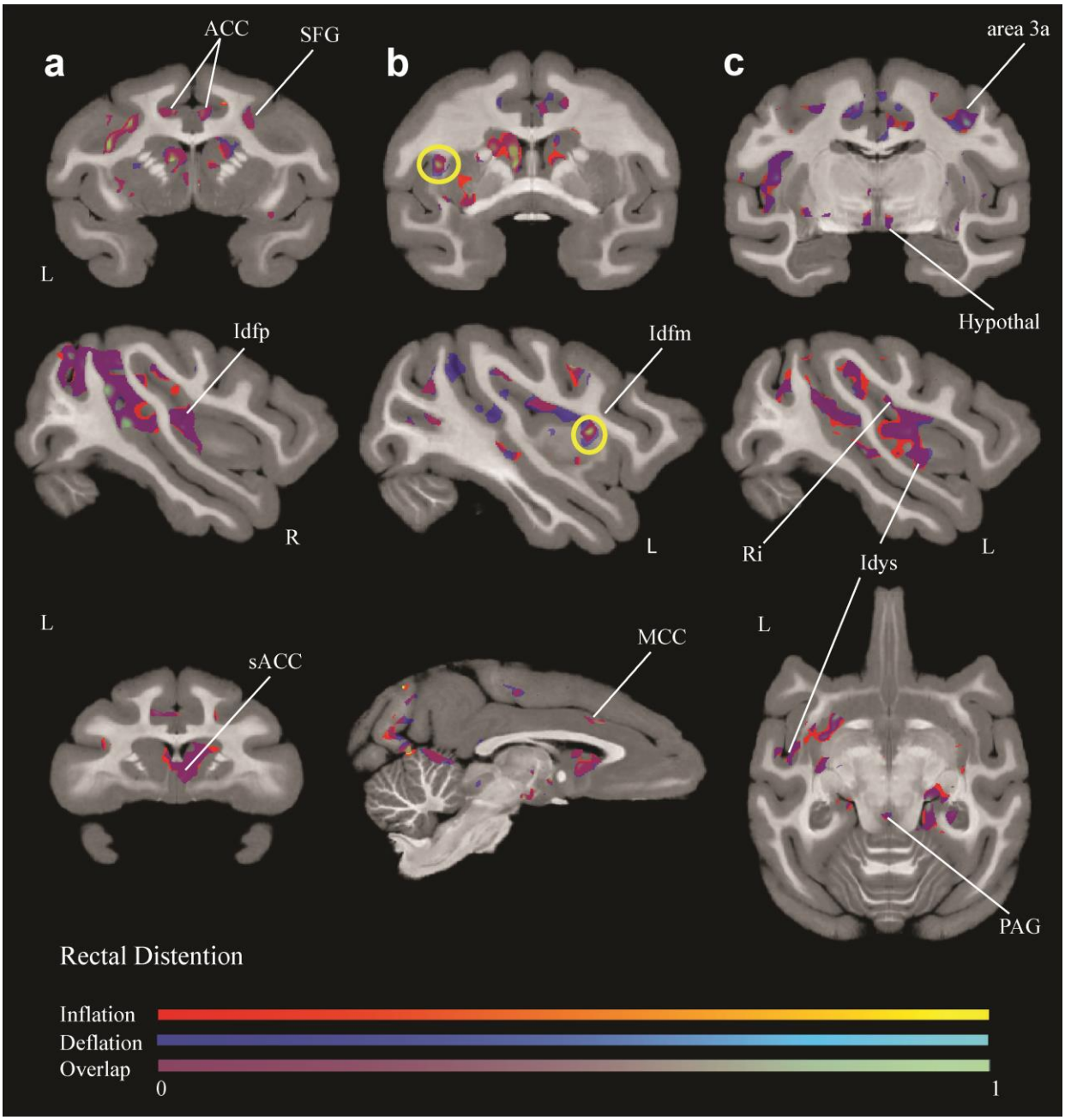

Fig. 2: Group-level representation of brain activity related independently to the inflation and deflation periods and a measurement of overlapping activity (purple – green scale bar). (**a**) – (**c**) Indicate different perspectives throughout the whole brain. Scale values were normalized and FWE-corrected at $p = 0.05$.

anatomically parcellated insular subregions: the granular (dAIC, Idfm, Idfp), dysgranular (Idys) and agranular (vAIC) regions (Fig. 3a). Functional connectivity results derived from the Pearson's correlation between intra-insular subregions found strong correlations ($r \geq 0.8$) between the left Idys and vAIC, right dAIC and Idfm (Fig. 3b) and contralateral dAIC and vAIC (Fig. 3c). Splitting the scans into odd and even runs and re-calculating the correlation did not reveal a significant difference in results (Pearson's coefficient variation ±0.05).

Further, a granular region posterior to the insular dorsal fundus, the retro-insula (Ri), was grouped with the ventroposterior granular insular cortex due to similar functional encoding of vestibular, auditory, whole-body and cardiovascular activity (Evrard, 2018; Gu, 2018; Remedios, Logothetis, & Kayser, 2009). From this parcellation, bilateral Ri activation was evident from the univariate analysis (group-level: Fig. 2; individual-level: Supplement 1) and the left Ri, in particular, was moderately correlated with the ipsilateral Idys and dAIC (Fig. 3b).

Building off the insight garnered from the Pearson correlations, a more unbiased measure of functional connectivity analysis was implemented to calculate the partial correlation between two insular regions without the confounding influence of activity in other anatomical areas (Fig. 4a). Modeling 4 insular nodes per hemisphere, we used the pairwise partial (conditional) correlation of these region to measure their connectivity. We conducted two analyses modeling Idfm and Idfp separately to further parse the functional circuitry would could represent cranial and spinal relays, respectively. The representation of functional connectivity between the insular cortex's subdivisions revealed a strong lateralized effect between the granular (Idfm/Idfp) – dysgranular (Idys) regions and between the dysgranular (Idys) – agranular (vAIC) regions. However, there was one notable distinction and that was the stronger coupling between Idfm and dAIC regions that minimized the strength of connectivity between the granular and dysgranular insular cortex. When modeling Idfp, the main source of functional connectivity with the dorsal anterior insular cortex (dAIC) was largely from the ventral agranular insula (vAIC) and from its contralateral counterpart. Overall, in terms of cross-hemispheric connectivity, each node along the posteroanterior gradient of the insula exhibited strong connectivity with its contralateral counterpart (Fig. 4b,d).

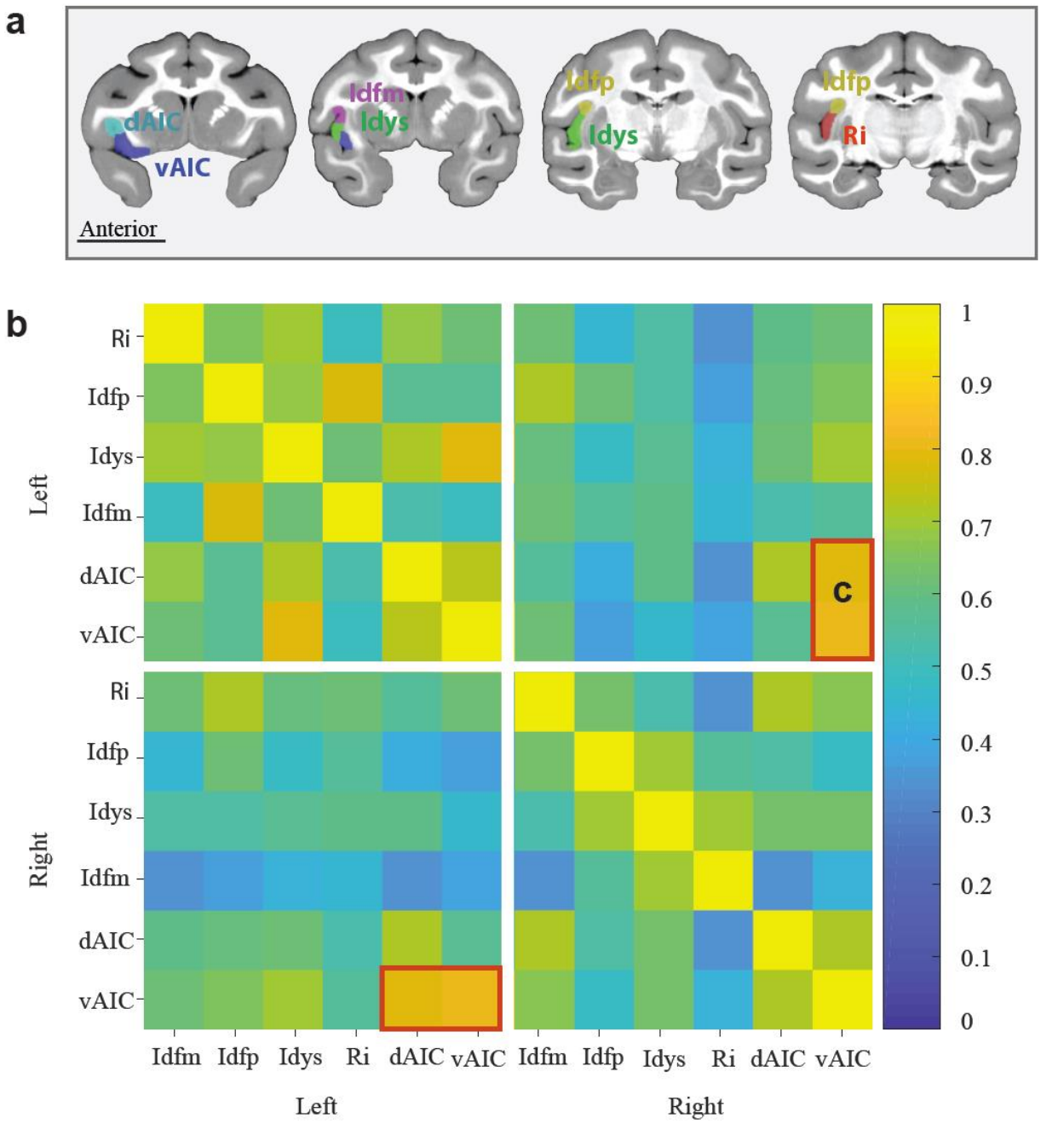

Fig. 3: Intra-insular functional connectivity, as measured by the Pearson's R correlation coefficient, calculated from the average normalized bandpass-filtered BOLD signal of all functional scans. (**a**) The anatomically subdivided insular regions - 6 regions per hemisphere. (**b**) Heat map depicting the strength of correlation between insular subregions and (**c**) the inter-hemispheric connectivity between the dorsal and ventral anterior insular cortex ($r > 0.85$).

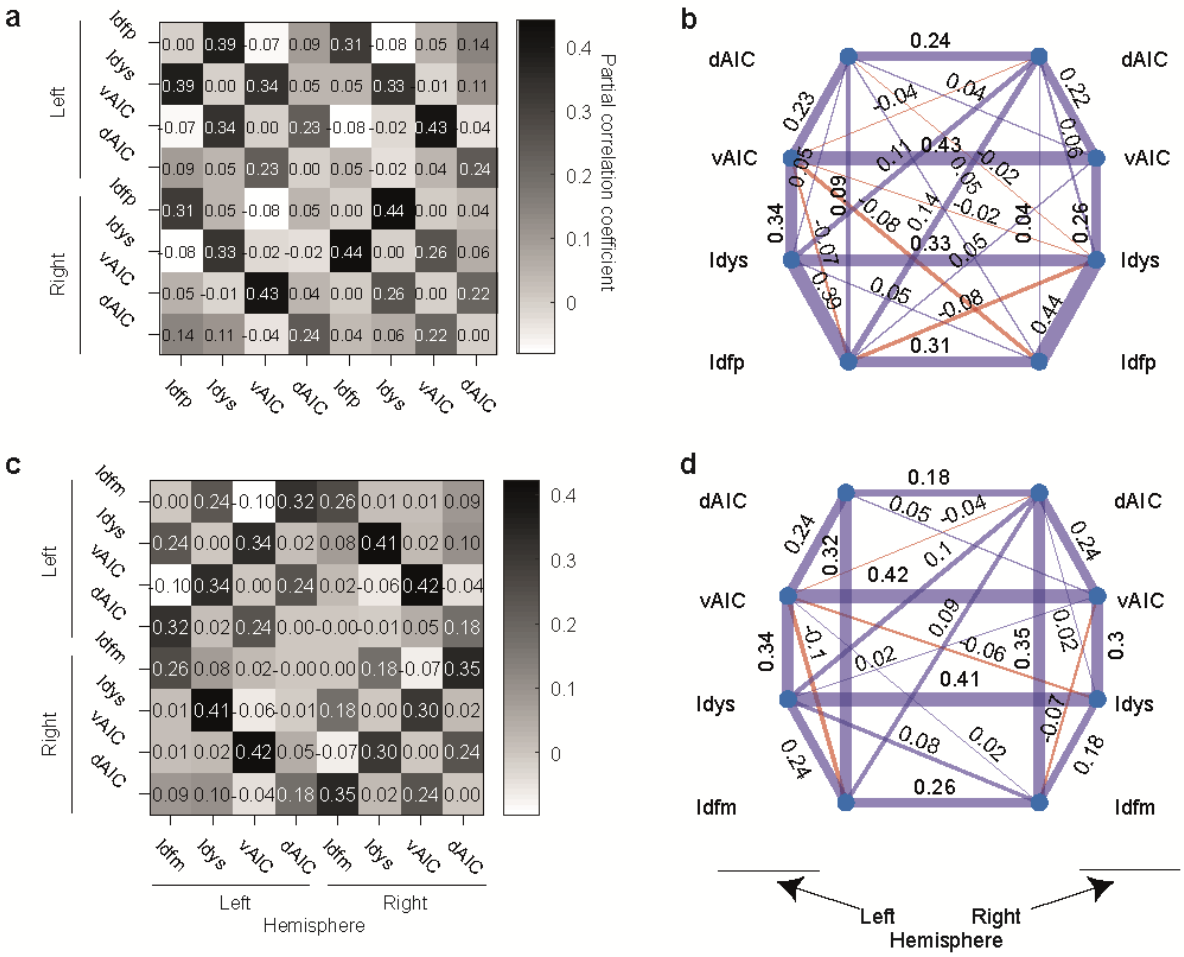

Fig. 4: The (**a, c**) partial correlation connectivity matrix was calculated between two regions with the effects of the remaining regions removed. This matrix was used to build an intrinsic insular connectivity graph with 4 insular nodes per hemisphere (**b**) with Idfp and (**d**) with Idfm to test the connectivity between two functionally different granular regions. To build this graph, only correlations significantly different from zero were used (Student's t-distribution test, $\alpha = 0.05$, Bonferroni's correction for 56 comparisons).

A further analysis of the functional connectivity between brain regions previously described as hubs involved in the homeostatic afferent and emotional arousal networks revealed bilateral PAG connectivity with the hypothalamus (Supplement 1). We also found moderate correlations (> 0.7) between the left habenula and the left pulvinar and bilateral midline thalamus. While the functional connectivity of PBN with most network regions was weak, there were mild correlations ($r \geq 0.6$) between PBN and the hypothalamus and PAG (Supplement 1). In most cases, the ventral extent of the fMRI slice acquisition excluded medullar nuclei (i.e. NTS and DMVN).

The electrogastrogram (EGG) was recorded in the macaque monkey at rest during our opiate-based anesthesia protocol. Channel 3 served as the ground and the power frequency spectrum of channels 1 and 2 were plotted, revealing peak gastric frequency between 0.02 – 0.11 Hz (Fig. 5b). The resulting frequency was compared to that of awake macaque monkeys and humans.

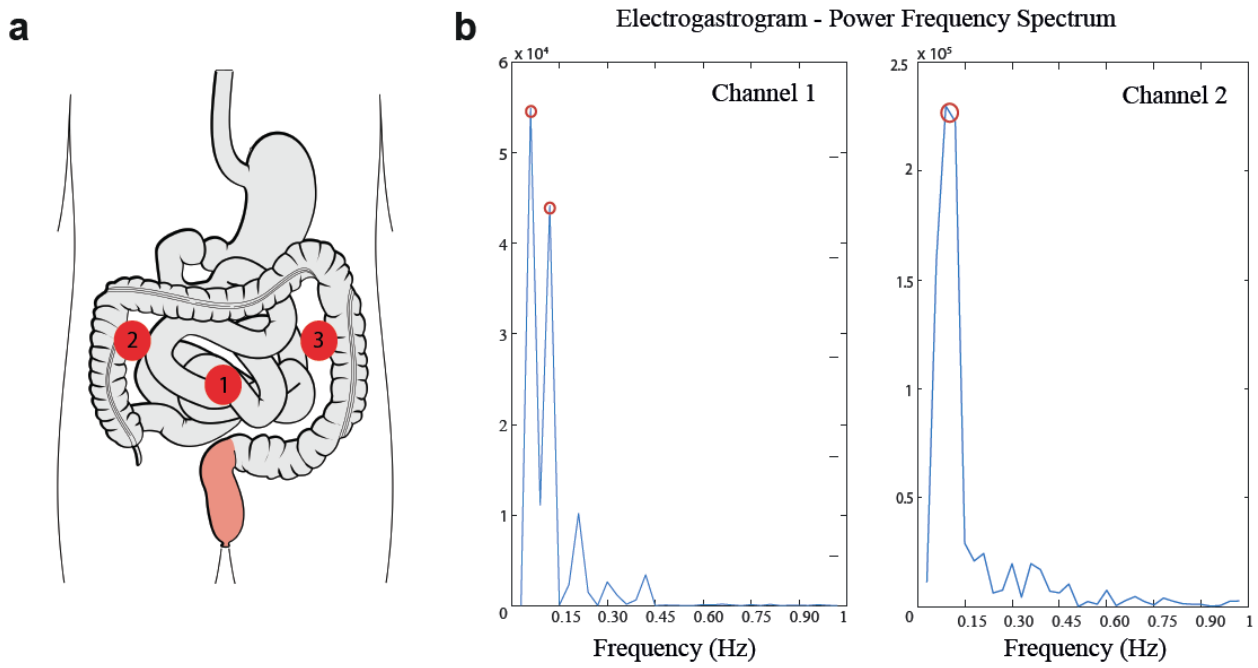

Fig. 5: The (**a**) attachment of electrode leads to the naval region of the macaque monkey resulted in the recording of resting gastric activity (electrogastrogam, EGG) under the opiate-based anesthesia protocol executed during these experiments. Channel 3 served as the ground and the (**b**) power frequency spectrum of channels 1 and 2 were plotted for one monkey, revealing peak gastric frequency between 0.02 – 0.11 Hz.

DISCUSSION

This work serves to elucidate the cortical and subcortical activations related to the processing of lower gastrointestinal activity within the context of interoceptive information relay from the body to the brain. Overall, the functional activation patterns related to the distention paradigm reflect the reception of visceral afferent information by the brain and suggest coordination between limbic and cortical structures involved in interoceptive processing and emotional arousal. Further, we aimed to understand the functional connectivity between cytoarchitectonically distinct subregions of the insular cortex.

From our in-depth analysis of the insula's intrinsic connectivity, it became apparent that distinct anatomical nodes within this cortical region were not only laterally connected in a specific

pattern but also cross-hemispherically. The functional connectivity results support the hypothesis of a re-representation of lateral spinothalamic afferents by the dysgranular insula (Idys) and relay of such information to higher-order insular regions, namely the vAIC and dAIC. However, it may be that cranial and vagal afferents that enter the CNS at the medullar level and innervate the granular insula more anteriorly, such as Idfm, are more connected with dAIC than Idys. This connectivity could represent two ascending streams relaying information from the gastrointestinal tract.

The AIC areas are involved in more complex aspects of sensory processing (e.g., the cognitive, emotional and social aspects). For instance, the AIC serves a crucial role in the affective evaluation of salient stimuli that may represent subjective differences in interoceptive processes. In our study, the spatial extent of AIC activity and its localization was variable across subjects, likely reflecting an individual difference in evaluating interoceptive processes (Chong, Ng, Lee, & Zhou, 2017) and visceral sensitivity (Icenhour et al., 2017). Such results indicate a degree of inter-individual variability and complexity in AIC activity as related to rectal distention. Since the dAIC activation, as shown by the GLM, is only evident at the individual subject level, its specific localization could vary amongst individual brain states. In this case, the dysgranular activity is more robust across experiments and may serve as a reliable area associated with vAIC processing.

Recent retrograde tract-tracer injections in the macaque stomach by Levinthal, Dumm and Strick (2018) provide anatomical evidence for the efferent connections from the "mid-ventral" insula to the gastrointestinal tract. Additionally, it has been shown that the Idys (mid-ventral insula) projects to the PBN (Saleh et al., 2016). This anatomical evidence seems to support a top-down pathway for the dysgranular insula to modulate ANS and visceral activity (e.g. peristalsis) and provide support for the gut-brain axis (Mayer et al., 2006; Small & Difeliceantonio, 2019).

With that said, we know that the vAIC also projects down to homeostatic relay centers in the brainstem (Chavez et al., 2018); however, the top-down modulation by vAIC may influence more emotional arousal centers (i.e., PAG) and emotive behavior. The dorsal anterior cingulate cortex, a higher-order region reciprocally connected to the vAIC, is also known to modulate effector systems (Mayer et al., 2006), together these regions may support more of the emotional processing, while the dysgranular insula supports the visceral homeostasis. One functional notion of support for such thought is provided by the effect of microstimulating the dysgranular insula of macaque monkeys, which results in a change in heart rate activity (Caruana et al., 2011).

Subcortical regions implicated in emotional arousal (e.g. dorsal striatum and PAG) were previously shown to respond to visceral sensations (Thayer & Lane, 2000). Furthermore, activity in higher-order cortical structures, such as the anterior cingulate and prefrontal cortices (Lane et al., 1997) and the SFG (Fried et al., 1998), were also implicated in emotional information processing. Here, we identified activity in such subcortical and cortical regions as correlated to the processing of visceral distention. Overall, it largely appeared that regions in both the emotional arousal and homeostatic afferent network were activated.

The physiological changes induced by the distention paradigm, such as, rectal sphincter relaxation and increased peristalsis, are largely mediated by the sacral parasympathetic nervous system (Kellow, Gill, & Wingate, 1987). While it is known that there is a lateralized innervation of the GI by vagal fibers, the GI is also innervated by unmyelinated and thinly myelinated fibers which ascend through the lamina I of the lateral spinothalamic tract (Umans & Liberler, 2018; Beyak & Vanner, 2004). DRG afferents ultimately enter the posterior part of the ventromedial nucleus in a topographically organized manner. We know that from studies of other interoceptive modalities where topography is maintained (Craig, 2014), this specific organization is also seen in the insular cortex (Craig et al., 2009). Thus, it would appear that the foot-to-head topography, whereby the foot is aligned posteriorly along the thalamic and insular axes, would situate inputs from the sacral spinal cord along posterior granular aspects of the insular cortex. We showed that Ri and Idfp were bilaterally activated and together may potentially represent a sacral representation. The left lateralized activation in the mid-anterior granular insular cortex (Idfm) may represent inputs from the vagal innervations, as literature has suggested that parasympathetic mechanisms predominantly drive left hemispheric activity (Oppenheimer, Kedem, & Use, 1996; Wittling et al., 1998) and support vagal interoception (Maniscalco & Rinaman, 2018).

Distention of the rectum entrains intrinsic slow-wave activity (Kellow et al., 1987) and signals for motor control over gastric motility (Huizinga & Lammers, 2009). An electrogastrogram (EGG) is often used to record the underlying slow-wave GI activity. In humans, the frequency of this activity amounts to 0.03 – 0.07 Hz and is phase-locked to neural activity at 0.5 Hz in gastric processing centers, as measured by electroencephalography (Richter et al , 2016) and BOLD fMRI (Rebollo et al., 2018). Independent recordings of the macaque GI, using EGG both under our opiate-based anesthesia protocol and during the awake-behaving state (Bruley et al., 1991), measured a peak gastric frequency between 0.02 – 0.11 Hz. With simultaneous EGG and neural measurements

in future studies, a claim could be made about the gut-brain connection in non-human primates and its similarity to the human gut-brain axis.

Tillisch, Mayer & Labus (2016) conducted a meta-analysis of rectal distention data from healthy controls and patients with IBS and found consistent activation in regions associated with visceral afferent processing (e.g. thalamus, insula, anterior mid-cingulate), irrespective of pathology. In previous studies, IBS patients have exhibited a greater engagement of regions associated with emotional arousal [limbic regions] and endogenous pain modulation, whereby the latter is functionally linked to midbrain (i.e., PBN) activity (Mayer et al., 2006; Song et al., 2006). Our work studied these networks under an opiate-based general anesthesia protocol, whereby the transmission of sensory information to the thalamus and cortical areas is similar to the awake state (Ku et al., 2011; Pfeuffer et al., 2004). However while the sensory afferent relay seems unperturbed, the PBN - a key regulator of endogenous arousal - appears to remain in an unmodulated, slow-wave state during general anesthesia (Yu et al., 2018). In our healthy subject pool, PBN responses were not as great as responses from other limbic regions during the stimulation (e.g., hypothalamus and PAG). This could signal a lack of emotional arousal at the midbrain level and recruitment of other limbic structures associated with this network. Whether recruitment of limbic structures in the anesthetized state is related to the salience of the stimulus remains to be determined.

Isolating pain-related responses from rectal distention here was not possible without indicative feedback on the presence of pain or from recordings of the viscera's innervating fibers. Using percept-related fMRI, feedback from participating subjects during non-painful and painful rectal distention was used to independently correlate sensations of distention and pain to different regions of activation (Kwan et al., 2005). It was noted that whether the distention was painful or not, the mid-insular cortex, left AIC, Idfp and Ri were activated in healthy participants. In an additional study of painful and non-painful rectal distention, the non-painful stimulus drove activation in the insula, anterior cingulate cortex and prefrontal cortex (Moisset et al., 2010; Ladabaum et al., 2007). Other rectal distention studies have localized ventromedial thalamus and insular activity (Tillisch & Mayer, 2016) and retro-insula (Larsson et al., 2012). With consideration to the work in humans, our fMRI results expose a gross similarity in functional patterns; however, the lateralization of AIC and PFC activation should be examined further as it appears to be related to the perceived intensity of distention pressure (Kwan et al., 2005; Bittorf et al., 2006).

It is evident from previous work done in monkeys (Pigarev, 1994; Pigarev, Almirall, & Pigareva, 2008) that the processing of stimuli from the viscera evokes activation in primary visual processing regions. Such heightened activity in visual areas could signal a necessary recruitment of additional sensory areas to efficiently process salient stimuli at the global level. Additional studies are needed to further examine the relationship between the processing of visceral, salient stimuli and the recruitment of additional sensory modality processing areas. Tallon-Baudry and colleagues had reported activations along the visual stream and lateral geniculate nucleus by rectal distention in humans, areas we found similarly activated in the macaque monkey. This group and others additionally showed activation in the posterior parietal cortex related to visceral processing (Rebollo et al., 2018; Mugie et al., 2017; Kwan et al., 2005). This could likely be explained by the presence of neuropeptides, synthetized by the gut, present in parietal areas, such as VIP and SST, and the link between these regions to the visual and limbic systems (Veit et al., 2017).

Overall, we obtained ultra-high field fMRI data during rectal distention (RD) in an unprecedented large sample of macaque monkeys. We analyzed the intrinsic functional connectivity of the insular cortex, the primary cortical region receiving afferents from the viscera, and provided strong evidence for a sequential processing of sensory information along the insula's posteroanterior granular gradient. Additional regions responding to lower GI stimulation paradigm were reported and two main networks were identified as responsive to stimulation: the homeostatic afferent and emotional arousal networks. Rectal distention has been shown to activate regions within these networks in human studies (Larsson et al., 2012; Moisset et al., 2010; Tillisch & Mayer, 2016), esp. the hypothalamus, cingulate, prefrontal, parietal and insular cortices. Our portrayal of homologous structural activation by the same functional modality in macaques likely indicates a conservation of ANS-driven activity in primates.

ACKNOWLEDGMENTS

We acknowledge Dr. Pedro Douay for performing the sonograms and providing medical insight on intraluminal balloon positioning. This work was supported by the Werner Reichardt Centre for Integrative Neuroscience (CIN) at the Eberhard Karls University of Tübingen (CIN is an Excellence Cluster funded by the Deutsche Forschungsgemeinschaft [DFG] within the framework of the Excellence Initiative EXC 307) and by the Max Planck Society. We acknowledge support by the Deutsche Forschungsgemeinschaft and Open Access Publishing Fund of University of Tübingen for the cost of publication.

CONFLICT OF INTEREST STATEMENT

The authors declare having no personal, professional or financial relationships that could potentially be construed as a conflict of interest.

REFERENCES

Adolfi, F., Couto, B., Richter, F., Decety, J., Lopez, J., Sigman, M., Manes F., Ibáñez, A. (2017). Convergence of interoception, emotion, and social cognition: A twofold fMRI meta-analysis and lesion approach. *Cortex*, *88*, 124–142. https://doi.org/10.1016/j.cortex.2016.12.019

Andrew D. and Craig AD. (2001). Spinothalamic lamina I neurons selectively sensitive to histamine: a central neural pathway for itch. *Nature*, *4*(1), 72–77.

Aziz, Q., Thompson, DG., Ng, VWK., Hamdy, S., Sarkar, S., Brammer, MJ., … Williams, SCR. (2000). Cortical Processing of Human Somatic and Visceral Sensation. *The Journal of Neuroscience*, *20*(7), 2657–2663. https://doi.org/10.1016/0959-4388(94)90053-1

Bernhardt, BC., & Singer, T. (2012). The Neural Basis of Empathy. *Annual Review of Neuroscience*, *35*(1), 1–23. https://doi.org/10.1146/annurev-neuro-062111-150536

Beyak, MJ., Ramji, N., Krol, KM., Kawaja, MD., Vanner SJ. (2004). Two TTX-resistant Na+ currents in mouse colonic dorsal root ganglia neurons and their role in colitis-induced hyperexcitability. *Am. J. Physiol. Gastrointest. Liver Physiol., 287,* G845-G855.

Bittorf, B., Ringler, R., Forster, C., Hohenberger, W., Matzel, KE. (2006). Cerebral representation of the anorectum using functional magnetic resonance imaging. *British Journal of Surgery, 93*(10), 1251-1257. https://doi.org/10.1002/bjs.5421

Bruley, S., Varannes, D., Mizrahi, M., & Dubois, A. (1991). Relation between postprandial gastric emptying and cutaneous electrogastrogram in primates. *Am. J. Physiol. 261,* G248-G255.

Kwan, CL., Diamant, NE., Pope, G., Mikula, K., Mikulis, DJ., Davis, KD. (2005). Abnormal forebrain activity in functional bowel disorder patients with chronic pain. *Neurology*, *65*(8), 1268–1277. https://doi.org/10.1212/01.wnl.0000180971.95473.cc

Cannon, WB. (1929). Organization for Physiological Homeostasis. *Physiological Reviews*, *9*(3), 399–431.

Carabotti, M., Scirocco, A., Maselli, MA., & Severi, C. (2015). The gut-brain axis: Interactions between enteric microbiota, central and enteric nervous systems. *Annals of Gastroenterology*, *28*(2), 203–209. https://doi.org/10.1038/ajgsup.2012.3

Caruana, F., Jezzini, A., Sbriscia-Fioretti, B., Rizzolatti, G., & Gallese, V. (2011). Emotional and social behaviors elicited by electrical stimulation of the insula in the macaque monkey. *Current Biology*, *21*(3), 195–199. https://doi.org/10.1016/j.cub.2010.12.042

Chavez, G., Saleh, TS., Horn FM., Evrard HC. (2018) Von Economo and Fork neuron projections to preautonomic nuclei in the macaque monkey. Poster, CIN-NIPS Symposium, 4-5 October.

Chong, JS. X., Ng, GJP., Lee, SC., & Zhou, J. (2017). Salience network connectivity in the insula is associated with individual differences in interoceptive accuracy. *Brain Structure and Function*, *222*(4). https://doi.org/10.1007/s00429-016-1297-7

Cox, RW. (1996). AFNI: Software for Analysis and Visualization of Functional Magnetic Resonance Neuroimages. *Computers and Biomedical Research, 29,* 162-173.

Craig, AD. (2015). *How do you feel?* Princeton University Pres.

Craig, AD. (2014). Topographically Organized Projection to Posterior Insular Cortex from the Posterior Portion of the Ventral Medial Nucleus (VMpo) in the Long-tailed Macaque Monkey. *J Comp Neurol*, *522*(1), 36–63. https://doi.org/10.1016/j.pestbp.2011.02.012.Investigations

Craig, AD. (2009). How do you feel — now? The anterior insula and human awareness. *Nature Reviews Neuroscience*, *10*(1), 59–70. https://doi.org/10.1038/nrn2555

Craig, AD. (2004). Lamina I, but not Lamina V, Spinothalamic Neurons Exhibit Responses That Correspond With Burning Pain. *J Neurophysiol*, *92*. https://doi.org/10.1152/jn.00385.2004

Craig, AD. (2002). How do you feel? Interoception: the sense of the physiological condition of the body. *Nature Reviews Neuroscience*, *3*(August), 655–666. https://doi.org/10.1038/nrn894

Craig, AD., Chen, K., Bandy, D., & Reiman, EM. (2000). Thermosensory activation of insular\rcortex. *Nature Neuroscience*, *3*(2), 184–190.

Eklund, A., Nichols, TE., & Knutsson, H. (2016). Cluster failure: Why fMRI inferences for spatial extent have inflated false-positive rates. *Proceedings of the National Academy of Sciences*, *113*(28), 7900-7905. https://doi.org/10.1073/pnas.1602413113

Evrard, HC., & Craig, AD. (2015). Insular Cortex. *Brain Mapping*, 387–393. https://doi.org/10.1016/B978-0-12-397025-1.00237-2

Evrard, HC. (2018). Von Economo and fork neurons in the monkey insula, implications for evolution of cognition. *Current Opinion in Behavioral Sciences*, *21*, 182–190. https://doi.org/10.1016/j.cobeha.2018.05.006

Fried, I., Wilson, CL., MacDonald, KA., Behnke, EJ. (1998). Electric current stimulates laughter. *Nature, 391*(6668), 650-650. https://doi.org/10.1038/35536

Führer, D., Zysset, S., & Stumvoll, M. (2008). Brain activity in hunger and satiety: an exploratory visually stimulated FMRI study. *Obesity (Silver Spring, Md.)*, *16*(5), 945–950. https://doi.org/10.1038/oby.2008.33

Gu, Y. (2018). Vestibular signals in primate cortex for self-motion perception. *Current Opinion in Neurobiology*, *52*, 10–17. https://doi.org/10.1016/j.conb.2018.04.004

Gwyn, DG., Leslie, RA., & Hopkins, DA. (1985). Observations on the afferent and efferent organization of the vagus nerve and the innervation of the stomach in the squirrel monkey. *The Journal of Comparative Neurology*, *239*(2), 163–175. https://doi.org/10.1002/cne.902390204

Huizinga, JD., & Lammers, WJEP. (2009). Gut peristalsis is governed by a multitude of cooperating mechanisms. *American Journal of Physiology-Gastrointestinal and Liver Physiology*, *296*(1), G1–G8. https://doi.org/10.1152/ajpgi.90380.2008

Icenhour, A., Witt, ST., Elsenbruch, S., Lowén, M., Engström, M., Tillisch, K., … Walter, S. (2017). Brain functional connectivity is associated with visceral sensitivity in women with Irritable Bowel Syndrome. *NeuroImage: Clinical*, *15*, 449–457. https://doi.org/10.1016/J.NICL.2017.06.001

James, W. (1884). What is an emotion? *Mind*, *9*(34), 188–205.

Jezzini, A., Rozzi, S., Borra, E., Gallese, V., Caruana, F., & Gerbella, M. (2015). A shared neural network for emotional expression and perception: an anatomical study in the macaque monkey. *Frontiers in Behavioral Neuroscience*, *9*(September), 1–17. https://doi.org/10.3389/fnbeh.2015.00243

Kellow, JE., Gill, RC., & Wingate, DL. (1987). Modulation of human upper gastrointestinal motility by rectal distension. *Gut*, *28*, 864–868. https://doi.org/10.1136/gut.28.7.864

Kriegeskorte, N., Simmons, W. K., Bellgowan, P. S. F., & Baker, C. I. (2009). Circular analysis in systems neuroscience: the dangers of double dipping. *Nature Neuroscience*, *12*(5), 535–540. https://doi.org/10.1038/nn.230

Ku, SP., Tolias, AS., Logothetis, NK., & Goense, J. (2011). FMRI of the Face-Processing Network in the Ventral Temporal Lobe of Awake and Anesthetized Macaques. *Neuron*, *70*(2), 352–362. https://doi.org/10.1016/j.neuron.2011.02.048

Ladabaum, U., Roberts, TP., McGonigle, DJ. (2007). Gastric fundic distension activates fronto-limbic structures but not primary somatosensory cortex: A functional magnetic resonance imaging study. *NeuroImage*, *34*(2), 724–732. https://doi.org/10.1016/j.neuroimage.2006.07.033

Lane, RD., Fink, GR., Chau, PML., Dolan, RJ. (1997). Neural activation during selective attention to subjective emotional responses. *NeuroReport, 8,* 3969-3972.

Larsson, MBO., Tillisch, K., Craig, AD., Engström, M., Labus, J., Naliboff, B., … Walter, SA. (2012). Brain responses to visceral stimuli reflect visceral sensitivity thresholds in patients with irritable bowel syndrome.

Gastroenterology, *142*(3), 463-472.e3. https://doi.org/10.1053/j.gastro.2011.11.022

Levinthal, DJ., Dum, RP., Strick, PL. (2018). Cortical control of the stomach and its potential relevance to Alzzheimer's disease. Poster. *Society for Neuroscience.* 6, November 2019.

Logothetis, NK., Eschenko, O., Murayama, Y., Augath, M., Steudel, T., Evrard, HC., … Oeltermann, A. (2012). Hippocampal-cortical interaction during periods of subcortical silence. *Nature*, *491*(7425), 547–553. https://doi.org/10.1038/nature11618

Lohmann, G., Müller, K., Bosch, V., Mentzel, H., Hessler, S., Chen, L., … von Cramon, DY. (2001). Lipsia—a new software system for the evaluation of functional magnetic resonance images of the human brain. *Computerized Medical Imaging and Graphics*, *25*(6), 449–457. https://doi.org/10.1016/S0895-6111(01)00008-8

Maniscalco, JW., & Rinaman, L. (2018). Vagal Interoceptive Modulation of Motivated Behavior. *Physiology, 33*, 151–167. https://doi.org/10.1152/physiol.00036.2017

Mayer, EA. (2011). Gut feelings: the emerging biology of gut-brain communication. *Nature Reviews. Neuroscience*, *12*(8), 453–466. https://doi.org/10.1038/nrn3071

Mayer, EA., Naliboff, BD., & Craig, AD. (2006). Neuroimaging of the Brain-Gut Axis: From Basic Understanding to Treatment of Functional GI Disorders. *Gastroenterology*, *131*(6), 1925–1942. https://doi.org/10.1053/j.gastro.2006.10.026

Menon, V., & Uddin, LQ. (2010). Saliency, switching, attention and control: a network model of insula function. *Brain Structure and Function*, *214*(5–6), 1–13. https://doi.org/10.1007/s00429-010-0262-0

Moisset, X., Bouhassira, D., Denis, D., Dominique, G., Benoit, C., & Sabaté, JM. (2010). Anatomical connections between brain areas activated during rectal distension in healthy volunteers: A visceral pain network. *European Journal of Pain*, *14*(2), 142–148. https://doi.org/10.1016/j.ejpain.2009.04.011

Nichols, TE., & Holmes, AP. (2002). Nonparametric permutation tests for functional neuroimaging: A primer with examples. *Human Brain Mapping*, *15*(1), 1–25. https://doi.org/10.1002/hbm.1058

Nummenmaa, L., Glerean, E., Hari, R., Hietanen, JK. (2014). Bodily maps of emotions. *Proceedings of the National Academy of Sciences of the United States of America, 111*(2), 646-651. https://doi.org/10.1073/pnas.1321664111

Oppenheimer, SM., Kedem, G., Martin, WM. (1996). Left-insular cortex lesions perturb cardiac autonomic tone in humans. *Research Paper Clinical Autonomic Research*, 6, 131-140.

Pfeuffer, J., Merkle, H., Beyerlein, M., Steudel, T., & Logothetis, NK. (2004). Anatomical and functional MR imaging in the macaque monkey using a vertical large-bore 7 Tesla setup. *Magnetic Resonance Imaging*, *22*(10 SPEC. ISS.), 1343–1359. https://doi.org/10.1016/j.mri.2004.10.004

Pigarev, IN. (1994). Neurons of visual cortex respond to visceral stimulation during slow wave sleep. *Neuroscience*, *62*(4), 1237–1243. https://doi.org/10.1016/0306-4522(94)90355-7

Pigarev, IN, Almirall, H., & Pigareva, ML. (2008). Cortical evoked responses to magnetic stimulation of macaque' s abdominal wall in sleep-wake cycle. *Acta Neurobiologiae Experimentalis (Warsaw)*, *68*, 91–96.

Rebollo, I., Devauchelle, AD., Béranger, B., & Tallon-Baudry, C. (2018). Stomach-brain synchrony reveals a novel, delayed-connectivity resting-state network in humans. *ELife*, *7*, 1–25. https://doi.org/10.7554/eLife.33321

Remedios, R., Logothetis, NK., & Kayser, C. (2009). An Auditory Region in the Primate Insular Cortex Responding Preferentially to Vocal Communication Sounds. *Journal of Neuroscience*, *29*(4), 1034–1045. https://doi.org/10.1523/JNEUROSCI.4089-08.2009

Reveley, C., Gruslys, A., Ye, FQ., Glen, D., Samaha, J., E. Russ, B., … Saleem, KS. (2016). Three-Dimensional Digital Template Atlas of the Macaque Brain. *Cerebral Cortex*, 1–15. https://doi.org/10.1093/cercor/bhw248

Richter, CG., Babo-Rebelo, M., Schwartz, D., & Tallon-Baudry, C. (2016). Phase-amplitude coupling at the

organism level: the amplitude of spontaneous alpha rhythm fluctuations varies with the phase of the infra-slow gastric basal rhythm. *NeuroImage*. https://doi.org/10.1016/j.neuroimage.2016.08.043

Rolls, ET., Grabenhorst, F., & Parris, BA. (2008). Warm pleasant feelings in the brain. *NeuroImage*, *41*(4), 1504–1513. https://doi.org/10.1016/j.neuroimage.2008.03.005

Rubio, A., Van Oudenhove, L., Pellissier, S., Ly, HG., Dupont, P., de Micheaux, HL., … Bonaz, B. (2015). Uncertainty in anticipation of uncomfortable rectal distension is modulated by the autonomic nervous system - A fMRI study in healthy volunteers. *NeuroImage*, *107*, 10–22. https://doi.org/10.1016/j.neuroimage.2014.11.043

Saleem, KS., Logothetis, NK. (2007). *Atlas of the Rhesus Monkey Brain*. Academic Press.

Saleh, TO., Logothetis NK., Evrard, HC. (2016). Insular projections to brainstem homeostatic centers in the macaque monkey. Poster. *Society for Neuroscience.* 6, November 2016.

Sanders, KM., Koh, SD., & Ward, SM. (2006). Interstitial Cells of Cajal as Pacemakers In the Gastrointesstinal Tract. *Annual Review of Physiology*, *68*(1), 307–343. https://doi.org/10.1146/annurev.physiol.68.040504.094718

Small, DM., & Difeliceantonio, AG. (2019). Processed foods and food reward. *Science*, *363*(6425), 346–347. https://doi.org/10.1126/science.aav0556

Song, GH., Venkatraman, V., Ho, KY., Chee, MWL., Yeoh, KG., & Wilder-Smith, C. H. (2006). Cortical effects of anticipation and endogenous modulation of visceral pain assessed by functional brain MRI in irritable bowel syndrome patients and healthy controls. *Pain*, *126*(1–3), 79–90. https://doi.org/10.1016/j.pain.2006.06.017

Thayer, JF. & Lane, RD. (2000). A model of neurovisceral integration in ER and dysregulation. *Journal of Affective Disorders, 61,* 201-216.

Tillisch K., Mayer, EA., Labus. JS. (2016). Quantitative Meta-Analysis Identifies Brain Regions Activated during Rectal Distension in Irritable Bowel Syndrome. *Gastroenterology*, *140*(1), 99662964. https://doi.org/10.1053/j.gastro.2010.07.053.Quantitative

Umans, BD. & Liberles, SD. (2018). Neural Sensing of Organ Volume. *Trends in Neurosciences, 41*(12), 911-924.

Wittling, W., Block, A., Genzel, S., & Schweiger, E. (1998). Hemisphere asymmetry in parasympathetic control of the heart. *Neuropsychologia*, *36*(5), 461–468. https://doi.org/10.1016/S0028-3932(97)00129-2

Yu, T., Jiao, Y., Cai, S., Zhang, Y., Yu, S., Yu, W., & Luo, T. (2018). Parabrachial Neurons Promote Behavior and Electroencephalographic Arousal From General Anesthesia. *Frontiers in Molecular Neuroscience*, *11*(December), 1–13. https://doi.org/10.3389/fnmol.2018.00420

Yuan, YZ., Tao, RJ., Xu, B., Sun, J., Chen, KM., Miao, F., … Xu, JY. (2003). Functional brain imaging in irritable bowel syndrome with rectal balloon-distention by using fMRI. *World Journal of Gastroenterology*, *9*(6), 1356–1360. https://doi.org/10.3748/WJG.V9.I6.1356

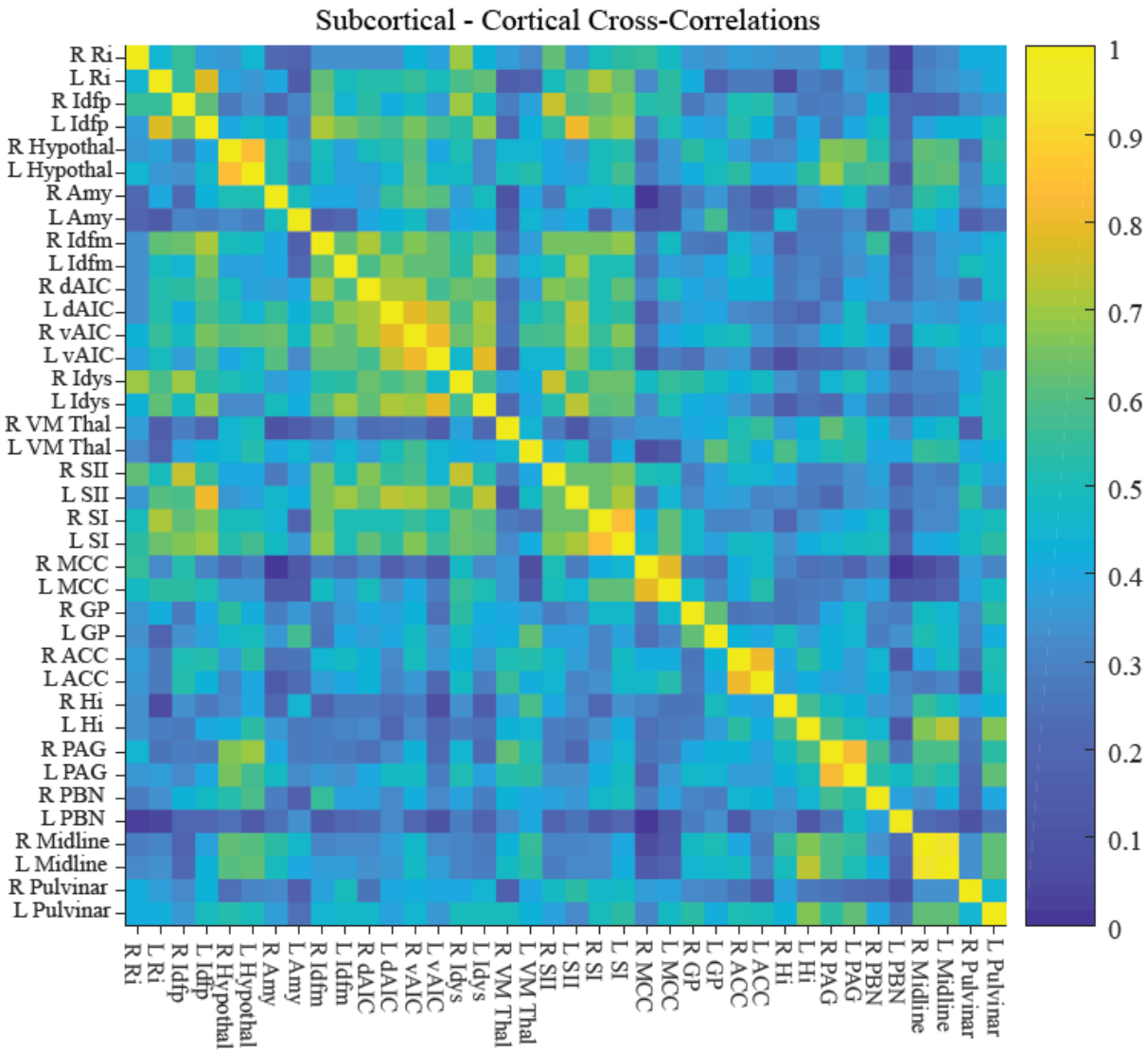

Supplement 1: Heat map depicting the strength of subcortical-cortical cross-correlations as measured by the Pearson's R coefficient. Data serves as an indicator of the underlying functional connectivity between ROIs. Correlations calculated from the average normalized bandpass-filtered BOLD signal of all functional scans.

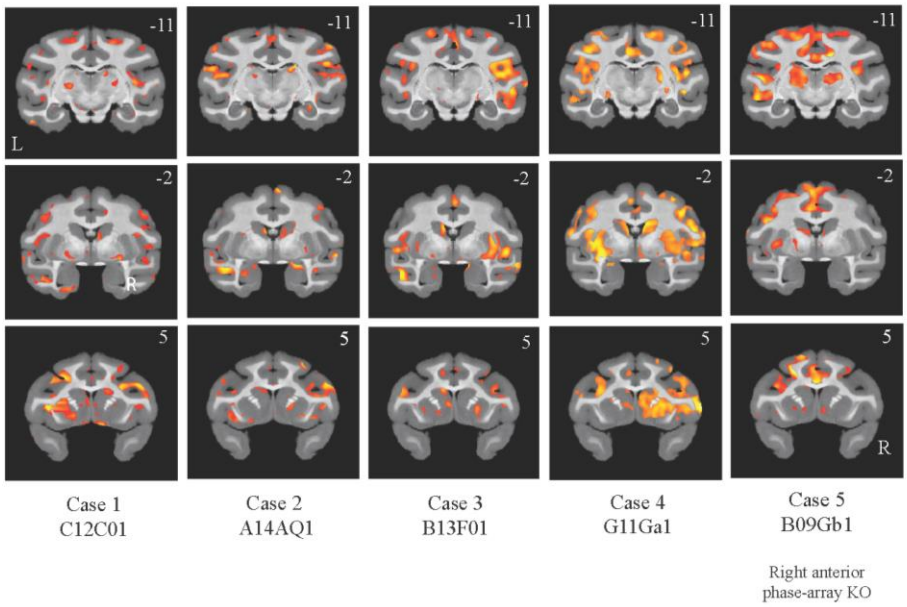

Supplement 2: Single-subject whole brain analysis revealed activations specifically related to rectal distention (balloon inflation period). A T-contrast weighting the distention period against the rest period revealed activation in the ventral anterior insular cortex (vAIC) and the ventral dysgranular insular cortex, along with activation in the granular insular cortex. Coronal and sagittal coordinates indicated in D99 template space. Case 5 data were collected during a knock-out (KO) of the right anterior phase-array scanner coil element.

4. THE INSULAR CORTEX'S INTEROTOPIC MAP

ABSTRACT

The macaque monkey is a common model organism used to study primate brain function and, without doubt, there are gross similarities in the functional neuroanatomical organization between macaques and humans. In both species, the insular cortex appears to be topographically innervated by interoceptive sensory afferents. However, the extent of topographic encoding and characterization of different functional modalities representing interoceptive inputs from foot-to-head has never been examined in one study. Thus, the topographic organization of interoceptive inputs within the insular cortex was investigated here in the anesthetized macaque. Neuroimaging data were collected during graded cooling and heating of the hand and foot, tastant delivery to the tongue, rectal distention and transcutaneous electrical stimulation of the auricular vagus nerve branch. Cutaneous thermal stimuli elicited activations in the posterior area of the dorsal fundus of the insula, while activations related to cranial nerve processing were localized more anteriorly. Electrophysiological recordings confirmed and refined this overall topography. The present study supports the idea that the primate insula represents interoception in a manner that preserves the spinocranial topography and the encoding of interoceptive modalities along distinct labeled-lines throughout the neuraxis. This refined representation of internal bodily signals plays a crucial role in emotional embodiment and in the homeostatically efficient shaping of cognitive processes by interoception, providing a basis for the evolutionary emergence of embodied subjective feelings in the human anterior insula. Our work suggests that the functional organization of the macaque insula resembles more that of the human insula, as previously thought, hinting at a conservation of the homeostatic afferent network and interoceptive processing in primates.

KEYWORDS

Interoception, primates, insular cortex, electrophysiology, neuroimaging, anatomical modeling

INTRODUCTION

While the insula - a primary cortical structure involved in receiving and relaying neuronal inputs from the body - is seated on the cortical surface in lissencephalic mammals (e.g. rodents), this cortical region appears sophisticatedly enveloped and progressively more convoluted in primates. Studies of the primate insular cortex have noted its evolution, expanded gyrification and number of cytoarchitecturally distinct subregions (Bauernfeind et al., 2013; Evrard et al., 2014). However, one should take caution to claim that the relatively larger anterior insular cortex (AIC) in humans, as compared to other primate species, is evidence enough that only humans possess the capacity to execute functions mediated by this region, such as, social-emotional functions (Kim et al., 2012), self-awareness (Craig, 2009) and emotional embodiment (Harrison et al., 2010). Contemporary electrical stimulation studies of the macaque insula provide evidence for an extrinsic AIC circuitry designed to output changes in emotional and social reactions (Caruana et al., 2011). However, what remains to be illustrated is the localization of sensory information encoded by the insula – a foundation for studies on neuronal propagation, emotional embodiment, and the manifestation of subjective, behavioral, and physiological responses. Our work shows that the sensory encoding aspects of the macaque insular cortex appears more similar to humans than previously believed (Craig, 2015; Hirata et al., 2005; Rolls, 2005).

This work has focused on mapping the insular cortex using an array of functional stimulation modalities during fMRI and electrophysiology experiments in an effort to collect empirical evidence for a potential body map in the insula, specifically along the dorsal granular cortex, as might be suggested from human neuroimaging (Segerdahl et al., 2015; Hua et al., 2005; Craig & Andrew, 2002) and tract-tracer injections of the thalamic relay centers (Craig, 2014; Pritchard et al., 1986). We introduced paradigms of graded cooling and heating stimuli to the hand and foot, tastants on the tongue, rectal distention (RD) and transcutaneous electrical stimulation of the auricular vagus nerve branch (ABVN) to glean insight into the mesoscopic organization of the insular cortex, including the retro-insular cortex (Ri) and adjacent opercula.

Previous electrophysiological recordings of sensory responses in the insula and adjacent opercula have only captured a small portion of the overall organization, even so that the work suggests functions, such as taste and oral somatosensation, occupy the entire rostral extent of the insular cortex (Hirata et al., 2005; Kadohisa, Verhagen, & Rolls, 2005; Scott et al., 1986). Such previous research was limited in its spatial scope of study, and would provide reason to presume the

macaque and human AIC were not homologous. However, a close review of those electrophysiology results indicate a limited number of taste-responsive neurons (2.1% of the sampled population) between the mid-dorsal to anterior insula and adjacent operculum (Scott et al., 1986), suggesting additional functional encoding capacity of this insular region. Our research aimed to further elucidate the underlying neuronal signature in the insular cortex.

Information crucial for maintaining homeostasis (e.g. itch, pain, cutaneous temperature) is relayed via thinly or unmyelinated fibers ascending the spinothalamic (or anterolateral) tract. Spinothalamic afferents relay to the superficial (lamina I) spinal dorsal horn and crossover immediately to the contralateral lemniscus, thereby ascending to the first homeostatic relay center in the brainstem – the nucleus tractus solitarius (NTS). The NTS also relays gustatory, vagal and baroreceptor afferents. The ventromedial thalamus (e.g. VMpo and VMb) receives direct spinal and brainstem projections and sends the incoming information to the insular cortex with some ancillary projections from VMpo to somatosensory area 3a. Interoceptive inputs are additionally received by the ventrocaudal portion of the mediodorsal (MDvc) thalamic nucleus and relayed to the anterior cingulate cortex (Craig, 2002). The functional stimuli (e.g. cutaneous temperature modulation, taste, rectal distention) used in this research were employed to activate the underlying vagal, gustatory, Aδ- and C-afferent fibers innervating the skin and viscera (Craig, 2014; Craig, Krout, & Andrew, 2001; Andrew and Craig, 2001; Dostrovsky & Craig, 1996; Light & Perl, 2003) to localize the correlated responses within the cortex.

As a recipient of sensory information from all areas of the body, including also specialized tissues and organs, the insular cortex has been shown to exhibit a unique neuroanatomical functional organization, whereby its dorsal granular portion is topographically organized in a way that mimics the afferent organization at the level of the relaying thalamic nuclei (Craig, 2014). Here, multi-modal functional mapping by fMRI and electrophysiological sampling has helped reveal the underlying neuronal organization to a greater extent. The current work extends the functional neuroanatomical knowledge of the macaque monkey, specifically of the insular cortex, and lays a foundation for next-generation studies on the higher-order functional processes attributed to the anterior insular cortex.

MATERIALS & METHODS

Subjects

A total of 16 rhesus macaque monkeys *(Macaca mulatta*; 7 females; average weight: 7.96 kg) were used in this study. Animals were treated according to the guidelines of the European Parliament

and Council Directive 2010/63/EU on the protection of animals used for experimental and other scientific purposes. All protocols were approved by the local German authorities and designed to continuously ensure the wellbeing of the animals.

Anesthesia

Before commencing an experiment, animals were pre-sedated with glycopyrrolate (Robinul, 0.01 mg/kg, i.m., anticholinergic) and ketamine (15 mg/kg, i.m., dissociative anesthetic). After transport to the experimental setup, they were anesthetized with sequential injections of fentanyl (3 µg/kg, i.v., analgesic), thiopental (5 mg/kg, i.v., hypnotic), and succinylcholine chloride (3 mg/kg, i.v., muscle relaxant). They were then intubated and ventilated (24 strokes/min) throughout the procedure, using 100% oxygen during preparation and craniotomies, and 21% oxygen during functional data acquisition. After intubation, anesthesia was maintained using a combination of remifentanil (1-3 µg/kg/min, analgesic and anesthetic) and mivacurium chloride (5-7 mg/kg/h, muscle relaxant) during fMRI and electrophysiological experiments. The anesthesia parameters had previously been optimized for imaging BOLD signal changes and recording neuronal activity (Logothetis et al., 2012). The physiological state of the animal was continuously monitored using infrared pulse oximetry (Nonin Medical Inc., Plymouth, MN, USA), electrocardiography (ECG), thermometry, and sphygmomanometry. A rectal thermometer continuously measured body temperature, which was regulated using a water-heating pad to maintain a body temperature within normal physiological range (38.3 – 38.8 °C). In order to attain physiological values optimal for fMRI, body temperature was maintained at 38-39ºC. Acidosis was prevented by the administration of lactated Ringer's solution with 2.5% glucose, infused at 10 ml/kg /h, and intravascular volume was maintained by the additional administration of colloids (hydroxyethyl starch, 20-30 ml over 1-2 minutes or 20 ml/kg/h).

Functional Imaging Data Acquisition

All fMRI experiments were conducted in a vertical 7 Tesla scanner with a 60 cm diameter bore (BioSpec 7/60v, Bruker BioSpin, Ettlingen, Germany) and a 75 mT/m actively shielded gradient coil (Bruker, BGA38S) of 38 cm inner diameter. The animals were positioned in a custom-designed MR-compatible chair. Their legs were wrapped from toe to pelvis to prevent venostasis. All physiological monitoring sensors (noted above) were secured with medical tape and the torso and arms were snugly wrapped in towels to maintain temperature to prevent obstruction of blood flow and airways. The head of the animals was immobilized using ear bars and mouthpiece fitted

with a custom-built quadrature volume radiofrequency (RF) coil in 13 animals (Logothetis et al., 2012) or a custom-built phased-array helmet in 3 animals (Hartig, Balla, Logothetis, Evrard, 2019).

Whole-brain functional scans were acquired with multi-shot gradient-echo echo planar imaging (GE-EPI; 1x1 mm^2 in-plane resolution; flip angle: 53°; TR/TE: 2000/19 ms; 20 axial slices) when using the quadrature coil, and with GRAPPA-accelerated parallel imaging (0.85x0.85 mm^2 in-plane resolution; flip angle: 53°; TR/TE: 1000/18 ms, 18 axial slices) when using the phased-array helmets. Slice volumes were acquired in contiguous sections. Both scan sequences had the same matrix size (128x128), field-of-view (FOV; 96x96 mm^2) and slice thickness (2 mm). During each experiment, a T2-weighted Rapid Imaging with Refocused Echoes (RARE) scan was collected to image the native structural space (FOV: 96x96 mm^2; matrix size: 256x256; 8 segments; flip angle: 8°; TR/TE: 4000-6500/25-48 msec; 40 slices). A three-dimensional anatomical scan was acquired for each subject using a T1-weighted modified driven equilibrium Fourier transform scan (MDEFT; FOV: 128x128 mm^2; matrix size: 256x256; 4 segments; flip angle: 20°; TR/TE: 15/4.5 msec; 136 slices).

fMRI Data Analysis and Modeling

Functional scans were motion-corrected and co-registered to their native anatomical scan using SPM12 (Statistical Parametric Mapping; Wellcome Department of Imaging Neuroscience, London, UK). Each animal's MDEFT scan was normalized to a high-resolution digital surrogate of the D99 atlas (Saleem & Logothetis, 2007) using AFNI (Cox, 1996) and open-source code (Reveley et al., 2016). The RARE scan was warped to fit the normalized MDEFT using an in-house MATLAB (Version 2017b, MathWorks, U.S.A.) function for nonlinear transformations. The resulting transformation matrix was applied to all functional scans before smoothing by a 2 mm FWHM Gaussian kernel.

The variation in BOLD signal was modeled using SPM12 with an event-related univariate general linear model (GLM). Each experimental condition was modeled separately and convolved with the canonical hemodynamic response function. Additionally, the six motion parameters obtained from the motion correction were included as parameters of non-interest in the model. The data were high-pass filtered with a cutoff of 128 sec and the temporal derivative was included. An additional low-pass filter was deemed unnecessary when modeling BOLD data convolved with the canonical hemodynamic response function; the technical reason relates to the Nyquist frequency of sampling rate (Matsuo, Hsu & Tseng, 2012). GLM parameter estimates (β-weights) were subjected

to a *t*-test ($p = 0.05$, corrected for false positives) to examine differential BOLD activity. The percent signal change and conditional effect (*t*-value) was calculated. A permutation of the individual condition contrasts revealed normalized activity at the group-level.

Electrophysiology

Anatomical targeting. In order to determine the stereotaxic coordinates for electrode placement, ROIs were drawn to-scale on each animal's high-resolution MDEFT anatomical scan. For each of the terminal experiments (n = 4), a 3D model of the left and right insula containing also the position of the ear canal and lower orbital bone (Frankfurt zero plan) was 3D-printed using Catia V5 (CAD Software, Dessault Systèmes, Vélizy-Villacoublay, France) and Form 2 (Formlabs, Berlin, Germany). For the preparation of the experiments, this model was placed in the stereotaxic head holder and the cardinal insular coordinates were recorded using micromanipulators (Kopf Instruments, Tujunga, CA, USA). Four independent micromanipulators were used: one pair was used to target separately the left and right dorsal fundus of the insula and dysgranular insula, while the other pair was used to target the left and right vAIC. This preparation using a 3D-printed model of the insula ensured accurate placement of the electrode arrays during the actual experimental recordings.

Data acquisition. The electrophysiological recordings were made during terminal (i.e., non-recovery) experiments, using a dedicated neurophysiological setup, outside the MRI scanner. Under stable anesthetic conditions (see above), the animal was transferred to the recording table and its head was fixed to the stereotaxic frame. The animal was then hyperventilated and a bilateral craniotomy (~18 x 23 mm^2) directed by the insula coordinates was performed to expose the underlying dura. All surgical procedures were performed under aseptic surgical conditions. During the experiment, the exposed area was continuously flushed with sterile saline to avoid tissue dryness and to keep the dura clean and free of occulting blood clots.

The anteroposterior extent of the dorsal fundus of the insula was sampled bilaterally using a pair of 4-electrode arrays (Fig. 1; 1 mm-spaced, 360 µm diameter shaft and 300 µm tip, 0.8-2.0 MΩ, 170 mm long, epoxylite insulated; FHC Inc., Bowdoinham, ME, U.S.A.). Each array was fixed to a micromanipulator, allowing for positioning along the relevant cardinal dimensions: the anteroposterior (AP), mediolateral (ML), and dorsoventral (DV) axes. Electrodes penetrated the tissue in 0.5 mm increments along the DV axis and in steps of 1 – 2 mm in both the AP and ML axes. Two additional arrays were positioned anteriorly in the vAIC region to concurrently record

activity from the VEN region. In the first terminal experiment (Case G11), arrays with an inter-electrode spacing of 0.5 and 2.5 mm were also tested. A silver wire was subcutaneously positioned adjacent to the craniotomy site. Extracellular signals were amplified (8,000) and filtered (1 Hz and 8 kHz) using an in-house 32-channel preamplifier with onboard subtraction and Alpha Omega multi-channel processor (Alpha Omega Engineering, Nazareth, Israel). Signals were digitized at 20.83 kHz with 16-bit resolution (National Instruments, Austin, TX, U.S.A.). An audio speaker and oscilloscope were used during the experiments to assess recording quality. The electrode arrays were built to accommodate a central microstimulation electrode (Fig. 1b), capable of eliciting biphasic-stimulation trains, with a pulse width of 1, 2 or 3 sec. Stimulation intensity and frequency ranges were 0.05 - 200 μA and 5, 40, 60 and 100 Hz, respectively. The electrical stimulation data will be analyzed subsequently within the framework of a larger research program.

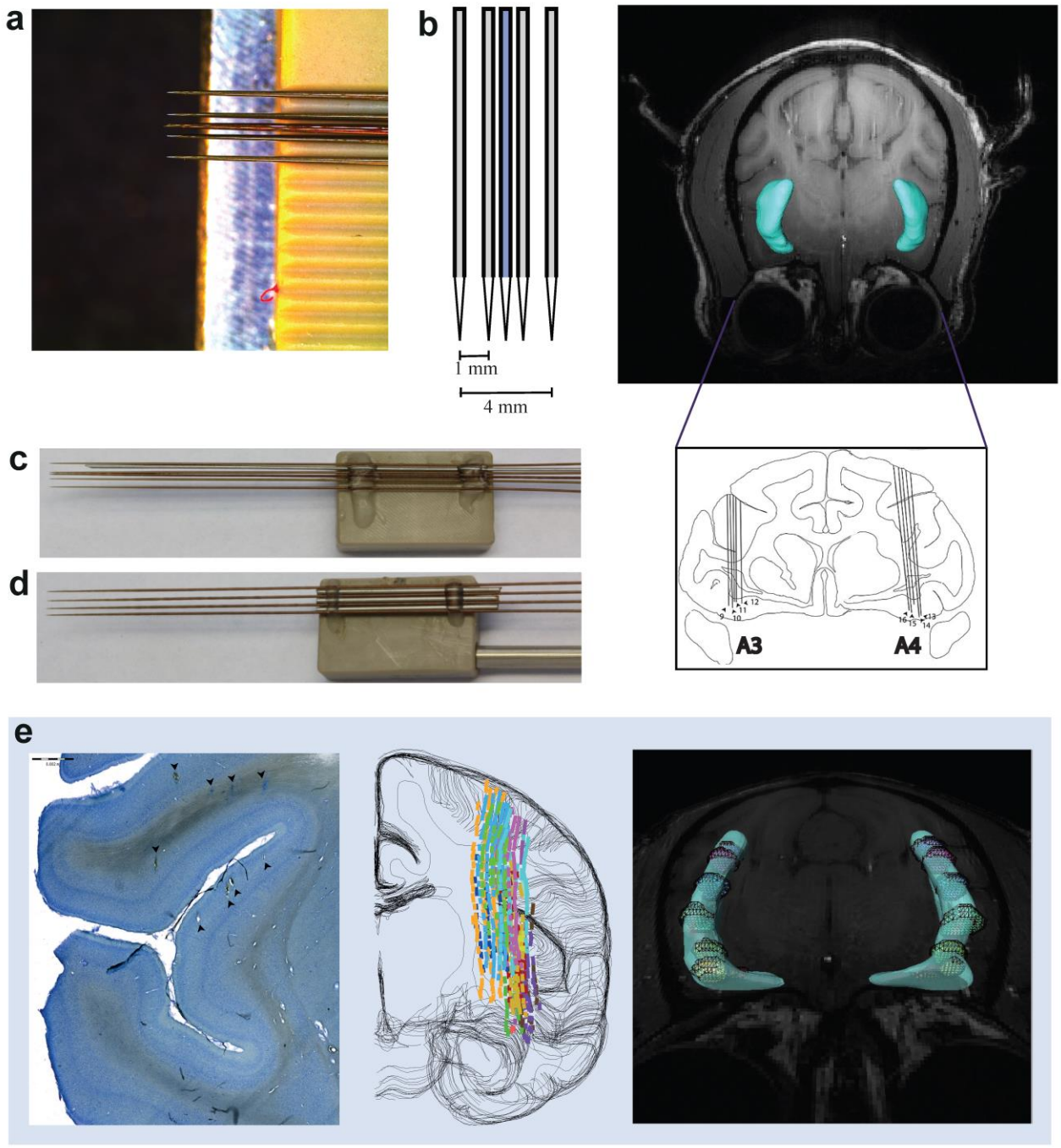

Fig. 1: Electrophysiology set-up and track reconstruction. (**a**) Photomicrograph of 0.5 mm-spaced electrode array tips. (**b**) Representation of the 1 mm-spaced electrode arrays mainly used during experiments. The blue electrode represents the position of the microstimulation electrode. (**c-d**) Images of different electrode array versions. (**e**) Track reconstruction process (from left-to-right): identification of electrode microlesions from Nissl stains; track annotations across the sampled region (different track insertions have their own color identity); and 3D modeling of the functional responses. (**f**) MDEFT image with to-scale insula outline: A1-A4 indicate the electrode array positioning, whereby A3-A4 remained stationary in the vAIC regions (see figure outset, the arrows represent different electrode channels).

MUA analysis. The electrophysiology data were subjected to a fourth order Butterworth high-pass filter (500 Hz cut-off) and temporally smoothed with a 0.3 msec Gaussian kernel before extracting the multi-unit activity (MUA). All sessions went through a noise detection procedure to remove high-amplitude artifacts, defined as data points exceeding six standard deviations from the mean of the filtered signal, occurring with the same polarity and at the same time in at least 9 out of 16 channels. These data points were then interpolated by replacing them with the nearest non-outlier data point. Spike trains were extracted from the clean MUA signal by applying a negative threshold. The threshold estimation was 5x that of the signal noise floor, or sum of all noise sources (Quiroga, Nadasdy, & Ben-Shaul, 2004)**.** Spike trains of sessions in which a stimulation modality was recorded were then separated into trials. Trials in which the duration of stimulation was less than 0.2 sec or longer than 18 sec were excluded to improve analytic consistency. Spike trains were aligned to the onset of the event and a baseline time was defined for the analysis 0.5 msec before stimulus onset. For ongoing sessions, in which no external stimulation was performed, the spontaneous physiological events (i.e., rhythmic cardiac activity) were analyzed with respect to recorded neuronal activity. Spike trains were epoched to each cardiac cycle and aligned to the R-peaks of the QRS complex.

During the terminal electrophysiological experiments, all sampled regions were probed with a defined set of sensory stimuli (see Functional Stimuli). However, due to time constraints, not every type of stimulation was recorded for all regions. For instance, if a given region was tested for all stimulation paradigms, but only clear responses were evoked by noxious warm stimuli, only the noxious warm responses were recorded for further analysis. Included sessions recorded from the same site were grouped and a one-way analysis of variance (ANOVA) was calculated to evaluate the effects of different functional modalities on neuronal activity. A Bonferroni correction was then performed to avoid inflated false-positive rates caused by multiple comparisons.

A histogram for each channel was created from non-overlapping bins of 500 msec. A spike-density function (SDF) was computed for each trial by convolving a 300 msec time window with a Gaussian kernel. Comparison plots display the average SDF over trials for different functional stimuli; the shaded regions represent the bootstrapped 95% confidence interval. Analyses were performed using the Field Trip toolbox in MATLAB (Oostenveld et al., 2011, Donders Institute for Brain, Cognition and Behaviour, Radboud University, Nijmegen, the Netherlands).

Power Frequency Spectrum

Electrophysiology data were bandpass (5 – 300 Hz) filtered to extract the local field potentials (LFPs). The spectral density underlying the LFP signal was extracted using the fast-Fourier transform (*fft)* function (MATLAB Version 2017b, MathWorks, U.S.A., Signal Processing Toolbox). The resulting spectrogram represents the power of each frequency envelop. To characterize the oscillatory profile of resting-state recordings and analyze the periodicity of ongoing neuronal data, auto-correlograms were constructed from 10 msec time bins and a maximum lag of 2 sec before undergoing a fast-Fourier transform with a simple Hanning window to compute the corresponding Lomb periodogram (Kaneoke & Vitek, 1996).

Functional Stimuli

Thermal stimulation. During the fMRI experiments, we used programmable thermodes (Medoc PATHWAY; CHEPS thermode, 27 mm diameter; ATS thermode, 16x16 mm^2; Medoc, Ramat-Yishai, Israel) gently affixed to the glabrous palmar surface of the hand or the foot. Care was taken to avoid pressing the thermodes against the skin. Four different stimulation paradigms were separately tested: innocuous warming (WARM), noxious heating (HOT), innocuous cooling (COOL), and noxious cooling (COLD). The COOL and COLD paradigms started from a basal temperature of 35°C, ramped down linearly to 20°C and 10°C, respectively, using a cooling of 0.5°C/sec, then ramped back to the basal temperature, using a rapid linear warming of 0.8°C/sec, and finally maintained at basal temperature for at least 90 sec, with jittered inter-stimulus time (ISI) interval, before the next stimulation ramp (Fig. 2c). The WARM and HOT paradigms started from a basal temperature of 33°C, ramped up to 40°C and 50°C, respectively, using a heating of 0.8°C/sec, before being brought back to basal temperature (0.8°C/sec), and finally maintained at basal temperature for 90 sec, with jittered ISI, before the next ramp (Fig. 2c). During functional scan sessions, an average of 15-30 trials were administered for each thermal paradigm, depending on the ISI. At least 3 runs per thermal paradigm executed during one experimental session were collected. These runs were concatenated and analyzed at the single-subject level, proportionately weighing the activity for each session.

Thermode device artifact compensation was unavailable for the electrophysiology recording setup, so alternative probes, previously shown to work efficiently (Craig, 2014), were applied during terminal recordings. Noxious heat stimulation was then provided by temperature-controlled forceps (maintained in 47°C water bath). Although this method did not allow for computing the respective

neuronal tuning curve, it ensured that the probe was above the threshold for responses of noxious heat cells (Craig et al., 2001). Noxious cold stimulation was provided by placing wet ice cubes in contact with the skin, similar to the method of (Andrew & Craig, 2001). These data were collected during a 2 min recording window of variable inter-stimulus timing due to manual control over recorded trials.

Noxious mechanical (pinch) stimulation. Similar to a previously described protocol (Craig & Andrew, 2002; Craig & Kniffki, 1985), pinch stimulation was delivered using a pair of forceps. The stimulus strength gradually increased during the pinch trial to elicit both non-painful and noxious mechanical sensations. Data were collected over a 2 min recording window of variable inter-stimulus timing due to manual control over recorded trials. The amplitude and rate of change in intensity were not recorded.

Rectal (visceral) Distention (RD). In both the fMRI and electrophysiology experiments, a lubricated biocompatible balloon was inserted into the rectum via the anus. The distal opening of the catheter was attached to a 3-port stopcock connecting a manometer (Soliton Laser- und Messtechnik GmbH, München), to continuously measure the pressure within the balloon, and extension tubing (total length: 5.5 m), which connected to the barostat pump (Distender II; G&J Electronics Inc, Toronto, Ontario, Canada). The barostat controlled the inflation and deflation of the balloon with air, and continuously monitored the volume and pressure inside the balloon. Once in place, the balloon unfolded by slowly injecting air under controlled pressure (<20 mmHg) and was then completely deflated.

The rectal distention (RD) paradigm (Fig. 2b) included three conditions: Inflation (I), Deflation (D) and Rest (R), whereby the period I consisted of a 4 sec graded increase in pressure, followed by a 6 sec sustained increase in intraluminal pressure (rectal balloon inflation), then by a graded 4 sec period over which the rectal balloon was deflated. The inter-stimulus trial rest period was between 16 - 36 seconds. This amounted to 15 - 20 trials per session in 10 min fMRI scans or 4 trials per sessions of 2 min in the electrophysiological recording.

Taste. In both the fMRI and recording experiments, taste stimuli were delivered to the mouth using programmable syringe pumps (Aladdin Pumps, World Precision Instruments, Sarasota, FL, U.S.A.) and deposited onto the anterior half of the tongue for 7 sec, encapsulating receptors for the processing of sweet, salt and sour tastants. Tastants included NaCl (salt, 0.8 M), sucrose (sweet, 0.5 M), and citric acid (sour, 80 mM). All stimuli were prepared using a base of artificial saliva in distilled water. Each delivery of tastant was succeeded by a 7 sec rinse of tasteless solution

(Veldhuizen et al., 2007), mimicking the concentration of saliva (7 seconds of 12.5 mM KCl + 1.24 mM $NaHCO_3$). Rinse cycles additionally served to negate the effects of stimulus habituation. There was a 2 sec waiting period between taste and rinse deposits to account for the lag in liquid drip from the delivery spout. The experimental paradigm (Fig. 2a) included a 15 sec wait period in-between taste-rinse cycles and 15 trials within on session. A total session was 10 min. The number of sessions recorded during electrophysiology and fMRI experiments is shown in Figure 3.

t-VNS. Using the NEMOS® device (t-VNS Technologies Erlangen, Germany), transcutaneous stimulation of the vagus nerve (t-VNS) was applied to the cymba concha, whereby

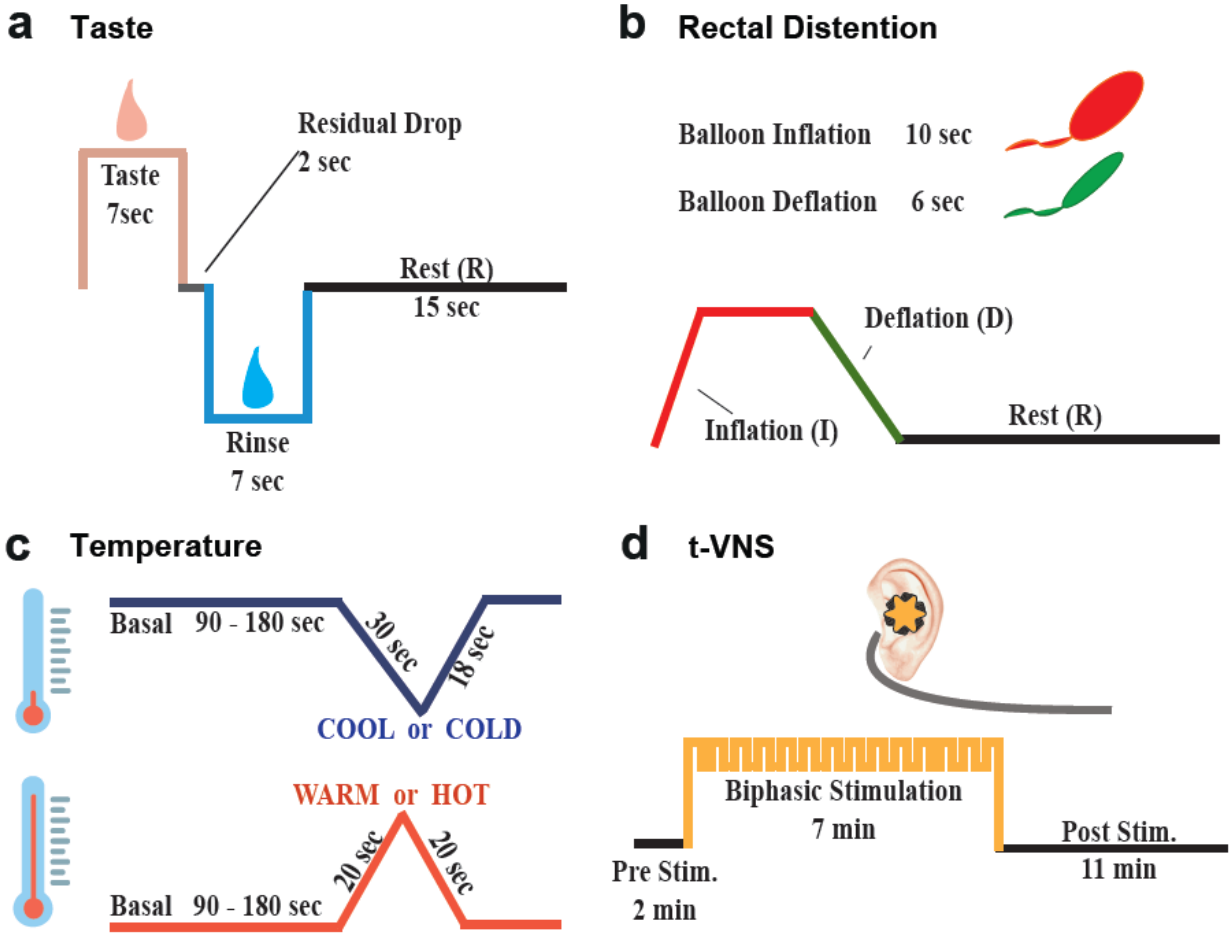

Fig. 2: The functional modalities employed during fMRI experiments. (**a**) Sweet, sour and salt tastants delivered before periods of rinse; (**b**) controlled timing of balloon inflation and deflation for rectal distention; (**c**) cutaneous temperature modulation with COOL/COLD, WARM/HOT paradigms; (**d**) transcutaneous stimulation of the auricular vagus nerve branch (ABVN) by t-VNS followed a pre-stimulation baseline period and preceded by a post-stimulation recording. These paradigms were modified to accommodate subsequent electrophysiology experiments (except for the external electrical stimulation, t-VNS, paradigm).

stimulating the underlying auricular vagus nerve branch (ABVN). For sham conditions, stimulation was applied to the earlobe activating the underlying vibro-receptive mechanoreceptors. The stimulation paradigms for t-VNS and sham stimulation were replicated from Frangos et al., (2015), whereby a pre-stimulation (baseline) recording preceded nerve stimulation, followed by a post-stimulation recording period. The paradigm for the t-VNS is shown in Figure 2d. This stimulation paradigm was only executed during fMRI sessions with the quadrature head coil as the custom helmet coils secured the ears in a fashion where additionally applying the stimulating electrodes would be uncomfortable for the subject. t-VNS was not included during electrophysiological measurements as the external stimulating current would produce extraneous noise within the recording arena that would result in low quality neuronal signal recordings.

Vestibular stimulation. Vestibular stimulation was performed by mechanical rocking of the floating recording table on which the subject was fixed. Vestibular stimulation was employed to help localize the posterior targeting of the dorsal fundus of the insular cortex – Idfp – the region adjacent to the retro-insular (Ri) cortex, or parietoinsular vestibular cortex (PIVC), where vestibular-responsive cells have been characterized (Brandt and Dietrerich, 1999). Data were collected during a 2 min recording window of variable inter-stimulus timing due to manual control over recorded trials.

Visual stimulation. To assess the BOLD activity during anesthesia and to substantiate our functional findings and control for effects specifically related to interoceptive stimulation, a visual flicker stimulus was also administered intermittingly throughout experimentation. The set-up and paradigm design was replicated from Logothetis et al., (2010). During electrophysiology experiments, a flash of light directed towards the subject helped to determine if electrodes had exceeded our target depth and hit the lateral geniculate nucleus (LGN).

Neuroanatomy

Tracer injections. Neuronal tract-tracers were injected into specific areas of the insular cortex throughout the terminal electrophysiological recording experiments using micropipettes (Hamilton Company, Reno, NE), with a 51 mm long needle. Dextran-conjugated fluorescent tracers (Rdex, Pdex) were manually injected by carefully inserting the syringe tip through guide tubes incorporated into the electrode arrays (Fig. 1c,d). An amount of 800 – 1,000 nL was injected over a period of 10-15 min. After the full volumetric amount was injected, the micropipette remained dormant in the tissue for 30 min.

Perfusion and histology. Animals were euthanized with a lethal dose of sodium pentobarbital (60-80 mg/kg i.v.). They were immediately perfused transcardially with saline (0.9%, RT), followed by 4% paraformaldehyde in phosphate buffer (PB; 0.1 M, pH 7.4, RT) and then by 4% paraformaldehyde and 5% sucrose in PB (0.1 M, pH 7.4, RT). The brain was removed and cryoprotected in 0.01 M PBS (pH 7.4), containing 30% sucrose and 0.1% sodium azide for at least 7 days at 4°C. After fixation, the entire brain was blocked coronally. Serial 50 μm thick coronal sections were cut frozen on a horizontal sliding microtome and collected in 0.01 M PBS. Sections were organized by either a 1-in-6 or 1-in-7 series, where the first section in the series was used for a standard (dehydrated) Nissl stain using cresyl violet (0.16% in 3.75% ethanol). Sections were subsequently scanned using a 10x planapochromatic objective (AxioImager.M2, Carl Zeiss, Goettingen, Germany).

Recording track reconstruction. The subcortical and cortical borders were contoured for each relevant Nissl section and two independent reviewers (AV and RH) plotted the corresponding anatomical labeling and physiological responses. Tracks were identified by comparing their ML, AP and depth level as recorded during the experiment with that measured from each subject's ex-vivo MDEFT. The reconstruction was done using custom-made software developed specifically to chart objects from the Carl Zeiss Image (CZI) format (HistoMapper; DA-Cons GmbH). For each subject, the series of coronal slices was aligned to the corpus callosum and optimized to reproduce the native alignment. The position coordinates for each section is in relation to the slice distance (in mm) from the anterior commissure.

Putative track locations were identified by characteristic microlesions caused by the electrode insertion (Fig. 1e). As tissue cutting was not orthogonal to the electrode insertions, track reconstruction was done by following the tip progression over sections. Tracks were identified by comparing the AP, ML and DV values recorded during the experiment, with special consideration of a tissue shrinkage factor (~20%) caused by the fixation process. Given the AP axis was sampled around every 1 mm and the slice sampling resolution was 0.35 mm, functional maps were adapted by merging three slices into one representative slice. This method ensured the equivalence of histological and experimental sampling resolution.

Tract-tracing analysis. Analysis of insular injection sites and retrograde labeling in the thalamus were made using an AxioImager.M2 (Carl Zeiss, Goettingen, Germany). DAB-reacted sections were analyzed under brightfield. Fluorescent sections were analyzed with epifluorescent

illumination using a fluorescein (B-2A) filter cube for Gdex, or custom-made filter cubes for Rdex and Pdex (Chroma Technology, Rockingham, VT).

Injection sites were localized cytoarchitectonically and documented with drawings of individual sections for each case, which were collated onto a standard atlas of coronal sections. Cytoarchitectonic delineations of the thalamic nuclei and sub-nuclei were made according to the method previously reported by Evrard & Craig (2008). Retrograde labeling was analyzed in the ventromedial thalamus both ipsi- and contralateral to the injection site by systematic scanning with 4×, 10×, 20×, and 40× planapochromic objectives under appropriate illumination.

RESULTS

In order to map the functional responses of interoceptive stimulation, we conducted a total of 40 anesthetized fMRI experiments, whereby 4 experiments were terminal and included electrophysiology. Two fMRI experiments were subsequently excluded either because of a mechanical or technical default relating to the stimulus paradigm or to the NMR signal transmitter

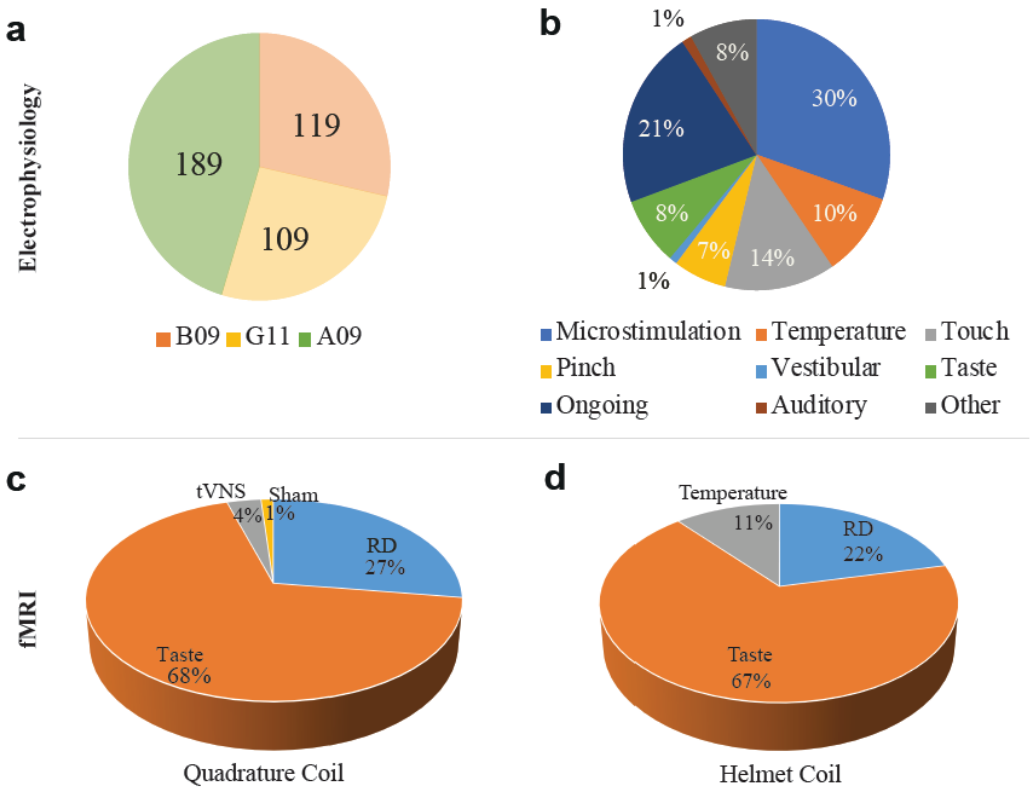

Fig. 3: Percentage of sessions across functional paradigms and experiment settings (fMRI or electrophysiology). Other category includes sessions that were not defined, or were recordings of visual and auditory stimulation.

coil. In total, 418 sessions across 3,762 electrode contacts were recorded in three of the four subjects that were part of this experiment. The fourth subject did not have any recorded sessions because of technical issues. A total of 417 recordings were performed between Cases A09 (189 recordings), B09 (119 recordings), and G11 (109 recordings), out of which 30 sessions met the exclusion criteria and were excluded from further analysis. For Cases A09 and G11, track reconstruction demonstrated that 101 valid sessions were recorded in the insula, representing a total 38% of the valid sessions, and 26 groups of sessions were recorded in the same area. Upon track reconstruction of Case B09, it was apparent that recordings predominantly targeted the putamen and a full posteroanterior mapping of insular responses was incomplete. However, with Case B09 taste responsive cells were recorded in the mid-insular cortex (Idfm) and illustrated here (Fig. 6b). Additionally, tract-tracer injections were made in this location and examination of the injection site revealed retrograde tracing in the basal portion of the ventromedial thalamic nucleus (VMb). The distribution of recordings per modality and region stimulated can be seen in Figure 3.

Neuronal populations responding to stimulation of the hindlimbs were observed in Idfp and Idys. Responses were predominantly elicited by stimulation of the contralateral side. For Case A09, an area with a predominant foot representation started at approximately AP -7 mm in the right hemisphere and at approximately AP -6 mm in the left hemisphere (FOOT area). This area seemed to be more extensive in the right insula than in the left; however, this likely reflected a sampling bias. Figure 4a shows selective responses of the contralateral foot to graded pinch stimulation as opposed to thermal stimulation (Case A09). Statistical analyses did not reveal a significant effect of modality on stimulus response, which could be a reflex of the graded response

- **Fig. 4:** Electrophysiology histograms and average response profiles. Electrophysiology recordings of insular activity during independent (**a**) cool, heat and pinch stimulation of the forelimbs and hindlimbs was conducted. The mean physiological response as well as multi-unit activity (MUA) are shown for Case A09 during targeted stimulation of the hand and foot. (**b**) Recordings from the vestibular cortex during stimulation, representation of single- and multi-unit activity in the denoted vestibular region. (**c**) Thermal and somatosensory stimulated responses of the orofacial region during electrophysiological sampling of the insular cortex.

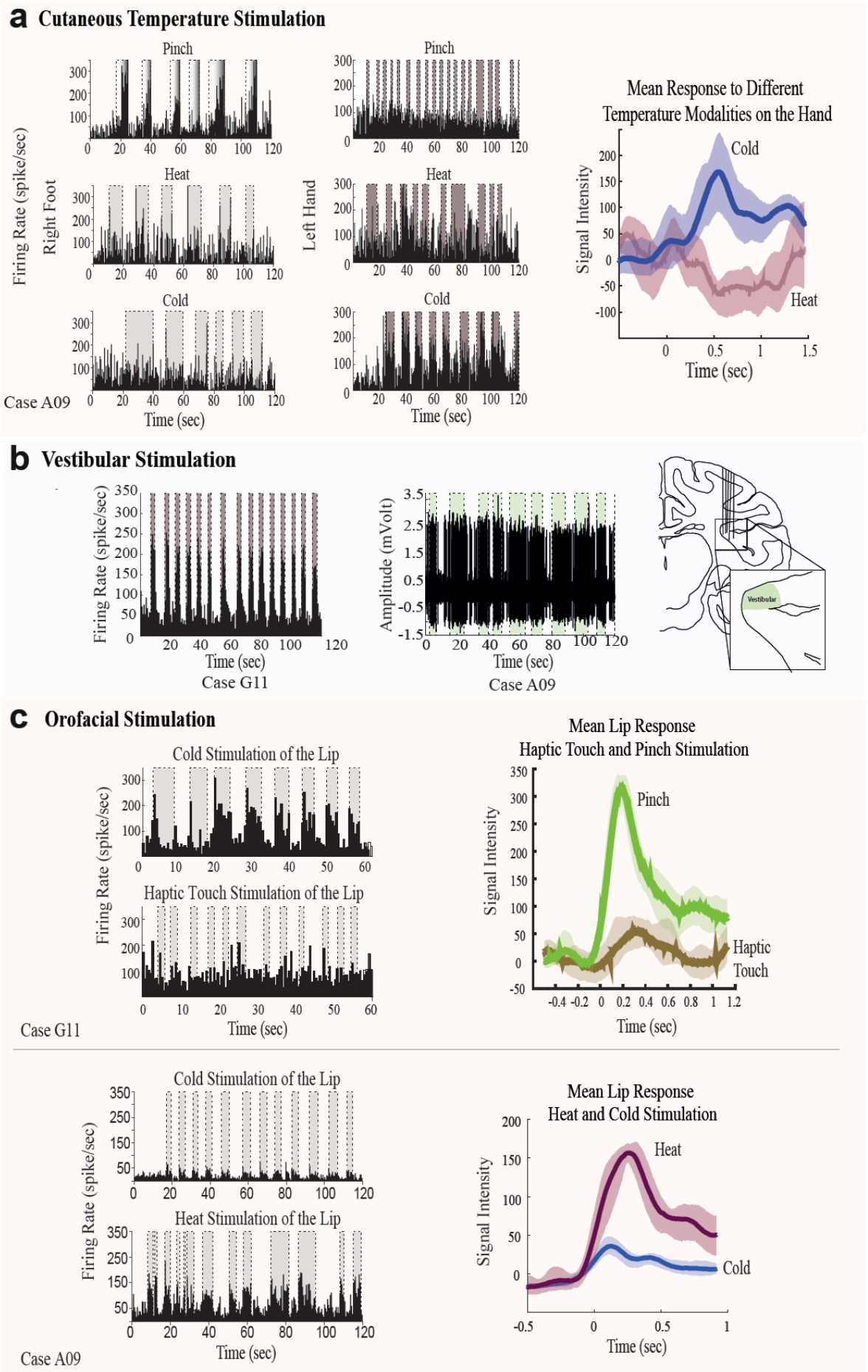
a Cutaneous Temperature Stimulation
Pinch
Heat
Cold
Firing Rate (spike/sec)
Right Foot
Left Hand
Case A09
Time (sec)
Mean Response to Different
Temperature Modalities on the Hand
Signal Intensity
Cold
Heat
Time (sec)
b Vestibular Stimulation
Firing Rate (spike/sec)
Time (sec)
Case G11
Amplitude (mVolt)
Case A09
Vestibular
c Orofacial Stimulation
Cold Stimulation of the Lip
Haptic Touch Stimulation of the Lip
Case G11
Mean Lip Response
Haptic Touch and Pinch Stimulation
Pinch
Haptic
Touch
Heat Stimulation of the Lip
Case A09
Mean Lip Response
Heat and Cold Stimulation
Heat
Cold

slope

as it seemed to be linearly correlated with the increase in noxious stimulation intensity. Observations of neurons with hindlimb receptive fields in Case G11 were scarce given the number of successful track targets in that region.

A transition area between the forelimb and hindlimb regions was found at approximately AP -6 mm in the right side of A09 and extending to AP -4 mm (HAND area). A significant effect of modality could be seen in the evoked responses in Figure 4 ($F(2, 21) = 11.31$, $p < 0.001$), where noxious cold of the hand evoked significantly stronger responses than cold and heat thermal stimulation (as shown by post-hoc analysis). This region was not so developed in Case G11 as the number of tracks sampling this region was less than that in Case A09. A cluster of hand-responsive cells could only be observed at approximately AP -9.8 mm in the right hemisphere.

The dorsal mid-insula, Idfm, contained a large representation of the orofacial cavity (MOUTH area) that extended from AP -2 mm to 3 mm in Case A09. Case G11 had a larger area representing the orofacial cavity, extending for 6 mm, from AP -3 mm to 3 mm. The dorsal mid-insula, Idfm, contained populations of neurons that encoded temperature, pinch, and touch of the mouth and face, as well as chemoreceptive cells that encoded specific tastants (Fig. 5b, sour taste). A population of neurons responding to cutaneous temperature stimulation, including both noxious heat ($F(1, 18) = 47.22$, $p<0.001$) and noxious cold ($F(2, 32)\ 26 = 8.9$, $p = 0.008$) stimulation of the lip were recorded (Fig. 4c). Similar to the FOOT and HAND area, pinch specific regions were also observed, however, responses were not reliably evoked in every trial, reflecting a possible variation on the pressure exerted manually, potentially below the response threshold. The nature of the MOUTH area seems to not only be somatosensory, as neurons encoding for movement of the subject's jaw were also seen in Case G11.

After track reconstruction, the functional composite maps for each hemisphere were plotted Figure 5. A bilateral topographic organization with a posteroanterior progression from vestibular and baroreceptive representations to foot, hand, face, and mouth representations was observed. This can best be seen in the right insular cortex of Case A09, as it was the most extensively sampled (22 tracks).

Regions of neurons that had very large and non-specific receptive fields and specific ongoing rhythmic activity were also observed in the Ri. Clusters of vestibular and heart responses were observed bilaterally in Ri, whereby vestibular responses were often located dorsally to the heart responses. Populations of neurons of the vestibular-profile type exhibited excitatory responses that were tonically maintained throughout the stimulation (Fig. 4b, Cases A09 and G11). Vestibular

representations extended less anteriorly than heart representations, which extended for more than two millimeters. The heart-responsive areas were usually characterized by ongoing spiking activity that increased in rate and was phase-locked with variable delay to the peak of the QRS complex. The heart-responsive population can be further sub-divided by their preferred

- **Fig. 5:** Electrophysiological sampling across the transverse axis of the insular cortex and adjacent opercula. Coronal sections from the left and right hemispheres of Cases (**a**) A09 and (**b**) G11. Slice number and AP level are written in light grey above each image. The AP level was defined as the distance from the anterior commissure. For better visualization, plotted responses were grouped, and responses here represent the evoked activation in a 1-mm range from the slice. Black arrows and numbers represent the corresponding figure number to the selected area response. Each section is functionally tagged with the relevant symbol indicating the underlying population characteristic (see Legend, upper right). Regions that were not reached by tracks or did not have specific responses were omitted.

a
G11 Right Hemisphere
G11 Left Hemisphere
Legend
pinch
temperature
vestibular
undefined cell
ongoing
touch
auditory
multimodal
heart
hindlimbs
forelimbs
face
b
A09 Right Hemisphere
A09 Left Hemisphere

delay from the QRS peak (Supplement 1). For instance, the populations of neurons recorded in the left hemisphere of Case A09 had an increase in firing rate 100 msec after the peak of the QRS complex, during the repolarization of the ventricles. In the right hemisphere of Case A09, an additional population fired more frequently 300 msec after the R-peak, during the systolic filling of the atrium. Different cells recorded from this area were tuned to different cardiac cycle phases, as indicated by the marked responses at -100 msec, 100 msec and 230 msec in. Similar ongoing activity

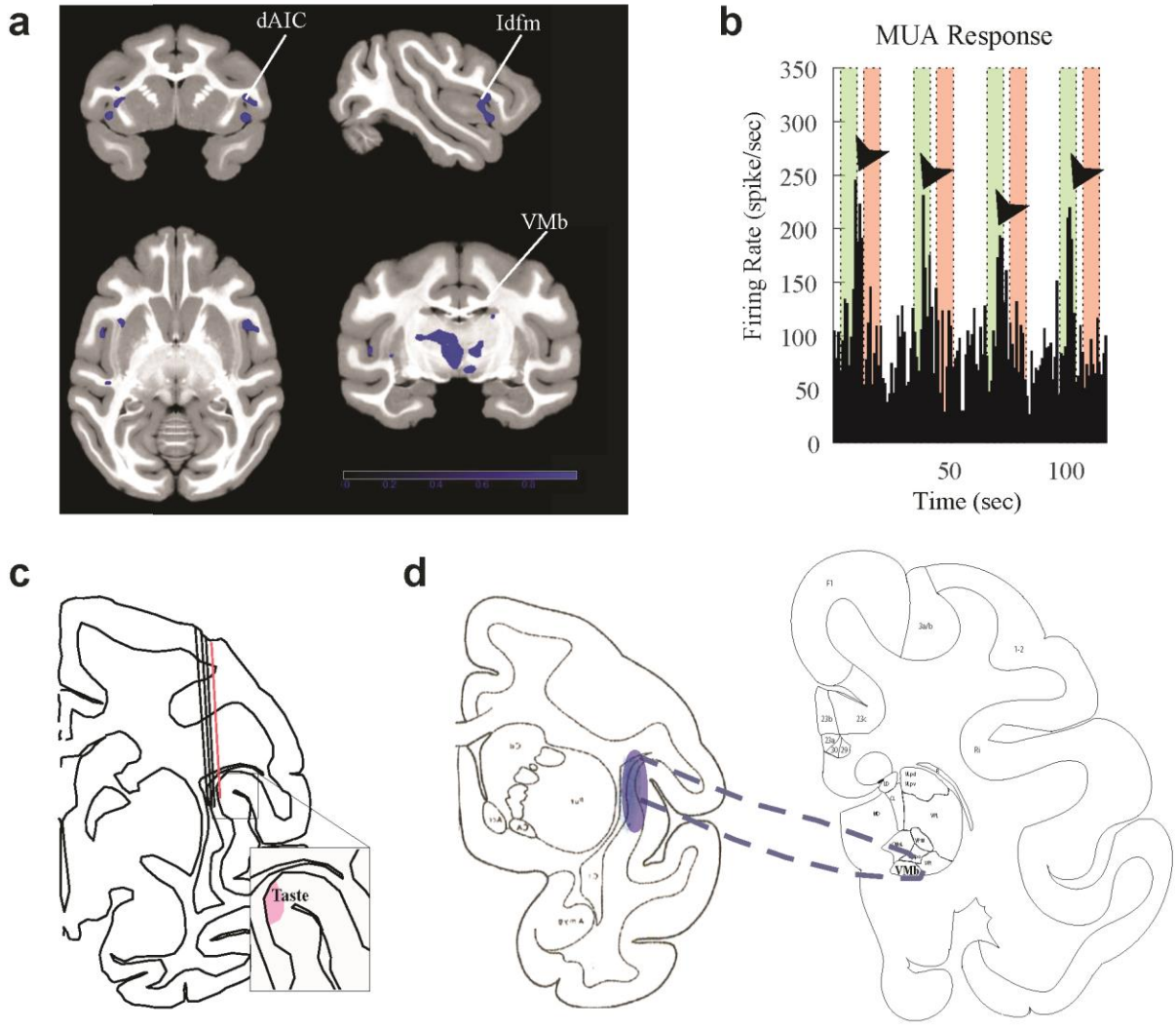

Fig. 6: Multi-modal localization of gustatory responses. (a) BOLD correlates of citric acid (sour) taste; (b) multi-unit activity (MUA) response to sour taste, firing rate averaged into 0.5 ms time bins and overlaid onto the corresponding taste stimulation paradigm, whereby green represents sour taste administration and the peach bar indicates the period of rinsing by artificial saliva. (c) Taste responses localized to the lateral electrode recording site in Idfm (highlighted in pink). (d) Plotted injection site onto atlas template and observed retrograde labeling to the ventromedial basal (VMb) nucleus.

was recorded in the anterior dorsal fundus in Case A09 but not in G11. For all recordings, the representative peak in the Lomb periodogram was around 2 Hz (Supplement 2). Overall, ongoing neuronal activity was observed throughout the insular cortex, most predominantly in the granular aspect (Fig. 5).

Neurons in Idfp responded either to noxious heat, pinch and cold (HPC cells), or were nociceptive-specific with responses to only noxious cold or pinch (NS cells). In the vAIC recording channels, we observed bilateral HPC responses, and also pinch responses, whereby the adjacent electrode (0.5 mm away), recording from a neighboring population, responded to HPC stimulation. Figure 7 highlights the similarity of neuronal responses in the posterior and anterior recording sites to interoceptive stimulation. This re-representation occurred almost simultaneously in both the left and right vAIC, but did not seem to be reliably evoked in every session. Further, these neuronal populations did not seem to have a preferred region or side of the body.

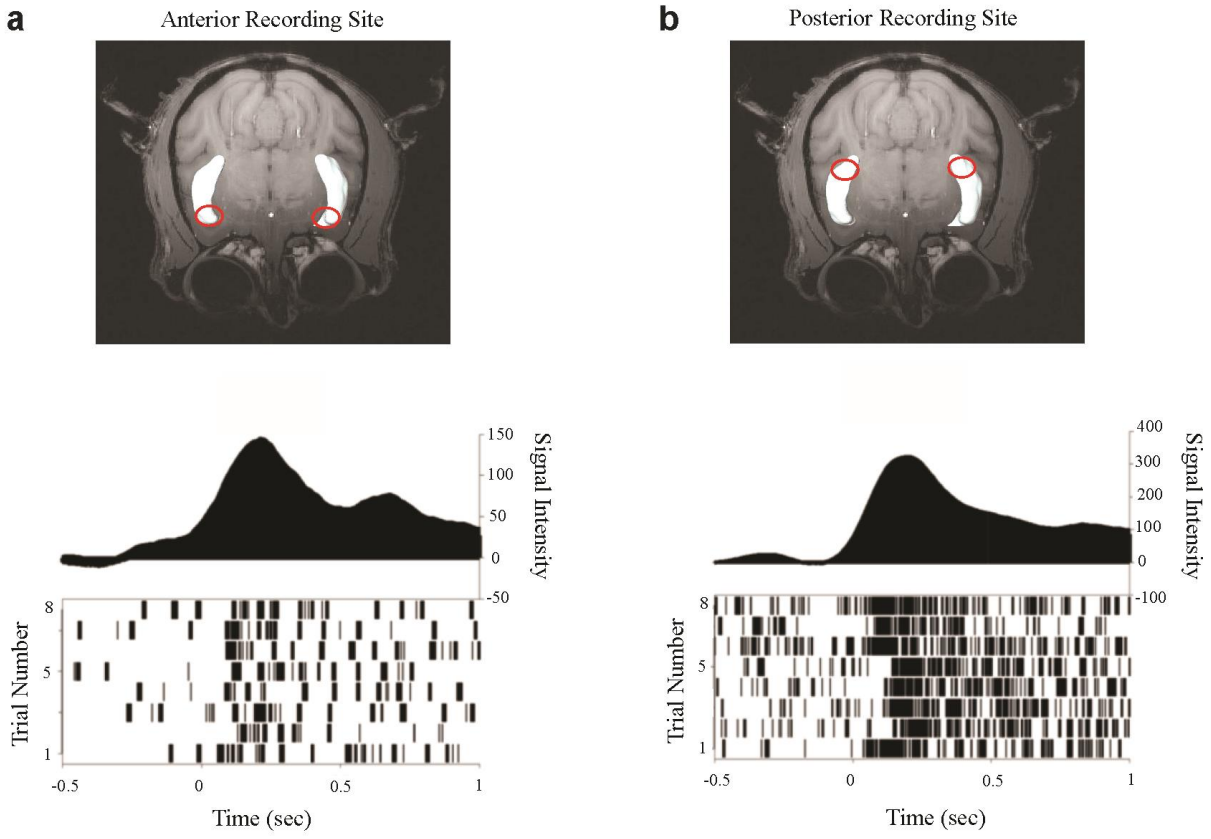

Fig. 7: Evoked responses in the granular and agranular insular cortex. The (**a)** anterior and (**b**) posterior recording arrays and corresponding activation to noxious cold stimulation of the upper lip (Case G11).

Prior to electrophysiological sampling of the insular cortex, a specific set of interoceptive stimuli (e.g. taste, visceral distention, and thermal stimulation) were introduced during anesthetized fMRI experiments. From these results, functional activation maps were first created at the individual-level to examine the anatomical localization of each type of stimulation. Functional activation maps for one individual are shown in Figure 8 (Case B09), whereby activation of the posterior dorsal fundus of the insula (Idfp) by thermal stimulation (Temperature) is evident. Stimulation of the auricular vagus nerve branch (ABVN) activated the mid-dorsal fundus of the insula (Idfm), an area that was also activated by rectal distention (GI 1) and taste (Taste 1). Additional activation regions were identified for rectal distention (GI 2) and taste (Taste 2) in the vAIC and dAIC, respectively.

Upon further analysis of these functional stimulations, it was observed that the localization of vAIC activation was different for each subject, and rather the more robust RD activation was localized posteriorly to Idfp/Ri (Fig. 7). On the contrary, dAIC activation by tastants was robust across individuals and at the group-level (Fig. 7). A multi-modal group-level map, as depicted by Figure 7, was constructed from the RD and taste sessions. Data from ABVN were not analyzed at the group level as the number of individual subjects and sessions were too few (Fig. 3). While there were sufficient sessions recorded during thermal stimulation, the group-level activation map was not overlaid in Figure 7 as most of these data were collected from a different cohort of subjects and need to be normalized in order to compare activation levels across functional modalities.

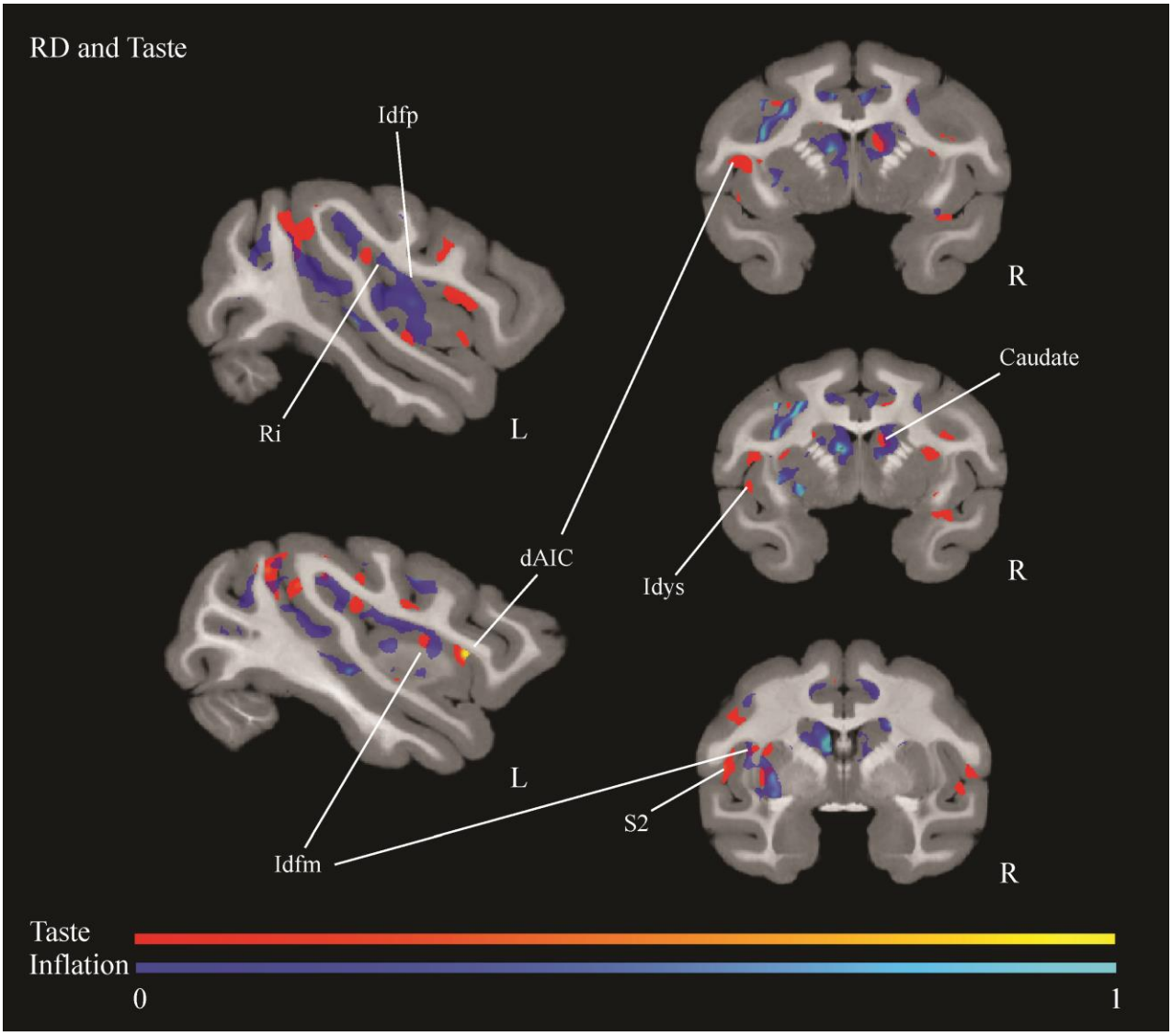

Fig. 8: Functional activation maps representing the group effects of taste and RD. The intensity of each modality was normalized for comparison. The activations in Idfp, Ri, Idfm, dAIC, Idys, S2 and the caudate have been labeled.

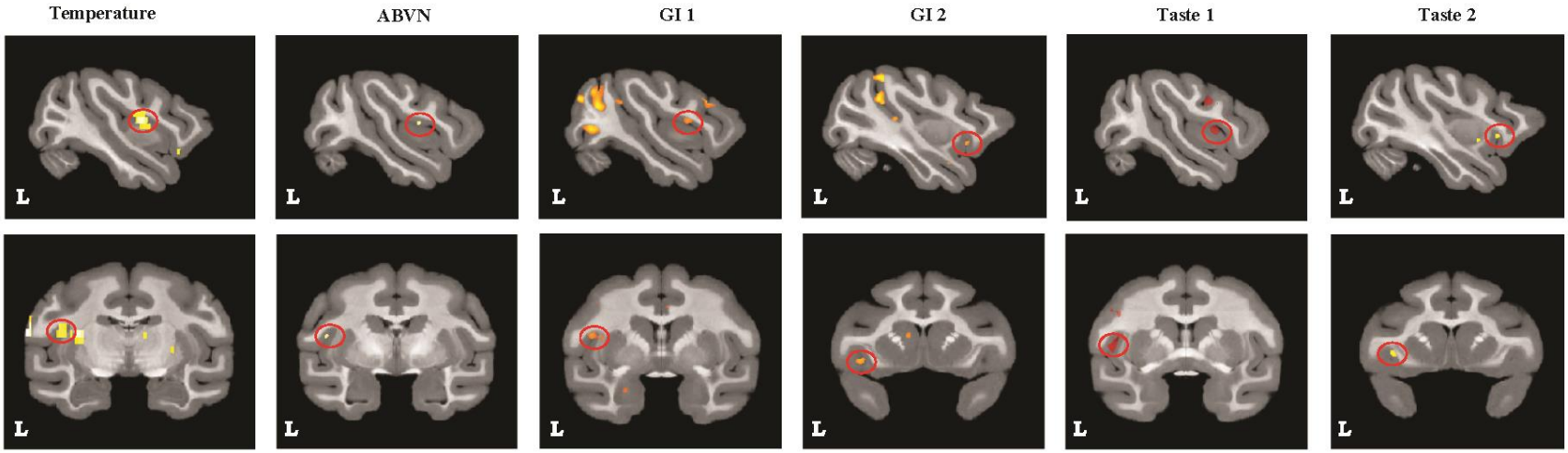

Fig. 9: Spatially normalized whole-brain representations of interoceptive and gustatory stimulus processing in the anesthetized macaque during 7T fMRI (Case B09), from left to right the BOLD correlates of (i) cooling of the right hand (Temperature), (ii) transcutaneous stimulation of the left auricular branch of the vagus nerve (ABVN) - electrodes positioned on the cymba concha, (iii) the dual-representation, anterior (GI 1) and posterior (GI 2) localization of distention of the lower gastrointestinal tract and (iv) the dual-representation of gustation, or taste, in the mid-dorsal fundus (Taste 1) and anterior insular cortex (Taste 2). All data were analyzed using a univariate parametric test to independently model each stimulus condition and the results portray the resulting t-contrast maps ($p = 0.001$, uncorrected).

DISCUSSION

Our results show that the macaque insular cortex encodes interoceptive information in a topographic manner reminiscent of that described for the human insula by fMRI studies with various interoceptive stimuli, including cutaneous temperature modulation (Craig & Andrew, 2002; Hua le et al., 2005), gustatory and interoceptive stimulation (Avery et al., 2015), as well as by electrical stimulation (Segerdahl et al., 2015; Mazzola et al., 2009; Ostrowsky et al., 2002). The characterization of the underlying responses highlights a gross foot-to-head topography along the posteroanterior insular axis. Our work provides additional insight into the underlying neuronal response properties and evidence for a re-representation of interoceptive information within the insular cortex.

Functional Organization of the Insular Cortex

The present study supports the idea that the primate insula represents interoception in a manner that preserves the spinocranial topography and the encoding of interoceptive modalities along distinct labeled-lines throughout the neuraxis. As the insula is the primary cortical recipient of interoceptive inputs, the manner in which this information is organized may help disclose how these inputs are relayed to form percepts of the body's physiological state and contribute to embodiment. It appears from our research that the insular cortex exhibits an organization of spinocranial afferents with modular domains denoted by the functional encoding of the underlying neuronal populations and receptor types. Such organization would be reminiscent of other primary sensory cortices, e.g., the somatosensory cortex (Sur, 1981).

There is evidence for a functional neuroanatomical conservation of the interoceptive sensory system, highlighting its importance for survival and evolution. While the VMpo thalamic subdivision exists only in primates, the C- and Aδ-fiber pathway exists in primordial form in cats and rats (Craig et al., 1994). Existence of such a conserved afferent pathway for interoceptive processing likely supports the maintenance of viscerototopic organization throughout the rodent neuraxis (Cechetto & Saper, 1987; Saper, 1982).

Afferent fibers innervating the gastrointestinal system ascend through two separate streams: one through the spinothalamic tract and another through the vagus nerve (Umans & Liberler, 2018; Beyak & Vanner, 2004). These two afferent streams are relayed by VMpo and VMb, respectively. Given the anatomical knowledge, our functional neuroimaging results can be interpreted as representing both ascending relay pathways.

Projections from VMb are concentrated to the anterior half of the dorsal fundus of the insula (Ito & Craig, 2009; Pritchard et al., 1986), the region where our results suggest taste is localized, albeit in two discrete regions: Idfm and dAIC, whereby Idfm appears to serve also as a multi-somatosensory mouth representation. Our fMRI data complement our electrophysiological findings, demonstrating clusters of voxels activated specifically to tastants in the mid-dorsal fundus of the insula (Idfm), next to where we observed the mouth representation. Further, from what we can see from ABVN stimulation, Idfm is also activated. The areal overlap in Idfm and its multi-modal activation could be indicative of VMb relay and the potential convergence of inter-related sensory information in terms of autonomic nervous system processing. Such convergence of multiple interoceptive functions in Idfm have been previously reported in humans (Avery et al., 2017).

The dysgranular insula (Idys) receives thalamic inputs in addition to the insular dorsal fundus (Craig, 2014), however, its topography likely reflects a dorsoventral re-representation of sensory afferent encoding by the granular insular cortex. Idys is responsive to multiple interoceptive modalities and already reflects predictive representations of incoming events, which are continuously updated by bottom-up sensory input (Sharvit et al., 2018).

Neuronal Characterization

The insular dorsal fundus is composed of neuronal populations that are preferentially tuned to noxious cold, noxious mechanical stimulation, innocuous heat and taste stimuli. Our functional mapping revealed a large and diverse neuronal population dedicated to the encoding of noxious stimuli. The major role of the insular cortex as a cortical center for pain representation has already been highlighted by fMRI (Duerden & Albanese, 2013; Peyron, Laurent, & Garcia-Larrea, 2000) and microstimulation studies (Ostrowsky et al., 2002). Our data not only largely corroborates these findings but also characterizes the response profile of nociceptive and thermoreceptive neurons in the insula. Our observed areas show an increase in firing activity time-locked to the onset of noxious cold stimulation, noxious heat, and graded mechanical noxious stimulation (pinch).

Few other studies were able to characterize neuronal activity in the macaque insular cortex. Verhagen, Kadohisa, and Rolls (2004) reported oral temperature-sensitive neurons, with differential response profiles to varying temperature, in a similar area to where we observed temperature neurons in Case G11. Zhang, Dougherty, and Oppenheimer (1999) have demonstrated pinch-neurons in the mid-insula with a similar response profile to the one observed in our data. However, the results of the statistical analyses of pinch stimulation in this manuscript should be considered carefully, as the

graded increase in pinch intensity was not always the same across trials. Therefore, the statistical results reported here for pinch stimulation might be biased by this inherent variability.

Sensory afferent fibers, connecting the body to the central nervous system, are characterized not only by anatomical relay but also by their responses to specific stimuli. Differences in neuronal response profiles between nociceptive (NS, not responsive to graded cool), cold, and HPC (heat-pinch-cold responding predominantly to burning pain) cells are related to cellular morphology and functional encoding in the insular cortex. Our electrophysiological sampling localized such neuronal cell types across the insula's neuroanatomical gradient.

Additional neuronal ensembles within the insula elicited ongoing activity, which may represent the rhythmic activity of physiological processes (e.g. respiration and cardiac activity). Such neuronal entrainment is evidenced by the population response to time-locked phases of the cardiac cycle (i.e. ventricular systole and the early or late phase of ventricular diastole) – this cardiometric encoding by insular neurons is further evidence of cortical monitoring of ongoing physiological processes. This observation seems to be aligned with the suggestion that a cardiac representation is not limited to subcortical structures in primates, but also includes a cortical representation in the insula (Nagai, Hoshide, & Kario, 2010; Oppenheimer & Cechetto, 2011).

The idea of heart chronometry is supported by previous studies reporting the same phenomenon at different levels of the neuraxis. Both vagal and sympathetic afferent fibers have spontaneous activity in phase to particular atrial or ventricular events in mammals (Malliani, Recordati, & Schwartz, 1973; Paintal, 1963). At the level of the pons, Sieck and Harper (1980) have demonstrated that PBN neurons display a correlation with the cardiac cycle, presenting variable phase preference when aligned with the peak of the QRS complex.

Oppenheimer (2016) published a review highlighting the capacity of the insula to monitor cardiac activity in humans and animals. Baroreceptor-related neurons had been previously observed in the macaque insula (Zhang et al., 1998). These baroreceptive cells described by Zhang et al. (1998) track and represent the slow modulation of blood flow. However, the exact extent of this cardiac, baroreceptive insular field is not completely resolved. A possible interpretation of our observed data is that a distinct population of neurons in the ventral Ri seems to act as a neural chronometer of the cardiac cycle that preserves characteristics already existing in lower levels of the neuraxis. The concept of a mechanism of cardiac chronometry had been suggested previously in the rodent insula (Oppenheimer & Cechetto, 1990).

While our finding of heart-responsive cells seems to be limited to the Ri and Idfp, the results from Zhang et al. (1998) suggest this area extends throughout the entire insular cortex. Indeed throughout the insular cortex, ongoing MUA was observed with a characteristic peak frequency at 2 Hz. This rhythmic activity might substantiate a complex representation contributing to the coupling of visceral rhythms.

Dorsal to the heart-responsive cells, a vestibular-responsive region in our sample contained neurons that increased their firing rate after movement of the whole body. Our observations are coherent with the current literature in the field, that the Ri contains vestibular responsive cells (Brandt & Dieterich, 1999; Akbarian et al., 1988). The close proximity between the heart and vestibular representations in the insular cortex may not be coincidental and rather related to the vestibulo-autonomic reflex, a well-described phenomenon in which changes in spatial orientation evoked changes in heart rate and blood pressure. Anatomical evidence links the vestibulo-autonomic reflex to the NTS (Balaban & Beryozkin, 1994). A possible interpretation of our data, taken together with reported findings in the literature, is that the Ri potentially represents our sense of self in space and time and influences cardiac function.

In addition to the aforementioned functional characterizations, neurons responding to movement of the jaw were also recorded in the insular cortex. Sensory input elicited by ergoceptors is also relayed by the lamina I spinothalamic pathway (Craig, 2002; Evrard, 2018). Thus, recordings of jaw movement in the dorsal fundus could be explained by this.

Refining the Working Model

Our study offers an unprecedented possibility to directly investigate the neuronal properties of the vAIC during our electrophysiological sampling across the insular cortex. Our data suggest the vAIC contains populations of neurons that bilaterally represent stimuli also encoded by the insular dorsal fundus. This re-representation seemed to be achieved through bursting activity that was time-locked to the stimulation. An examination of all recording sessions led to the revelation that a specific relationship between modality tested and position of the electrode tip in the vAIC exists.

The almost concomitant re-representation of a sensation in different cortical areas has previously been observed by Nicolelis et al. (1998), where researchers recorded simultaneously in three of the primate sensory cortices (areas 2 and 3b, and S2) and observed distinct neuronal ensembles simultaneously representing the same tactile stimulation using different encoding strategies. Nicolelis and colleagues hypothesized that neurons in individual cortical areas using a

wide variety of encoding strategies interact extensively to form a unified representation of stimuli. Similarly, the insular cortex might represent different aspects of the stimuli in its sub-regions that interact to form a cohesive representation of the sensation as a whole. The non-specificity of the vAIC responses to a region or side of the body suggests that the observed evoked responses are not topographically organized in the seemingly trans-modal agranular aspect. It is during dynamic emotional experiences that the vAIC integrates the internal and external milieu (Nguyen, Breakspear, Hu, & Guo, 2016). A possibility to explain this observed pattern is that while the dorsal fundus represents the stimulus as a whole, including its spinocranial localization, laterality, intensity and duration, the vAIC might separately represent specific aspects of the stimulation that are behaviorally relevant, such as, its saliency.

Finally, the vAIC representation may speak in favor of a previously suggested functional specialization of each AIC hemisphere (Craig, 2009). According to this framework, while the left AIC is associated with affiliative emotions and behaviors; the right AIC is associated with arousing stimuli (e.g., nociceptive). If these two regions are involved in divergent subjective feelings, it seems logical that both sides should receive information about relevant events to substantiate appropriate behavioral responses. This should require an almost simultaneous representation of the event details, performed throughout the insular dorsal fundus, and a representation of the event's behavioral relevance, possibly represented in the vAIC. These findings fit with prior reports of the vAIC as a cortical center for predictive coding (Seth & Crithley, 2012; Barrett & Simmons, 2015) and region supporting interoceptive awareness (Craig, 2009; Critchley et al., 2004).

Our results suggest a common pattern that bridges the gap between how humans and non-human primates encode bodily sensations, as the topographic representation seen here is similar to what has been previously reported in human studies (Avery et al., 2015; Craig, 2002, 2009; Craig & Andrew, 2002; Hua le et al., 2005; Segerdahl et al., 2015). This refined representation of internal bodily signals plays a crucial role in emotional embodiment and in the homeostatically efficient shaping of cognitive processes by interoception, providing a basis for the evolutionary emergence of embodied subjective feelings.

ACKNOWLEDGMENTS

This work was supported by the Werner Reichardt Centre for Integrative Neuroscience (CIN) at the Eberhard Karls University of Tübingen (CIN is an Excellence Cluster funded by the Deutsche Forschungsgemeinschaft [DFG] within the framework of the Excellence Initiative EXC 307) and by the Max Planck Society. We acknowledge support by the Deutsche Forschungsgemeinschaft and Open Access Publishing Fund of University of Tübingen for the cost of publication.

CONFLICT OF INTEREST STATEMENT

The author declares having no personal, professional or financial relationships that could potentially be construed as a conflict of interest.

REFERENCES

Akbarian, S., Berndl, K., Gruesser, OJ., Guldin, W., Pause, M., Schreiter, U. (1988). Responses of single neurons in the parietoinsular vestibular cortex of primates. *Annals of the New York Academy of Sciences, 545*(1), 187-202.

Andrew, D. & Craig AD. (2001). Spinothalamic lamina I neurons selectively sensitive to histamine: a central neural pathway for itch. *Nature*, *4*(1), 72–77.

Avery, JA., Gotts, SJ., Kerr, KL., Burrows, K., Ingeholm, JE., Bodurka, J., … Simmons, KW. (2017). Convergent gustatory and viscerosensory processing in the human dorsal mid-insula. *Human Brain Mapping*, *38*(4), 2150–2164. https://doi.org/10.1002/hbm.23510

Avery, JA., Kerr, KL., Ingeholm, JE., Burrows, K., Bodurka, J., & Simmons, WK. (2015). A common gustatory and interoceptive representation in the human mid-insula. *Hum Brain Mapping*, *36*(8), 2996–3006. https://doi.org/10.1002/hbm.22823

Balaban, CD. & Beryozkin, G. (1994). Vestibular nucleus projections to nucleus tractus solitarius and the dorsal motor nucleus of the vagus nerve: potential substrates for vestibulo-autonomic interactions. *Experimental Brain Research, 98*(2), 200-212.

Barrett, LF., & Simmons, WK. (2015). Interoceptive predictions in the brain. *Nature Reviews Neuroscience*, *16*(7), 419–429. https://doi.org/10.1038/nrn3950

Bauernfeind, AL., de Sousa, AA., Avasthi, T., Dobson, SD., Raghanti, MA., Lewandowski, AH., … Sherwood, CC. (2013). A volumetric comparison of the insular cortex and its subregions in primates. *J Hum Evol*, *64*(4), 263–279. https://doi.org/10.1016/j.jhevol.2012.12.003

Beyak, MJ., Ramji, N., Krol, KM., Kawaja, MD., Vanner SJ. (2004). Two TTX-resistant Na+ currents in mouse colonic dorsal root ganglia neurons and their role in colitis-induced hyperexcitability. *Am. J. Physiol. Gastrointest. Liver Physiol., 287,* G845-G855.

Brandt, T., & Dieterich, M. (1999). The Vestibular Cortex: Its Locations, Functions, and Disorders. *Annals of the New York Academy of Sciences*, *871,* 293–312. https://doi.org/10.1111/j.1749-6632.1999.tb09193.x

Caruana, F., Jezzini, A., Sbriscia-Fioretti, B., Rizzolatti, G., & Gallese, V. (2011). Emotional and social behaviors elicited by electrical stimulation of the insula in the macaque monkey. *Current Biology*, *21*(3), 195–199. https://doi.org/10.1016/j.cub.2010.12.042

Cechetto, DF., & Saper, CB. (1987). Evidence for a viscerotopic sensory representation in the cortex and thalamus in the rat. *Journal of Comparative Neurology*, *262*(1), 27–45. https://doi.org/10.1002/cne.902620104

Cox, RW. (1996). AFNI: Software for Analysis and Visualization of Functional Magnetic Resonance Neuroimages. *Computers and Biomedical Research, 29,* 162-173.

Craig, AD. (2015). *How do you feel?* Princeton University Pres.

Craig, AD. (2014). Topographically Organized Projection to Posterior Insular Cortex from the Posterior Portion of the Ventral Medial Nucleus (VMpo) in the Long-tailed Macaque Monkey. *J Comp Neurol*, *522*(1), 36–63. https://doi.org/10.1016/j.pestbp.2011.02.012.Investigations

Craig, AD. (2009). How do you feel — now? The anterior insula and human awareness. *Nature Reviews Neuroscience*, *10*(1), 59–70. https://doi.org/10.1038/nrn2555

Craig, AD. (2004). Lamina I, but not Lamina V, Spinothalamic Neurons Exhibit Responses That Correspond With Burning Pain. *J Neurophysiol*, *92*. https://doi.org/10.1152/jn.00385.2004

Craig, AD. (2002). How do you feel? Interoception: the sense of the physiological condition of the body. *Nature Reviews Neuroscience*, *3*(August), 655–666. https://doi.org/10.1038/nrn894

Craig, AD. & Andrew, D. (2002). Responses of Spinothalamic Lamina I Neurons to Repeated Brief Contact Heat Stimulation in the Cat. *Journal of Neurophysiology*, *87*(4), 1902–1914.

https://doi.org/10.1152/jn.00578.2001

Craig, AD., Krout, K., & Andrew, D. (2001). Quantitative Response Characteristics of Thermoreceptive and Nociceptive Lamina I Spinothalamic Neurons in the Cat. *Journal of Neurophysiology*, *86*(3), 1459–1480. https://doi.org/10.1152/jn.2001.86.3.1459

Craig, AD., Chen, K., Bandy, D., & Reiman, EM. (2000). Thermosensory activation of insular cortex. *Nature Neuroscience*, *3*(2), 184–190.

Craig, AD., Bushnell, MC., Zhang, ET., Blomqvist, A. (1994). A thalamic nucleus specific for pain and temperature sensation. *Nature*, *372*(6508), 770–773. https://doi.org/10.1038/372770a0

Craig, AD., & Kniffki, KD. (1985). Spinothalamic Lumbosacral Lamina I Cells Responsive to Skin and Muscle Stimulation in the Cat. *J. Physiol* (Vol. 365).

Critchley, HD., Wiens, S., Rotshtein, P., Ohman, A., Dolan, R. J., Öhman, A., … Dolan, RJ. (2004). Neural systems supporting interoceptive awareness. *Nat Neurosci*, *7*(2), 189–195. https://doi.org/10.1038/nn1176

Dostrovsky, JO., & Craig, AD. (1996). Cooling-specific spinothalamic neurons in the monkey. *Journal of Neurophysiology*, *76*(6), 3656–3665. https://doi.org/10.1152/jn.1996.76.6.3656

Duerden, EG., Arsalidou, M., Lee, M., & Taylor, MJ. (2013). Lateralization of affective processing in the insula. *NeuroImage*, *78*, 159–175. https://doi.org/10.1016/j.neuroimage.2013.04.014

Evrard, H. C. (2018). Von Economo and fork neurons in the monkey insula, implications for evolution of cognition. *Current Opinion in Behavioral Sciences*, *21*, 182–190. https://doi.org/10.1016/j.cobeha.2018.05.006

Evrard, HC., Logothetis, NK., & Craig, A. (2014). Modular architectonic organization of the insula in the macaque monkey. *Journal of Comparative Neurology*, *522*(1), 64–97. https://doi.org/10.1002/cne.23436

Evrard, HC., & Craig, AD. (2008). Retrograde analysis of the cerebellar projections to the posteroventral part of the ventral lateral thalamic nucleus in the macaque monkey. *Journal of Comparative Neurology*, *508*(2), 286–314. https://doi.org/10.1002/cne.21674

Frangos, E., Ellrich, J., & Komisaruk, BR. (2015). Non-invasive access to the vagus nerve central projections via electrical stimulation of the external ear: FMRI evidence in humans. *Brain Stimulation*, *8*(3), 624–636. https://doi.org/10.1016/j.brs.2014.11.018

Harrison, N, Gray, M., Gianaros, PJ., & Critchley, HD. (2010). The embodiment of emotional feelings in the brain. *Journal of Neuroscience*, *30*(38), 12878–12884. https://doi.org/10.1523/JNEUROSCI.1725-10.2010

Hirata, S., Nakamura, T., Ifuku, H., & Ogawa, H. (2005). Gustatory coding in the precentral extension of area 3 in Japanese macaque monkeys; comparison with area G. *Exp Brain Res*, *165*(4), 435–446. https://doi.org/10.1007/s00221-005-2321-y

Hua lH., Strigo, IA., Baxter, LC., Johnson, SC., & Craig, AD. (2005). Anteroposterior somatotopy of innocuous cooling activation focus in human dorsal posterior insular cortex. *Am J Physiol Regul Integr Comp Physiol*, *289*(2), R319–R325. https://doi.org/10.1152/ajpregu.00123.2005

Ito, SI., & Craig, AD. (2005). Vagal-evoked activity in the parafascicular nucleus of the primate thalamus. *Journal of Neurophysiology*, *94*(4), 2976–2982. https://doi.org/10.1152/jn.00235.2005

Kadohisa, M., Rolls, ET., & Verhagen, JV. (2004). Orbitofrontal cortex: Neuronal representation of oral temperature and capsaicin in addition to taste and texture. *Neuroscience*, *127*(1), 207–221. https://doi.org/10.1016/j.neuroscience.2004.04.037

Kaneoke, Y., & Vitek, JL. (1996). Burst and oscillation as disparate neuronal properties. *Journal of Neuroscience Methods*, *68*(2), 211–223. https://doi.org/10.1016/0165-0270(96)00081-7

Kim, EJ., Sidhu, M., Gaus, SE., Huang, EJ., Hof, PR., Miller, BL., … Seeley, WW. (2012). Selective frontoinsular von economo neuron and fork cell loss in early behavioral variant frontotemporal dementia. *Cerebral Cortex*, *22*(2), 251–259. https://doi.org/10.1093/cercor/bhr004

Light, AR., & Perl, ER. (2003). Unmyelinated afferent fibers are not only for pain anymore. *Journal of Comparative Neurology*, *461*(2), 137–139. https://doi.org/10.1002/cne.10691

Logothetis, NK., Eschenko, O., Murayama, Y., Augath, M., Steudel, T., Evrard, HC., … Oeltermann, A. (2012). Hippocampal-cortical interaction during periods of subcortical silence. *Nature*, *491*(7425), 547–553. https://doi.org/10.1038/nature11618

Logothetis, NK., Augath, M., Murayama, Y., Rauch, A., Sultan, F., Goense, J., … Merkle, H. (2010). The effects of electrical microstimulation on cortical signal propagation. *Nature Neuroscience*, *13*(10), 1283–1291. https://doi.org/10.1038/nn.2631

Malliani, A., Recordati, G., Schwartz, P. (1973). Nervous activity of afferent cardiac sympathetic fibres with atrial and ventricular endings. *J. Phsyiol., 229*(2), 457-469.

Matsuo, K., Hsu, YC., Tseng, WYI. (2012). Effects of low pass filtering and autocorrelation on resting state fMRI as investigated using a regression model in SPM8. *Proc. Intl. Soc. Mag. Reson. Med., 20.*

Mazzola, L., Isnard, J., Peyron, R., Guénot, M., & Mauguière, F. (2009). Somatotopic organization of pain responses to direct electrical stimulation of the human insular cortex. *PAIN*, *146*(1–2), 99–104. https://doi.org/10.1016/J.PAIN.2009.07.014

Nagai, M., Hoshide, S., & Kario, K. (2010). The insular cortex and cardiovascular system: A new insight into the brain-heart axis. *Journal of the American Society of Hypertension*, *4*(4), 174–182. https://doi.org/10.1016/j.jash.2010.05.001

Nicolelis, MAL., Ghazanfar, AA., Stambaugh, CR., Oliveira, LMO., Laubach, M., Chapin, JK., … Kaas, JH. (1998). Simultaneous encoding of tactile information by three primate cortical areas. *Nature Neuroscience*, *1*(7), 621–630. https://doi.org/10.1038/2855

Nguyen, VT., Breakspear, M., Hu, X., & Guo, CC. (2016). The integration of the internal and external milieu in the insula during dynamic emotional experiences. *NeuroImage*, *124*, 455–463. https://doi.org/10.1016/J.NEUROIMAGE.2015.08.078

Oostenveld, R., Fries, P., Maris, E., & Schoffelen, JM. (2011). FieldTrip: Open source software for advanced analysis of MEG, EEG, and invasive electrophysiological data. *Computational Intelligence and Neuroscience*, *2011*. https://doi.org/10.1155/2011/156869

Oppenheimer, S. (2016). The Insular Cortex and the Regulation of Cardiac Function. *Comprehensive Physiology*, *6*(April), 1081–1133. https://doi.org/10.1002/cphy.c140076

Oppenheimer, SM. & Cechetto, DF. (1990). Cardiac chronotropic organization of the rat insular cortex. *Brain Research, 533*(1), 66-72.

Oppenheimer, SM. & Cechetto, DF. (2010). The insular cortex and the regulation of cardiac function. *Comprehensive Physiology, 6*(2), 1081-1133.

Ostrowsky, K., Magnin, M., Ryvlin, P., Isnard, J., Guenot, M., & Mauguière, F. (2002). Representation of pain and somatic sensation in the human insula: a study of responses to direct electrical cortical stimulation. *Cerebral Cortex (New York, N.Y. : 1991)*, *12*(4), 376–385. https://doi.org/10.1093/cercor/12.4.376

Paintal, A. (1963). Vagal afferent fibres. In *Ergebnisse der physiologie biologischen chemie und experimentellen pharmakologie.* Springer. 376-385.

Peyron, R., Laurent, B., García-Larrea, L. (2000). Functional imaging of brain responses to pain: A review and meta-analysis. *Neurophysiologie Clinique/Clinical Neurophysiology*, *30*(5), 263–288. https://doi.org/10.1016/S0987-7053(00)00227-6

Pfeuffer, J., Merkle, H., Beyerlein, M., Steudel, T., & Logothetis, N. K. (2004). Anatomical and functional MR imaging in the macaque monkey using a vertical large-bore 7 Tesla setup. *Magnetic Resonance Imaging*, *22*(10 SPEC. ISS.), 1343–1359. https://doi.org/10.1016/j.mri.2004.10.004

Pritchard, TC., Hamilton, RB., Morse, JR., & Norgren, R. (1986). Projections from thalamic gustatory and lingual

areas in the monkey, Macaca fascicularis. *Journal of Comparative Neurology*, *244*(2), 213–228. https://doi.org/10.1002/cne.902440208

Quiroga, QR., Nadasdy, Z., & Ben-Shaul, Y. (2004). Unsupervised Spike Detection and Sorting with Wavelets and Superparamagnetic Clustering.

Reveley, C., Gruslys, A., Ye, F. Q., Glen, D., Samaha, J., E. Russ, B., … Saleem, KS. (2016). Three-Dimensional Digital Template Atlas of the Macaque Brain. *Cerebral Cortex*, 1–15. https://doi.org/10.1093/cercor/bhw248

Reveley, C., Gruslys, A., Ye, FQ., Glen, D., Samaha, J., E. Russ, B., … Saleem, KS. (2016). Three-Dimensional Digital Template Atlas of the Macaque Brain. *Cerebral Cortex*, 1–15. https://doi.org/10.1093/cercor/bhw248

Saleem, KS., Logothetis, NK. (2007). *Atlas of the Rhesus Monkey Brain*. Academic Press.

Saper, C. B. (1982). Convergence of autonomic and limbic connections in the insular cortex of the rat. *The Journal of Comparative Neurology*, *210*(2), 163–173. https://doi.org/10.1002/cne.902100207

Scott, TR., Yaxley, S., Sienkiewicz, ZJ., Rolls, ET. (1986). Gustatory responses in frontal opercular cortex of the alert cynomolgus monkey. *Journal of Neurophysiology*, *56*(3), 876–890.

Segerdahl, AR., Mezue, M., Okell, T. W., Farrar, JT., & Tracey, I. (2015). The dorsal posterior insula subserves a fundamental role in human pain. *Nature Neuroscience*, *18*(4), 499–500. https://doi.org/10.1038/nn.3969

Seth, AK. and Friston, KJ. (2016). Active interoceptive inference and the emotional brain. https://doi.org/10.1098/rstb.2016.0007

Sharvit, G., Corradi-Dell'acqua, C., & Vuilleumier, P. (2018). Modality-specific effects of aversive expectancy in the anterior insula and medial prefrontal cortex. https://doi.org/10.1097/j.pain.0000000000001237

Sieck, GC. and Harper, RM. (1980). Discharge of neurons in the parabrachial pons related to the cardiac cycle: changes during different sleep-waking states. *Brain Research, 199*(2), 385-399.

Sur, W. & K. (1981). Modular Segregation of Functional Cell Classes Within the Postcentral Somatosensory Cortex of Monkeys. *Science*, *212*(29), 1059–1061. https://doi.org/10.1126/science.7233199

Umans, BD. & Liberles, SD. (2018). Neural Sensing of Organ Volume. *Trends in Neurosciences, 41*(12), 911-924.

Veldhuizen, MG., Bender, G., Constable, RT., Small, DM. (2007). Trying to detect taste in a tasteless solution: Modulation of early gustatory cortex by attention to taste. *Chemical Senses*, *32*(6), 569–581. https://doi.org/10.1093/chemse/bjm025

Verhagen, JV, Kadohisa, M., Rolls, ET. (2004). Primate Insular/Opercular Taste Cortex: Neuronal Representations of the Viscosity, Fat Texture, Grittiness, Temperature and Taste of Foods. *Journal of Neurophysiology*, *92*(3), 1685–1699. https://doi.org/10.1152/jn.00321.2004

Zhang, ZH., Dougherty, P., Oppenheimer, S. (1999). Monkey insular cortex neurons respond to baroreceptive and somatosensory convergent inputs. *Neuroscience, 94*

Zhang, ZH., Dougherty, P., Oppenheimer, S. (1998). Characterization of baroreceptor-related neurons in the monkey insular cortex. *Brain Research, 796*(1-2), 303-306.

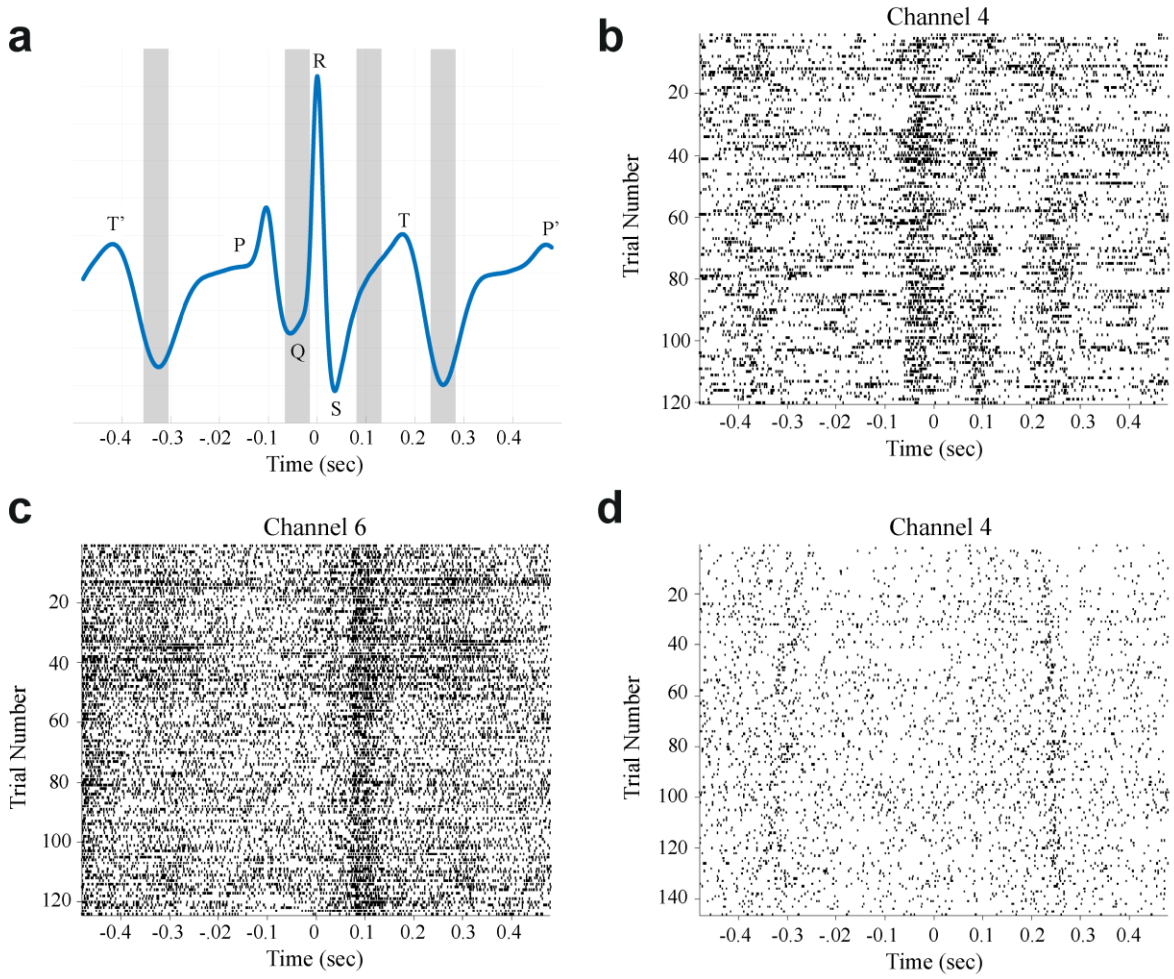

Supplement 1: Heart responses recorded in different sites of the retroinsula (**Ri**) in Case A09. (**a**) Example of one of the cardiac cycle trials; gray columns indicate the time points to which neurons were specifically tuned. MUA signals were aligned to the R peak of the QRS complex and epoched with a time window of 0.8 sec. (**b**) Heart-responsive area that displays a complex response pattern, in which time-locked activation can be observed during the deep Q wave, during the ascending slope of the RT interval, and during the deep valley after the T-wave. (**c**) A heart-responsive region with ongoing activity responsive to the ascending slope of the RT interval. (**d**) A heart-responsive region recorded with an ongoing activity that is responsive during the trough after the T-wave.

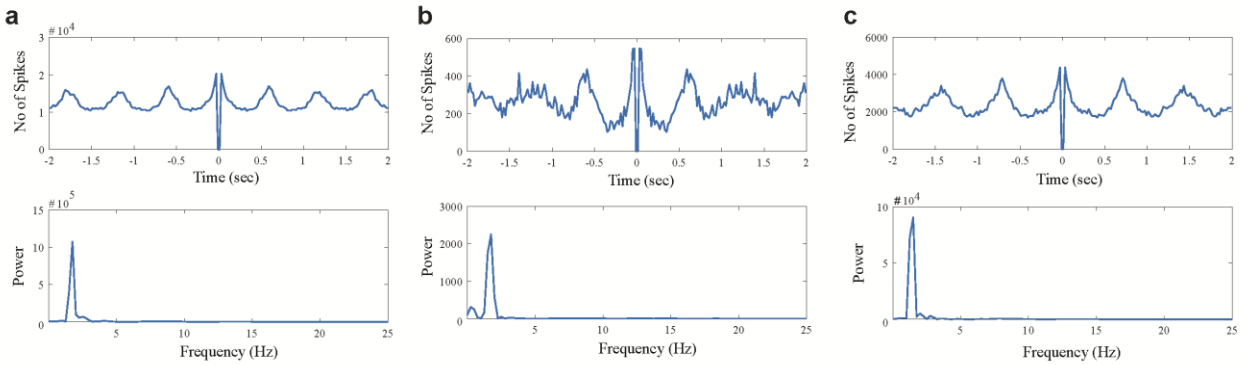

Supplement 2: Oscillatory activity registered in the dorsal fundus. (**a**-**b**) are from recordings performed in Case A09, and (**c**) shows a recording performed in Case G11. Autocorrelograms were not normalized and the y-axis indicates the raw correlograms values. All oscillatory activities had a peak at 2 Hz. Recording locations can be seen in the respective functional maps.

ACKNOWLEDGEMENTS

The doctoral candidate acknowledges Henry Evrard for his continuous support and for leading the Comparative Neuroanatomy Laboratory at the Center for Integrative Neuroscience (CIN) (Tübingen, Germany). Research funding was provided by the CIN and the Max Planck Institute (MPI) for Biological Cybernetics (Department of Physiology of Cognitive Processes, directed by Nikos K Logothetis). There was no declaration of financial interests influencing this research.

All work associated with this dissertation was carried out at the MPI campus in Tübingen. Logothetis is acknowledged for providing access to his experimental facilities and scientific support. Anesthetized NMR experiments were conducted by the doctoral candidate with the assistance of trained anesthesiologists (Mirko Lindig, Deniz Ipek), veterinarians (Pedro Douay, Silvia Slesiona-Kuenzel and Daniel Havel), and technical assistants (Thomas Steudel and Micheal Beyerlein). A team of animal caretakers (Matthias Neuscheler, Mariana Kallinger and Hannes Goehring) maintained the animal husbandry around the clock and assisted with post-experimental and post-op surveillance of the animals. Surgeries and chamber cleanings proceeded by a coordinated effort between the anesthesiologists, veterinarians, animal caretakers and researchers. For terminal experiments, members of the Functional and Comparative Neuroanatomy Lab, who were trained and FELASA certified, assisted with anesthesia monitoring (Marcel Hertl, Felicitas Horn, and Jennifer Smuda). For invasive terminal recordings, Eduard Krampe assisted directly and wholeheartedly with the design, creation and implementation of the electrode arrays. In addition to the aforementioned, Gianfranco Chavez, Ana Vedoveli, Carsten Klein and Henry Evrard provided experimental and technical assistance during the terminal electrophysiology experiments. Data collected from those experiments were meticulously organized by Ana Vedoveli, who spearheaded the development of the SOP for electrophysiological and physiological (i.e. ECG, pulse oximetry, blood pressure) signal processing and analysis. Histological (i.e. Nissl) sections were digitized and contoured by Renee Hartig, Didem Ergul, Laura Seidel and Ana Vedoveli. Whereby, Hartig and Vedoveli reconstructed the track locations for all terminal electrophysiology recordings and Vedoveli helped tremendously with the electrophysiology figures by developing the analysis pipeline - without her this work would certainly not be where it is today. Marcel Hertl coordinated much of the histology and slice preparation along with Matthias Krockenberger and Albert

Langensiepen. Support was received from experienced macaque experimentalists David Balla and Yusuke Murayama who shared their methodological, technical and analytical expertise. IT consultation on data organization and protection was provided by Michael Schnabel and Joachim Werner. In particular, Werner helped greatly with the technical interfacing between various experimental devices and the NMR or electrophysiology set-ups. For consultation in all topics related to physics, electromagnetic compensation and electrical noise there was Axel Oeltermann. Matthias Arndt, who built the low-pass feedthrough filter which Oeltermann conceptualized for the tVNS-fMRI paradigm, and Joshi Walzog, who replaced the phased-array NMR coil fuses on-the-spot in a matter of minutes. Manifestation of the experimental set-up was assisted by the MPI workshop, particularly by mechanical engineers Mirsat Memaj, Bledor Kadriu and Jannik Romanowski. They helped create the hardware for the multi-electrode array design and fMRI-compatible taste delivery system for humans and macaques. Also, Johannes Bolt for constructing and printing our intra-cranial chambers and 3D insula models. Measuring BOLD responses to select gustatory stimuli in the awake monkey was done with Frederico Azevedo. Advice on fMRI experimental paradigms and scan sequences was sought from imaging experts, such as, Andreas Bartels and David Balla. Some assistance with Matlab, C++ and Linux computer programming was provided by Celia Foster, Ali Karimi, Eric Lacosse, Ana Vedoveli and Joachim Werner. I am truly grateful to all those listed here and cherish all that I have learned from my interactions over the past few years.